Motion of a space tether system in the atmosphere

Thesis submitted in accordance with the requirements of the University of Chester under the auspices of Glyndŵr University for the degree of Doctor of Philosophy by

Dmitrii Elenev

February 2019

The material being presented for examination is my own work and has not been submitted for an award of this or another HEI except in minor particulars which are explicitly noted in the body of the thesis. Where research pertaining to the thesis was undertaken collaboratively, the nature and extent of my individual contribution has been made explicit.

07 February 2019

ABSTRACT

Motion of a space tether system in the atmosphere

Dmitrii Elenev

The space tether system under consideration consists of two rigid bodies with significantly different ballistic coefficients. Because of this difference one of the bodies acts as a stabilizer for the main body – a spacecraft – during the motion of the tether system in the atmosphere.

The investigations are focused on the stability of motion of the tether system in the atmosphere. During its motion in the atmosphere the tether system makes use of torques from aerodynamic forces to maintain a desired orientation. This aerodynamic method of stabilization is passive and does not require energy expenses.

Such a tether system can be used to stabilize the motion before landing onto the surface of Earth or other planets with atmospheres. The aerodynamic tether system is helpful for returning payloads from outer space, especially using small landing modules. It is also possible to utilize in the removal of space debris by reducing the altitude of their orbits. By achieving the spacecraft motion stability during descent the tether system enables a reduction in the target landing area at the final stage of the descent.

The modelling of motion of the tether system includes two parts – *(i)* the deployment of the tether system, and *(ii)* the descent of deployed tether system through the dense layers of the atmosphere.

The motion of the deployed tether system is investigated with regard to the terms of its stability. The tether system can be in stable motion even if either or both bodies are statically unstable. The stability of the system is assessed relative to the parameters – the mass, the geometrical dimensions of the bodies and the length of the tether. It is found that increasing the length of the tether, as a controlled part of the deployment process during descent, can provide an additional stabilizing factor for the tether system.

The model of the deployment process, based on the model of an elastic tether, represents the tether as a set of nodes with mass and with elastic connections. The control of the deployment is based on the length and the rate of change of the length of the tether. The aerodynamic resistance of the tether and its mass characteristics are both taken into consideration during modelling of the deployment.

The described and numerically realized mathematical models allows the parameters for the space tether system motion in the atmosphere to be determined.

ACKNOWLEDGEMENTS

I am truly grateful to my principal supervisor, Professor Alison McMillan, for her patient guidance and valuable suggestions.

I sincerely appreciate the help from Professor Yuriy Zabolotnov, his guidance and support in the research for years.

I would like to acknowledge my employer, Samara National Research University, for the financial support for my study and for providing with facilities for my research.

I am thankful to my parents, Valerii Elenev and Galina Eleneva, for their mental support and motivation, and to my wife Alena and to my sons for inspiring me.

TABLE OF CONTENTS

LIST OF FIGURES

NOMENCLATURE

Indices $i = 1$ and $i = 2$ are used for the spacecraft and the stabilizer respectively,

α_i – angle of attack,

C_{x1}, C_{y1} – non-dimensional aerodynamic force coefficients of the spacecraft,

C_{x2}, C_{y2} – non-dimensional aerodynamic force coefficients of the stabilizer,

C_{xv} – drag coefficient,

$\Delta\vec{r}_1$ – radius-vector of centre-of-pressure position relative to the spacecraft centre of mass,

$\Delta\vec{r}_2$ – radius-vector of centre-of-pressure position relative to the stabilizer centre of mass,

Δx_1 – projection of vector $\Delta\vec{r}_1$ onto the axis of symmetry of the spacecraft, (see §5.1),

Δx_2 – projection of vector $\Delta\vec{r}_2$ onto the axis of symmetry of the stabilizer, (see §5.1),

$\vec{e}_{1i}$ – unit vectors in the coordinate systems associated with vectors $\overrightarrow{V_i}$ and $\overrightarrow{r_i}$ (see §6.1),

$F_{\text{control}}(t)$ – control force (see §6.1),

$F_{\min}$ – minimum deceleration force that the tether release mechanism can provide (see §6.1),

$g = g(h)$ – acceleration due to gravity,

$\vec{g}_e$ – gravitational force,

G – gravity constant,

h – altitude above sea level,

I_{xi}, I_{yi}, I_{zi} – moments of inertia (rotational inertia) of the bodies with respect to axis of the coordinate system $Ox_iy_iz_i$,

k – spring constant,

K – kinetic energy (see §4.4),

$\vec{l}$ – net total angular momentum,

l_{full} – full length of the non-stretched tether (see §7.1),

L – perturbed length of the tether during deployment (see §6.4),

$\dot{L}$ – perturbed rate of change of the length of the tether during deployment (see §6.4),

L_{ND} – length of non-deformed tether (see §6.1),

$L_p(t)$ – program dependence of tether length with respect to time during deployment (see §6.4),

$\dot{L}_p(t)$ – program dependence of the rate of change of length of the tether with respect to time during deployment (see §6.4),

m_1 – mass of the spacecraft,

m_2 – mass of the aerodynamic stabilizer,

M_E – mass of the Earth,

M – Mach number (see §4.3),

$Ox_iy_iz_i$ –coordinate system based on the body *i* (see §4.2),

$Ox_ky_kz_k$ – trajectory coordinate system (see §4.2),

p_L, p_V – feedback coefficients during deployment (see §6.4),

$q = \rho V^2/2$ – dynamic pressure of the air flow (see §4.3),

r_1 – distance between the point of attachment of the tether to the spacecraft and the centre of mass of the spacecraft,

r_2 – distance between the point of attachment of the tether to the stabilizer and the centre of mass of the stabilizer,

r_3 – length of the tether for the deployed tether system,

$\vec{r}_a$ – radius vector for the tether attachment points on the spacecraft,

$\vec{r}_b$ – radius vector for the tether attachment points on the stabilizer,

$\vec{r}_{ab}$ – vector representation of the tether,

R_E – radius of Earth,

$\vec{R}_i$ – aerodynamic force,

$R_{ixk},\ R_{ixk},\ R_{1yk},\ R_{2yk}$ – projections of the aerodynamic forces $\vec{R}_i$ onto the axes of the trajectory coordinate system $Ox_ky_kz_k$,

$\rho = \rho(h)$ – density of the atmosphere (as a function of altitude),

S_1 –reference area of the spacecraft (see §4.3),

S_2 – reference area of the aerodynamic stabilizer (see §4.3),

t – time,

T – tension of the tether,

$\mathrm{T_{orbit}}$ – orbit period on the initial orbit (see §6.2),

θ – path inclination

$\vec{\tau}_{C_1}(\vec{R}_1) = \Delta\vec{r}_1 \times \vec{R}_1$ – external torque from aerodynamic force $\vec{R}_1$ (see §4.3),

$\vec{\tau}_{C_2}(\vec{R}_2) = \Delta\vec{r}_2 \times \vec{R}_2$ – external torque from aerodynamic force $\vec{R}_2$ (see §4.3),

$\tau = t/\mathrm{T_{orbit}}$ – dimensionless time (see §6.2),

V – magnitude of velocity of the oncoming air flow,

V_r – velocity of the separation (see §6.2),

$\omega_1, \omega_2, \omega_3$ – natural frequencies of the system (see §5.1),

$\vec{\omega}_i$ – angular velocities for each body.

1. INTRODUCTION

1.1. Context of the research

The space tether system can be used for a wide number of applications and purposes.

The most obvious application of an aerodynamic tether system is to provide the appropriate orientation of a spacecraft during descent. This method does not require any energy expenses, works basing on aerodynamic forces and requires only the presence of the atmosphere. Therefore, the aerodynamic stabilization using the tether system can be used not only during descent to Earth, but to stabilize the motion before landing onto the surface on other planets. It is not possible to use this method to explore the closest space object – Moon – but there is a possibility to use such tether system on the orbit of, for example, Mars or Venus.

The aerodynamic tether system is applicable for returning payloads from outer space to the surface of the planet, especially using small landing modules from the space station. The payload in small modules can include, but is not limited to, the materials manufactured in the absence of gravity, the devices for service and maintenance or examples of space objects. In this case, the tether system is helpful to lower the orbit of the landing module before descent and to obtain stable motion during the second stage of descent.

Tethered aerodynamic stabilization can be used to target the detachable stages of rocket launchers after their separation from the launcher with greater accuracy towards the desired landing site area.

The problem of reducing the search area over which detachable parts of the launchers might land has a great economic and ecological significance, because without aerodynamic stabilization these areas can cover up to thousands of square kilometres. Solutions to this problem have been researched for a long time, but so far experts have not agreed on any particular stabilization method, which can be both easily implemented from the design point of view, and economically profitable.

The tether system can be used for ecological purposes by collecting space debris and burning them out in the atmosphere. For specific debris with dangerous contents it may be preferable to collect them into the landing module for descending onto the surface of the Earth and further recycling. Aerodynamic tether systems can help to solve this problem by

predictable reduction of the altitude of the orbit during deployment and reducing the landing area at the final stage.

The tether system can establish a connection between space objects like space stations. This connection can be used for transportation of payloads between spacecraft and space station without docking and berthing of spacecraft.

1.2. Summary of the novel contributions to science

This section describes the contents of the following chapters and obtained results.

Chapter 2, literature survey, refers to the investigation previously made on tether systems. Here there is a review of: major models of the tether, methods used for mathematical modelling of the tether systems, and, in short, real tether space experiments.

Chapter 3 describes the background of the stabilization of motion of the tether systems. The definition of stability of motion, which is used in the following chapters, is made here. As the following chapters address the aerodynamic stabilization which is passive stabilization of motion of a spacecraft, the terms and ideas are described there. The description of models of the atmosphere and numerical methods are also included.

Chapter 4 concentrates on the mathematical model for 3D motion of the deployed tether system in the dense layers of the atmosphere. The definitions and assumptions for the tether system itself, the forces acting on the mechanical system, and for the coordinate systems used for deriving the governing equations are described. The use of the second body as an aerodynamic stabilizer enables the stable motion of the spacecraft during descent. The mathematical model is presented here. The described mathematical model is the basis for determining the conditions of stability of motion of the system.

Chapter 5 investigates the influence of parameters of the tether system on its motion. The tether system is stable when it is able to sustain a previously defined orientation during its motion. Here, the conditions of static stability, which are necessary conditions of stability, are determined based on the undisturbed motion of the tether system. It is found, that the tether system can be in stable motion even if either or both bodies are statically unstable. The dependence of stability on the natural frequencies of the system is assessed relative to the parameters. Here, the method for choosing the parameters of the tether system is offered to obtain stable motion. These parameters are the mass, the geometrical dimensions and the

length of the tether. It is found that the deployment process during descent can add the stabilization to the motion of the tether system.

Chapter 6 describes the process of deployment of a tether system. This process is based on the aerodynamic forces. The initial condition for the deployment model is that of a spacecraft with a rigidly connected stabilizer in a circular orbit about the planet. Because of the difference in ballistic coefficient of the bodies, the tension of the tether enables the deployment of the tether system. The deployment is then controlled by the tether release mechanism on the time and tether parameters bases. The tether release mechanism unreels the tether and controls the rate at which the tether is unreeled, but is not able to pull the tether back in. Different methods of deployment and system dynamics are investigated. The model uses elastic tether, but its mass and aerodynamic force are not considered.

Chapter 7 is focused on the modelling tether system as a system with distributed parameters. The modelling is based on the model obtained in previous chapter. The tether is split into a number of parts by intermediate nodes, and the multi-point model includes the series of separations of material points, describing stabilizer and nodes on the tether, from the spacecraft. The multi-point model takes into consideration the elasticity of the tether and aerodynamic forces acting on the tether. This model allows to calculate numerically elastic deformations and curvature of the tether.

The comparison of results obtained by the two-point and multi-point models is made. The change in mass after adding each node and the influence of aerodynamic forces acting on the tether leads to differences in values of the tension force and angles describing the orientation of the bodies. Therefore, the model allows to make a more accurate estimation of specified parameters.

Chapter 8 makes the conclusions of work done in previous chapters and gives the recommendations for further work. The origins of perturbations and possible applications are also discussed there.

1.3. Assumptions

The motion of the tether system considered in the following chapters includes the deployment process of the tether system and the motion of previously, or already deployed tether system.

The major assumption made for modelling purposes, is that the aerodynamic influence caused by one body on the other or on the tether can be disregarded.

The assumed path that the tether system takes is through low density gas, for which the hypothesis of the diffuse reflection of gas molecules is applicable. This assumption means that vectors of the aerodynamic forces are co-linear with the vectors of velocities of the bodies. This assumption is valid for low atmospheric density and avoids having to do complicated CFD calculations. The typical change of Mach numbers of spacecraft during descent are described below in §4.3.

During the motion through the atmosphere, the dynamic pressure arising from the airflow creates the aerodynamic force that acts on all of the components of the tether system: the spacecraft, the stabilizer and the tether. The possibility of a wake effect is not taken into consideration in the modelling, as the aerodynamics in the model is limited to the diffuse reflection of gas molecules hypothesis. However, the aerodynamic forces acting on the bodies and on the thin tether can be comparable if the tether is long enough. The definitions for short and long tether in terms of modelling are made below in §7.2.

In the modelling of the deployed tether system, in which the motion is assumed to take place in the dense layers of the atmosphere, the gravity torque is ignored because of its small value in comparison to the aerodynamic torque. At this stage of motion, the mass of the tether is considered to be equal to zero, thus providing a geometric constraint between the spacecraft and the stabilizer. The variation in the acceleration due to gravity within the size of the system is assumed to be negligible since the tether system is comparatively small. The full list of assumptions made for motion of deployed tether system can be found in §4.3.

The deployment of tether system takes place in higher layers of atmosphere where aerodynamic torques are not significant in comparison to the gravity torques, and the gravity torque is taken into consideration. There is a simplification in the model of unreeling device. It is assumed that it works on unreeling only and cannot pull the tether back in. The multipoint model of the tether splits the tether in massless parts, but the mass of the tether is represented by a number of intermediate nodes.

2. LITERATURE SURVEY

2.1. The ideas for space tether systems

First space tether system was described by K. E. Tsiolkovsky who proposed the idea of artificial gravity on a space station in 1903 (Levin, E., 2007). The spacecraft is connected by the tether with a body with equal mass, and the tether system rotates around its centre of mass. A few years later, F. Zander (Zander F., 1977) proposed another idea of a space elevator from the surface of Moon to the direction of Earth. The length of the tether to be used in this project should be more than 60 thousand km, extending further than the Earth-Moon Lagrange point; at this point the effect of the centrifugal force becomes equal to the effect from Moon's gravity force. The loose part of the tether would be prevented from falling onto the surface of the Moon by Earth's gravity. Later, Zander found that the existing materials were not acceptable for such tether system.

These ideas were improved by Yu. Artsutanov, who showed that the space elevator can have no connection with the surface of the Earth (Artsutanov, Yu., 1969). The orbital and rotational parameters of a spacecraft and the motion of the tether system connecting two satellites can be selected to enable one satellite to hang over the surface of the Earth for a short period, to take the payload and move it into orbit. This idea was invented by H.Moravec and called a "non-synchronous orbital skyhook" (Moravec, H., 1977).

The artificial gravity arising from the rotation of the tether system, even when its value is small, simplifies the experience of living on a spacecraft by removing the problems of micro-gravity, such as motion of unrestrained objects, and problems with the transfusion of liquids such as water and fuel. The idea of application of a tether system as an electrodynamic system was proposed by M. Grossi (Grossi, M., 1973). It was suggested that an orbital conducting tether could be used as a dipole antenna. These ideas for an electrodynamic space tether system were tested during the TSS-1 (1992) and TSS-1R (1996) space experiments.

The tether systems can be used to investigate the high layers of the atmosphere by using a light probe connected to the spacecraft (Colombo, G., 1975).

The investigations of tether systems focus on two major processes – *(i)* the motion of the deployed tether system, and *(ii)* the process of deployment of a tether system.

The most comprehensive investigations of tether systems were associated with National Aeronautics and Space Administration (NASA). The results are included into the book (Cosmo, M. L., 1997), where the models of motion and deployment are described, as well as results of experiments on tether systems. The estimations of heating and deformations of the tether under the influence of gravity forces are included into this book.

Tether systems are applicable to investigations of the higher layers of the atmosphere, where the flight of traditional aircraft is not possible (Kumar, K. 2006, Alpatov, A.P., 2010), to stabilize the motion of spacecraft (Levin, E., 2007), for removing space debris (Aslanov V.S., 2014, Sabatini, M., 2016) and for deep space investigations (Mantellato, R., 2015).

The tether system with an atmospheric probe is a prospective technology for gathering important information about higher layers of the atmosphere of Earth, at altitudes about 100-150 km. The density of the atmosphere at these heights is too low for normal aircraft operations, on the other hand, traditional spacecraft would meet comparatively high aerodynamic drag. This problem can be solved by using an atmosphere probe, connected by tether to a spacecraft operating at altitude about 200 km (Levin, E, 1993, Johnson, L., 1999).

E. Levin also investigated electromagnetic space tether systems. He found that direct current can lead to motion instability in the tether system, and that, by changing the amperage in the tether, it is possible to stabilize the motion of the tether system.

The tether system can provide deceleration of the spacecraft before landing, but it is necessary to mention that in this case the tether tension force is significantly higher than for upper atmospheric use (Puig-Suari, J., 1991).

It is necessary to mention that all tether systems, and especially tether systems with long tethers, are vulnerable for micrometeorite attacks and space debris impact. For example, the tether in the real space tether system SEDS-2 was cut a few days after the deployment (Cosmo, M. L., 1997).

2.2. Mathematical models of motion

The motion of the space tether system is a motion of a system with distributed parameters. The placement of each rigid body can be defined by the position of the centre of mass of the body and the orientation of the body in space. The orientation of the body is described by its rotation around its centre of mass, and, as Euler’s rotation theorem states,

an arbitrary rotation can be described by three angles. Therefore, the rigid body in space is described by six parameters.

The tether system is a complex non-linear dynamical system where parameters are distributed. In general, the tether is a flexible mechanical connection which has a distributed mass along its length. Within the tether, there are complex longitudinal, bending and torsion oscillations.

It is possible to name the following types of model for tethers.

1. The *model of the rigid rod*. This model is a simple model of the tether that ignores its extensibility and flexibility. In other words, the tether has infinite rigidity. This model was used for an estimation of the possibility to use tether system for atmosphere investigations (Pradeep, S., 2003).

2. The *model of the elastic rod*. Like the previous model, the tether is a straight rod, but it can be stretched axially. This model ignores the flexibility of the tether, but the extensibility is taken into consideration (Jin, D., 2006, Williams, P, 2006).

3. The *billiard model* takes into consideration both the axial stretch ability and bending flexibility of the tether. The tether in this model is a weightless flexible spring. The model allows the bending oscillations to be described, and enables limitations on transversal displacements of the tether to be made (Beletsky, 1996). This model is inappropriate for describing the dynamics of parts of the tether. This model makes it possible to research the motion of the tether system in the gravity field of the planet.

4. The *model of rigid rods with swivel joints* was used (Williams, P. 2008, Williams, P. 2010) to find the parameters of optimal deployment of the tether. This model has zero torsional stiffness and does not take into consideration the longitudinal oscillations and encounters difficulties in describing the sag of the tether.

5. The *beads model* describes the tether by a number of material points, also called nodes, with masses. The nodes have masses and are connected to neighbouring nodes by weightless springs. A number of points is defined during the mathematical modelling. The more intermediate points included into the mathematical model, the more accurate is the model; however, increase in the number of nodes leads to increase in the number of degrees of freedom thus greatly increasing the number of equations and time required for calculations. Therefore, this model is commonly used to validate other models (Zhong, R. 2011, Zabolotnov, 2015, Dong, 2017).

Mathematical models of the tether system can be obtained using different but equivalent methods, including the Lagrange Equations, Newton's Laws (Mankala, K.K., 2008) and Kane's method originally called Lagrange's form of the D'Alembert principle (Kane, T.R., 1980).

The Lagrange Equations are widely used to build the mathematical model of motion of the tether systems and other mechanical systems. Newton's Laws have the most simple implementation and are useful for a mathematical model with distributed parameters. Kane's method does not use functions of energy thus allowing the mathematical model to be built without differentials.

The implementations of space tether systems require a method for the control of the deployment process. Tether systems with non-electrical tethers use rocket engines for centre of mass motion correction, and special devices to control the unreeling of the tether (Wen, H., 2008). The control of the unreeling can be with or without feedback.

It is necessary to discuss the validation of the various mathematical models. The complexity of the dynamics of a tether system means that the mathematical model can be fully validated only by orbital experiment, because the results of experiments on the deployment and the subsequent motion of the deployed tether system cannot give accurate results while under the influence of gravity that they would experience if they were to take place on the surface of the Earth or in the lower layers of the atmosphere. Therefore, the results of the mathematical modelling should be compared with previously obtained research results and should be demonstrated not to contradict known results from experiments.

The aim of the real space experiments described below in section §2.4 was to validate mathematical models of deployment and the subsequent motion of a space tether system in space and in the higher layers of the atmosphere (Cosmo, M. L., 1997). The major difficulty in space tether experiment lies in the deployment process because of the risk of breakage of the long tether or jamming in the unreeling device. These accidents were the cause of previous of the TSS-1 and TSS-2 (NASA Science, 2016) tether space experiment failures.

There are investigations in related scientific areas that can be of interest for the modelling of the tether. For example, the dynamics of the tether are similar to the dynamics of a three-dimensional elastic string pendulum attached to a rigid body (Lee, T., 2010) or the dynamics of extensible cables (Tjavaras, 1996).

2.3. Tethers

The tether is a component that joins two space objects to make the tether system. The properties of the tether have high significance for the deployment and operation of the tether system. The tether, on the one hand, should have a high tensile strength and, on the other hand, low density to have minimal mass.

Zander's idea for a space elevator met the difficulties with suitable materials for the tether. The best steels existing during the beginning of 20^{th} century were too heavy to make such a tether system possible.

The simplest synthetic material for the tether is nylon – a polyamide material which is inexpensive, but its properties are not as good as those of the newer fibre called Dyneema®.

The Dyneema® fibre is a lightweight and stronger material made from high performance poly ethylene (HPPE).

Kevlar®, and analogues such as Technora®, Nomex® and others, are aramid fibres. The most significant difference between these materials and Dyneema® is that they have a high melting temperature. This property can be of great value during the descent through the denser layers of the atmosphere.

Carbon nanotubes, or CNTs, are allotropes of carbon with a cylindrical nanostructure. Carbon nanotubes may by formed by rolling up a single or multiple sheets of graphene. These nanotubes are very lightweight but their tensile strength greatly exceeds other materials. For example, the carbon nanotube has at least 100 times the specific strength of steel and 30 times that of Kevlar®.

The more general utilization of carbon nanotubes is limited by the current level of manufacturing technology. When there are only a few topological defects in the carbon nanotube, its mechanical performance decreases greatly (Zhu, Wang and Ding, 2016).

The tether, during its motion through the magnetic field of the planet, could be used to generate electrical power needed for the spacecraft. This opportunity could be very important for orbital space stations connected by the tether, but for tether systems used for stabilization prior and during the descent, the amount of electrical current going through the tether could change the parameters of motion of the tether system. Such tether systems would require of the tether to be made of conducting material.

2.4. Tether space experiments

For testing the tether systems on Earth before implementation in space, different experiments may take place on Earth using special devices for modelling space conditions.

As a result of such investigations, a number of real tether space experiments took place. The list of these experiments is shown in Table 1.1. It is necessary to pay attention to some of them.

In the controlled deployment of space tether systems it is assumed that the tether length is regulated (Alpatov, A.P., 2010). There are programs set to ensure a constant rate of change of the tether length, or to provide a rate of change of tether length based on the length of an already deployed tether.

The deployment of the tether system with control, based on the rate of change of the length of the tether, was implemented in joint NASA and Italian Space Agency experiments on Space Shuttles Atlantis (TSS-1, 1992) and Columbia (TSS-1R, 1996) with proposed length of the tether equal to 20 km (NASA Science, 2016). This experiment was to verify the concept of tether gravity stabilization, and to investigate physics and electrodynamics. The separating spacecraft had engines to accelerate a satellite at the beginning of separation. During the first experiment, the tether was deployed to a length of 256 meters before getting stuck. During the second experiment, the tether almost reached its full length, but then broke.

All methods of space tether system deployment for which the tether length is regulated have a common disadvantage; the inability to avoid the longitudinal oscillations of the tether system caused by the elasticity of the tether. Should the intensity of the longitudinal oscillations increase sharply, the tether may sag and snatch, thus causing the deceleration device to fail in operation. It is likely that this disadvantage was the underlying reason for the failure of those two experiments.

In 1992 and 1994 NASA performed tether experiments SEDS-1 and SEDS-2 (Small Expendable Deployer System Experiments). These experiments (Carroll, J., 1995) used a 20 km tether and showed the possibility to use a tether system for placement of a re-entry capsule into the re-entry orbit. The experiment used the deployment control model based on the tension of the tether. This method allows damping of the longitudinal oscillations during the deployment.

Table 2.1 – Tether systems in space

Tether system	Country	Year
Gemini-11/12	USA	1966
TPE-1	USA /Japan	1980
TPE-2	USA /Japan	1981
Charge-1	USA / Japan	1983
Charge-2	USA / Japan	1984
Charge-2B	USA / Japan	1992
Oedipus-A/C	Canada / USA	1989/1995
TSS-1	USA / Italy	1992
PMG	USA	1993
SEDS-1	USA	1993
SEDS-2	USA	1994
TSS-1R	USA / Italy	1996
TiPS	USA	1996
YES	European project	1997
ATEx	USA	1998
MAST	USA	2007
YES2	Europe	2007
T-REX	USA / Japan	2010

The Young Engineers' Satellite 2 (YES2) tether system was implemented is 2007 to collect experiment data on the Space Mail concept (Kruijff, M., 2008). This concept uses a tether system to return small payloads from space to Earth. The final length of the tether reached 30 km and the deployment was successful, but the landing capsule was not found after descent to the surface of the Earth. At the present time, this project holds the record for the longest tether implemented in space.

3. BACKGROUND

3.1. Methods of stabilization of spacecraft motion

The orientation, or attitude, is the part of the description of the placement that the rigid body occupies in space. The other component of placement is its linear position. The attitude is defined by the angles between the longitudinal axis of the spacecraft and some reference line or plane (Space Primer, 2009) such as the vector of velocity of the air flow. In this context, "stabilization" means the process of maintaining attitude during motion or tending to restore the original attitude after receiving a displacement or perturbation. For a spacecraft, attitude control is the process of achieving and maintaining a desired orientation in space by a corrective action.

The attitude control can be active or passive. Active control methods use hardware and algorithms of making decisions to ensure the motion remains stable. These methods use thrusters, electromagnets, and reaction wheels (Space Primer, 2009). Active methods have significant energy expenses.

Methods of passive stabilization enable the maintenance of the attitude by making use of torques from the environment. Methods of passive stabilization use gravity forces, solar sails or, for lower orbit, where the density of the atmosphere is high enough, aerodynamic forces.

The choice of the method of control is highly dependent on the mission of the spacecraft.

3.2. Passive stabilization

Methods of passive spacecraft motion stabilization are widely used for control of spacecraft motion. If design properties are chosen properly, these methods are considerably more effective and easier than methods of active stabilization that invariably require energy expenditure. Methods of passive stabilization are based on different physical principles. Depending on the nature of the harnessed environmental force to be applied – gravitational, aerodynamic or magnetic – the appropriate method of stabilization of the spacecraft motion can be distinguished.

In the physical sense, any type of passive spacecraft motion stabilization involves the generation of a stabilizing torque. This torque provides steady oscillations with respect to the appropriate direction. Depending on the type of stabilization, this direction can be:

- Local vertical, for gravitational stabilization;
- The direction of the magnetic field, for magnetic stabilization;
- The direction of the velocity relative to the air flow, for aerodynamic stabilization.

The stabilizing torque is provided by the appropriate choice of parameters for the mechanical system. For example, during gravitational stabilization, the axis of to the spacecraft's minimal rotational inertia makes a periodic motion relative to the local vertical axis. The magnetic stabilization uses the axis through the poles of a magnet placed on a spacecraft. The aerodynamic stabilization axis goes through centre of mass of the spacecraft and through its centre of pressure.

When passive stabilization is used, it is possible to include dissipative torques to obtain asymptotic stability of equilibrium of the system.

The application of tethered space systems opens up new opportunities for the use of any type of passive spacecraft stabilization, but for the tether system, as a mechanical system with distributed parameters, the problem is to know how to choose design parameters to obtain stable motion since these systems cannot be regarded as rigid bodies.

3.3. Aerodynamic stabilization

The aerodynamic motion stabilization method is the main method for providing steady motion for uncontrolled spacecraft, including landing modules and capsules, through the dense layers of the atmosphere, when returning payloads from space to the surface of the Earth or other planets.

The stability condition for the spacecraft moving through the atmosphere is rather simple: the centre of mass of the spacecraft should be located between the front part of the spacecraft (with thermal protection) and the centre of the aerodynamic forces, or aerodynamic centre. When using a tethered space system with an aerodynamic stabilizer, the analysis of the motion and the choice of parameters becomes complex because the relative position of the bodies changes within the system. At the same time, the position of the centre of mass of bodies relative to the centre of mass of the system changes continuously.

The idea of using a tethered system to enable the aerodynamic stabilization of spacecraft motion was proposed by K.K. Alekseev (1974). In order to enhance the stabilizing action of the aerodynamic moment it was proposed to use stabilizers attached by tethers. Various design-layout schemes for tethered aerodynamic stabilization systems for spacecraft motion are reported. Figures 3.1 and 3.2 illustrate spherical and planar shaped stabilizers, for use at different altitudes, as suggested by Alekseev.

Stabilizers should have a foldable or inflatable construction in order to be stored conveniently within the limited space within the spacecraft, and to enable an easy deployment of the stabilizer into orbit (Wilson A., 1981, Babuscia, A., 2014).

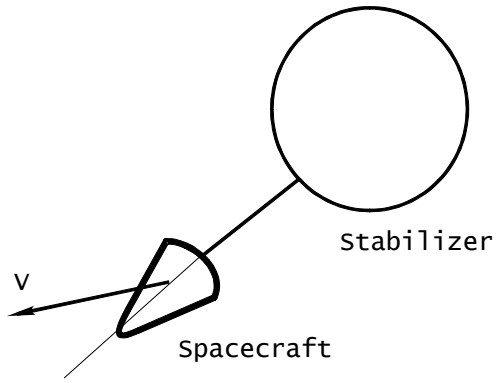

Figure 3.1 – Spacecraft with a spherical stabilizer

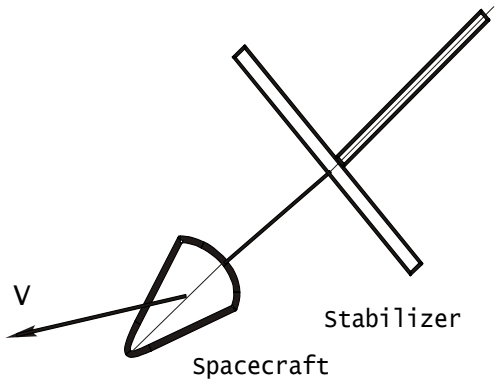

Figure 3.2 – Spacecraft with a planar stabilizer

The aerodynamic stabilization can be used to stabilize the motion of rocket launchers. Some theoretical and experimental studies of aerodynamic stabilization for the example of stages from the Proton and Rus launchers was carried out by Central Research Institute of Mechanical Engineering (TSNIImash, 2017). It was noted that if the stabilizers were not used during the active part of the flight, then including the stabilizers for stages as a part of

design of the launcher would increase the mass of the rocket and thus reduce its effectiveness (Daydkin, A.A. 2002). In answer to this criticism, it is proposed to re-use elements from the rocket/stage construction to act as stabilizers.

The effectiveness of the aerodynamic stabilization method for the first stage of the Proton launcher and second stage of the Rus launcher was investigated experimentally on scaled models. The models used parts from the fuel tanks as stabilizers. Models were made at two scales: the large model 1:25 and the small model 1:50, because the drop altitude for the large model was insufficient for the steady flight mode to be reached. Drop tests of models at subsonic flight speeds were conducted from the altitude of 20 m. The length of the tether varied from 0.6 to 8.6 of the diameter of the models. According to the experimental results, by connecting a fuel tank with a tether to a stage enables a significant improvement in the stability of the fall to Earth of that stage.

According to preliminary estimates and the results of test models during free flight at subsonic speeds, these stabilizing devices reduce the amplitudes of oscillations within the system, thus allowing to reduce the possible landing area by up to 10 times.

It is necessary to note that comprehensive analysis of motion of tether systems in the atmosphere, taking into account shape, mass and inertial properties of the spacecraft and the stabilizer, had not been carried out before.

A similar problem of stabilizing the motion of an uncontrolled body in the atmosphere arose when considering the delivery of a small payload from a near-Earth orbit by means of a descent capsule (project YES2 – “Space Mail”). YES2 is the second project in the Young Engineers Satellite programme. The goal of the project was to test and produce data on the Space Mail concept, where a tether system is used instead of conventional chemical propulsion, to return material from space to Earth (Kruijff, M., 2008).

This project was implemented in an experiment in September 2007 by the use of the Foton spacecraft. Initially, the capsule with payload was located on the spacecraft moving in a low orbit of the Earth at an altitude about 300 km. The tethered capsule system was deployed to an altitude of about 270 km. The full length of the tether in this experiment was 30 km (Kruijff, M., 2011).

After that, the tether was cut from both sides and the capsule moved freely through the high layers of the atmosphere and entered the dense layers (altitude about 100 km) for landing in the predetermined area. Initially, the capsule was designed to be conical with a spherical apex with a cone angle equal to 90 degrees. A large cone angle means a large

midsection area of the capsule, thus providing sufficiently low landing velocity (about 25 m/s) to make a parachute system unnecessary for the Space Mail application.

Computational studies of the dynamics of such a capsule showed that the large cone angle conical capsule has a dynamic instability of motion. The amplitudes of the oscillations of the capsule begin to increase and the angle of attack of the capsule reaches unacceptable values of about 90° (Zabolotnov, Y.M., 2003). Therefore, as an alternative descent scheme, tethered aerodynamic stabilization was employed. This method of stabilization makes it possible to provide dynamic stability of the motion of the large cone angle capsule throughout the complete descent.

3.4. Models of the atmosphere

The atmosphere is the environment through which the spacecraft moves during its descent. The motion of the spacecraft in the atmosphere depends on the properties of the atmosphere, because the atmosphere is the source of the aerodynamic forces and damping, and which leads to heating of the spacecraft. The most important parameters of the atmosphere include its density, temperature, pressure and winds. The listed parameters depend on the altitude, latitude, season, time of the day, activity of Sun and other factors.

For modelling purposes, a model of the atmosphere requires atmosphere parameters at the given position. Usually such a model of the atmosphere comprises a conditional distribution of density, pressure and temperature of the air, expressed as a function of altitude above mean sea level. Such a model of the atmosphere is based on average values. The deviations of parameters from the standard values, and the phenomenon of wind, are atmospheric disturbances that would also have influence on the motion of the body.

“Wind” is any motion of the air relative to the surface of Earth, arising as a result of differences in air pressure in different parts of the atmosphere. Wind is a chaotic phenomenon, but in some cases winds have a large scale structure where the average properties like the velocity of air flow remain almost the same on a length scale of tens to hundreds of kilometres. The “monsoon” is an example of such wind.

Such global motions are accompanied by local motions of air flow called “turbulence” which are chaotic states of the airflow.

Here, it is necessary to mention that the motion of a spacecraft takes place through different layers of the atmosphere, and the velocity of the spacecraft decreases as the altitude reduces as a result of the influence of the aerodynamic forces.

The most commonly used model of the atmosphere is the International Standard Atmosphere published by the International Organization for Standardization as an international standard ISO 2533:1975. This standard consists of the values of parameters of the atmosphere at various altitudes as a table of values. The intermediate values can be obtained by interpolation. The International Standard Atmosphere does not provide any meteorological information with current conditions of the atmosphere. It models a standard day without difference in time of the day or season. The International Standard Atmosphere was extended to the altitude of 80 km by The International Civil Aviation Organization Standard Atmosphere in 1993. This model of the atmosphere provides accurate parameters of the atmosphere for the altitudes up to 80 km above mean sea level.

The U.S. Standard Atmosphere (U.S. Standard Atmosphere, 1976) gives values for density, pressure and temperature of the atmosphere for a wider range of altitudes. This model of the atmosphere coincides with the International Standard Atmosphere for altitudes from 0 to 32 km.

U.S. Air Force Space Command and Space Environment Technologies provides a model of the atmosphere named JB2008. This model gives values of parameters of the atmosphere from 120 to 2000 km and takes into account solar irradiances and time evolution of geomagnetic storms. This standard is widely recommended for mass density where drag is a significant factor.

The atmospheric models listed above are based on tabylated values. Their disadvantage is the complexity of calculating the parameters of the atmosphere at a given altitude. Therefore, for preparatory numerical modelling, simpler and faster models of the atmosphere are used for the calculations in the following chapters of this thesis.

The exponential model of the atmosphere provides a method to find the density of the atmosphere at given altitude based on a simple dependence

$$\rho(h) = \rho_0 e^{-\lambda h}$$

where $\rho_0 =$ is the density of the atmosphere at mean sea level, $\lambda \approx 1/7000$ 1/m is the logarithmic density coefficient and is constant.

For altitudes over 140 km the density of the atmosphere can be approximated more accurately by the equation

$$\rho(h) = e^{-(a_0+a_1h+a_2h^2+a_3h^3+a_4h^4+a_5h^5)}$$

where a_k , $k = 0..5$ are constants. Figure 3.3 shows the change in density of the atmosphere with respect to the altitude according to this model.

It is necessary to mention that these two last models of the atmosphere are used for computational time saving purposes, they are not part of the mathematical model and can be replaced by more accurate models of the atmosphere if needed.

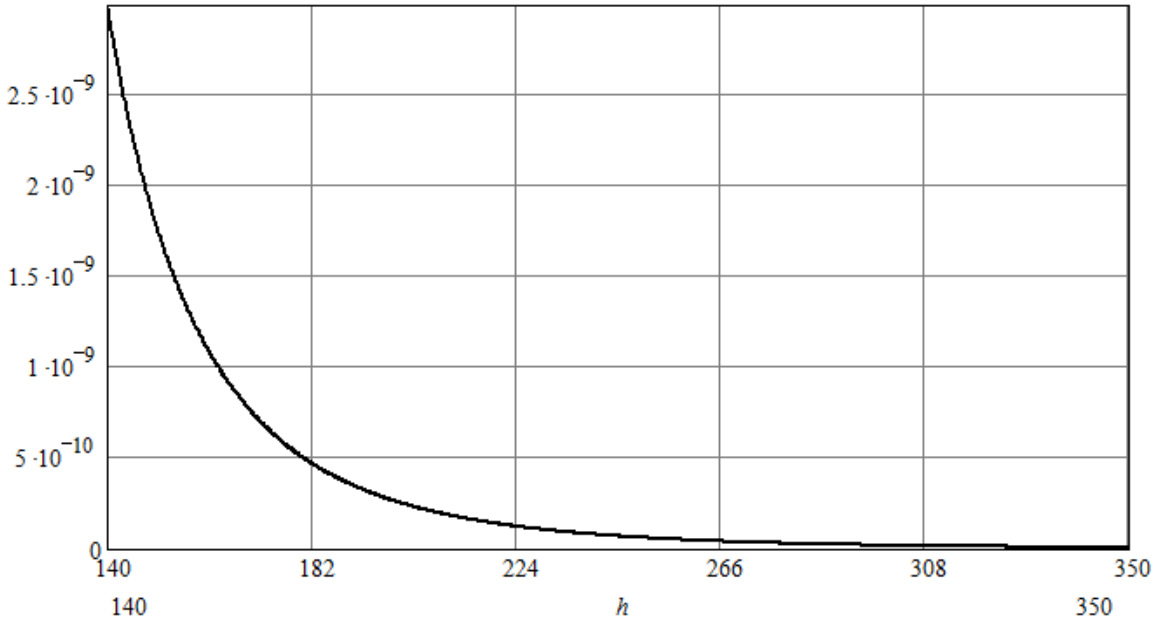

Figure 3.3 – Density of the atmosphere

For the mathematical models in the following chapters, the major parameter of the atmosphere is its density. The density of the atmosphere and the velocity of the spacecraft define the dynamic pressure of the airflow, which has high importance in calculating the aerodynamic forces. Even at high altitudes, when the density of the atmosphere is comparatively low, the velocity of entry of a spacecraft into the atmosphere is about 7800 km/s, and any change in density leads to a corresponding change in the aerodynamic force acting on a body.

3.5. Numerical methods used for modelling

As will be demonstrated in the following chapters, the motion of the tether system is described by a system of ordinary differential equations, including dynamic and kinematic equations, and the equations for the centre of mass of the system.

These ordinary differential equations are written in matrix form, and it is necessary to solve for the variables. At this stage, the systems of dynamic equations can be treated as a system of linear equations with respect to the differentials. The most widely used method is Gauss–Jordan elimination which inverts the matrix by using of three types of elementary row operations to reduce the matrix to row echelon form, thus expressing the variables in the system of equations. The calculations can be made either analytically and numerically. The numerical calculations mean that prior to matrix inversion the matrix coefficients are calculated numerically.

Because of the complexity of the dynamic equations, it is not possible to find the solutions of the system of equations analytically using symbolic computation; however, it is possible to find a numerical approximation of the solution.

The calculations will show how the parameters of the system vary during the descent for a given set of initial conditions, meaning that it is necessary to solve the initial value problem also known as Cauchy problem (Hirsch, M., 1974).

Methods that can be used for solving such initial value problems are divided into two main groups: linear single-step methods and multistep methods. Single-step methods use only one previous point to determine the current value, while multistep methods make use of results from previous steps to obtain high numerical efficiency. Runge-Kutta methods are multistep methods that use intermediate steps instead of keeping results of previous steps.

The most widely used Runge-Kutta method is the explicit fourth-order Runge-Kutta method with the total accumulated error of the order of $O(h^4)$, where $h > 0$ is the step size.

Classical Runge-Kutta methods use a constant step size, but for "stiff equations", meaning the equations where the frequencies of variables are high, it is necessary to use a small step size. The small and constant step size with many additional calculations is very time and memory consuming, so the fourth order Runge-Kutta method with variable step size is used in following chapters to calculate the motion of the tether system during descent and deployment.

4. MODELLING THE MOTION OF THE SYSTEM IN THE ATMOSPHERE

Modelling of the motion of the tether system requires definitions for the tether system itself, for the forces acting on the mechanical system, and for the coordinate systems used for deriving the governing equations. For the purposes of this chapter, the motion is assumed to take place in dense layers of the atmosphere. The tether system considered here is a system of two rigid bodies connected by a massless and relatively short tether. The use of the second body as an aerodynamic stabilizer is made possible by the difference in dimensions and masses between the two bodies. This enables the stable motion of the spacecraft (the first body) during descent. The modelling uses some assumptions, those are described in this chapter.

The derivation of the mathematical model for spatial motion is presented here. The conditions of undisturbed motion are described at the end of the chapter. The undisturbed motion provides the basis for determining the conditions of stability of motion of the system that will be examined in Chapter 5. The validation of mathematical model is made numerically using the integrals of undisturbed motion of the tether system.

4.1. Forces acting on the system

Let us consider the derivation of the dynamic equations of motion of two rigid bodies, connected by a tether, governing their spinning motion in the atmosphere. Every rigid body in the atmosphere is affected by aerodynamic force $\vec{R}$ and gravity force $\vec{G}$. Usually, when obtaining the equations for the rotating motion of rigid bodies in the atmosphere, the gravity torque is ignored because of its small value in comparison to the aerodynamic torque $\vec{\tau}$ (Zabolotnov Yu.M, 2012). The resultant of the aerodynamic forces of each body acts at pressure centres, the positions of which are determined by the given aerodynamic characteristics of the spacecraft and the aerodynamic stabilizer. In addition to aerodynamic and gravity forces, each body is also affected by the tether tension force $\vec{T}$. When deriving the equations of the mechanical system motion let us consider that the tether has zero mass, treating it as a geometric constraint between the bodies of the system. Hereinafter, indices 1 and 2 are used for the spacecraft and stabilizer respectively.

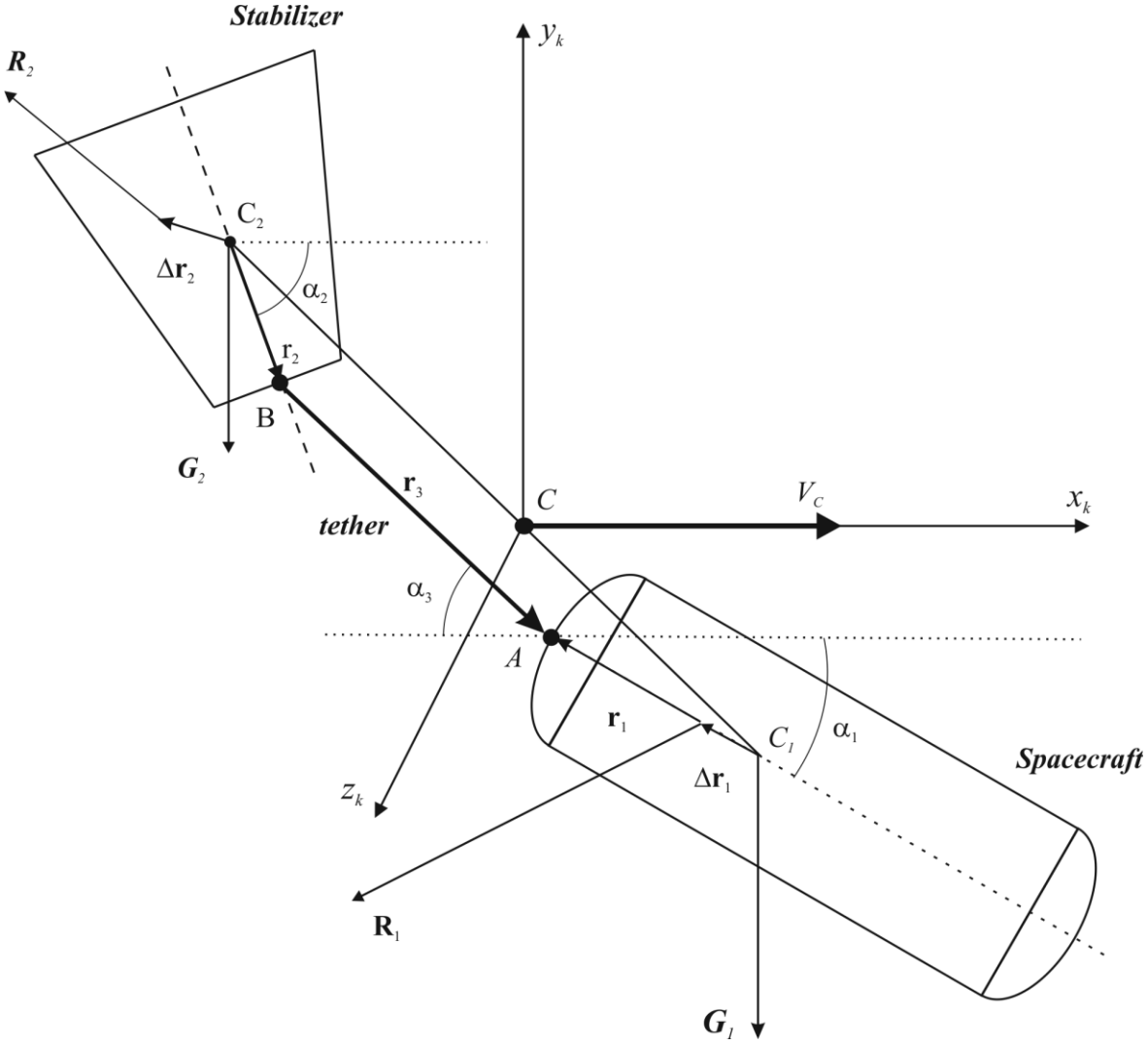

Figure 4.1 – Forces acting on the mechanical system

Figures 4.1-4.3 depict forces, acting on the whole mechanical system, spacecraft and aerodynamic stabilizer.

It is possible to make an assessment to show how the acceleration due to Earth gravity changes within the system. The formula for the acceleration due to gravity at any given altitude h is

$$g(h) = \frac{GM}{(R_E + h)^2}, \tag{4.1}$$

where G is the gravitational constant, $G = 6.674 \times 10^{-11}$ m^3/(s^2·kg), $M = 5.972 \cdot 10^{24}$ kg is the mass of Earth, $R_E = 6.357 \cdot 10^6$ m – radius of Earth.

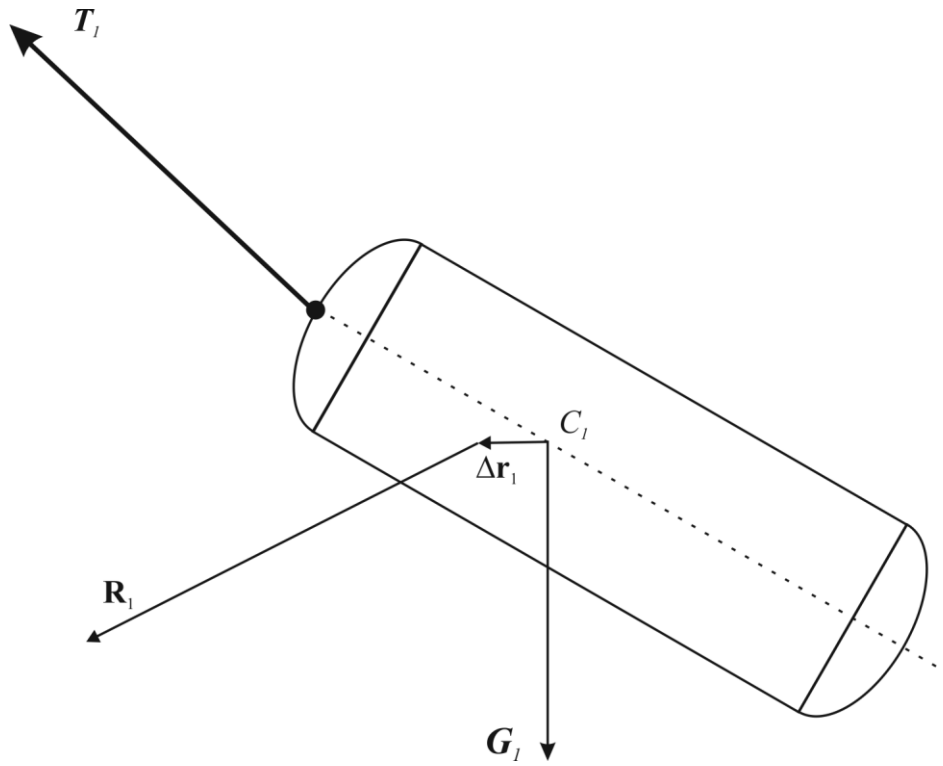

Figure 4.2 – Forces acting on the spacecraft

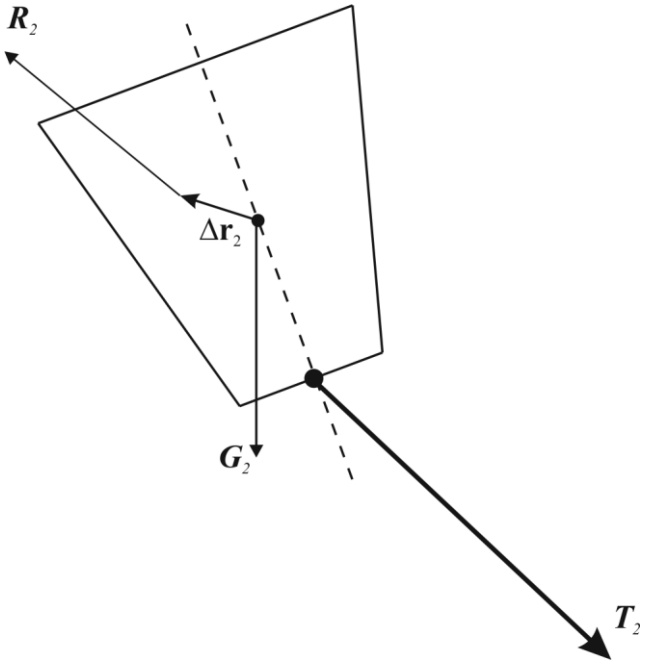

Figure 4.3 – Forces acting on the aerodynamic stabilizer

According to this formula, the maximum difference in acceleration due to gravity between the spacecraft and the stabilizer occurs when the system is oriented vertically and the difference in height is equal to difference in tether length. It is obvious that

$$\Delta g = \frac{g\left(h - \frac{d}{2}\right) - g\left(h + \frac{d}{2}\right)}{g\left(h - \frac{d}{2}\right)},$$

where d is the size of the system defined by the length between centres of mass of spacecraft and stabilizer.

Figure 4.4 shows the results of assessment made for short tether systems with sizes of 0.1, 0.2, 0.5 and 1.0 km. The relative change of the acceleration due to gravity depends mostly on the dimension of the system. For a system with a short tether of less than 100 metres, the value for $g(h)$ varies by less than 4×10^{-3} of one percent within the dimension of the system, at any atmospheric altitude. On this basis, it is reasonable to ignore gravitational force variation within the tether system.

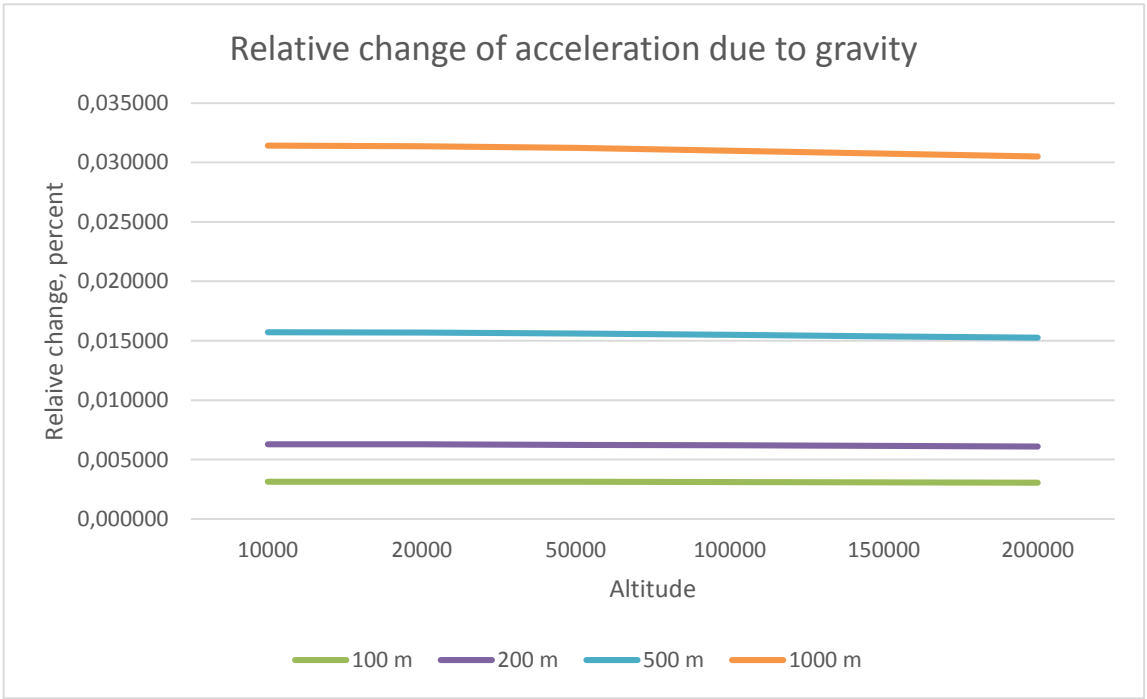

Figure 4.4 – Relative change of acceleration due to gravity

4.2. Coordinate systems

For derivation of equations for each body let us use the following coordinate systems (Figure 4.5).

The bound coordinate system $Oxyz$. This coordinate system is based on the body and rotates with the body. The origin of the coordinate system, *O,* is in line with the centre of mass of each body, the *Ox* axis – longitudinal body axis, is ideally coincident with its line of symmetry, the *Oy* and *Oz* axes generate a right-handed coordinate system along with *Ox* axis.

The Ox axis defines the reference line of the body, and the angle between the Ox axis and the direction of the oncoming air flow is the angle of attack, α.

The $Oxy_\alpha z_\alpha$ ***coordinate system is related to the angle of attack*** $\boldsymbol{\alpha}$. Here the *Ox* axis is coincident with the axis of the $Oxyz$ coordinate system, the Oy_α axis is situated in the plane of the angle of attack α, and the Oz_α axis completes the right-handed coordinate system.

The $Ox_K y_K z_K$ ***trajectory coordinate system***: The Ox_K axis is directed to the $\vec{V}$ velocity vector of the body, the Oy_K axis is directed upwards perpendicular to the vertical plane of flight, defined by $\vec{V} \times \vec{G}$, the Oz_K axis completes the right-handed coordinate system.

These coordinate systems are related to each other by a series of rotational transformations. The angles of rotation of these coordinate systems are shown in Figure 4.5, where α –angle of attack, φ – aerodynamic banking angle (roll), γ – banking angle of the plane of the angle of attack relative to vertical plane (yaw).

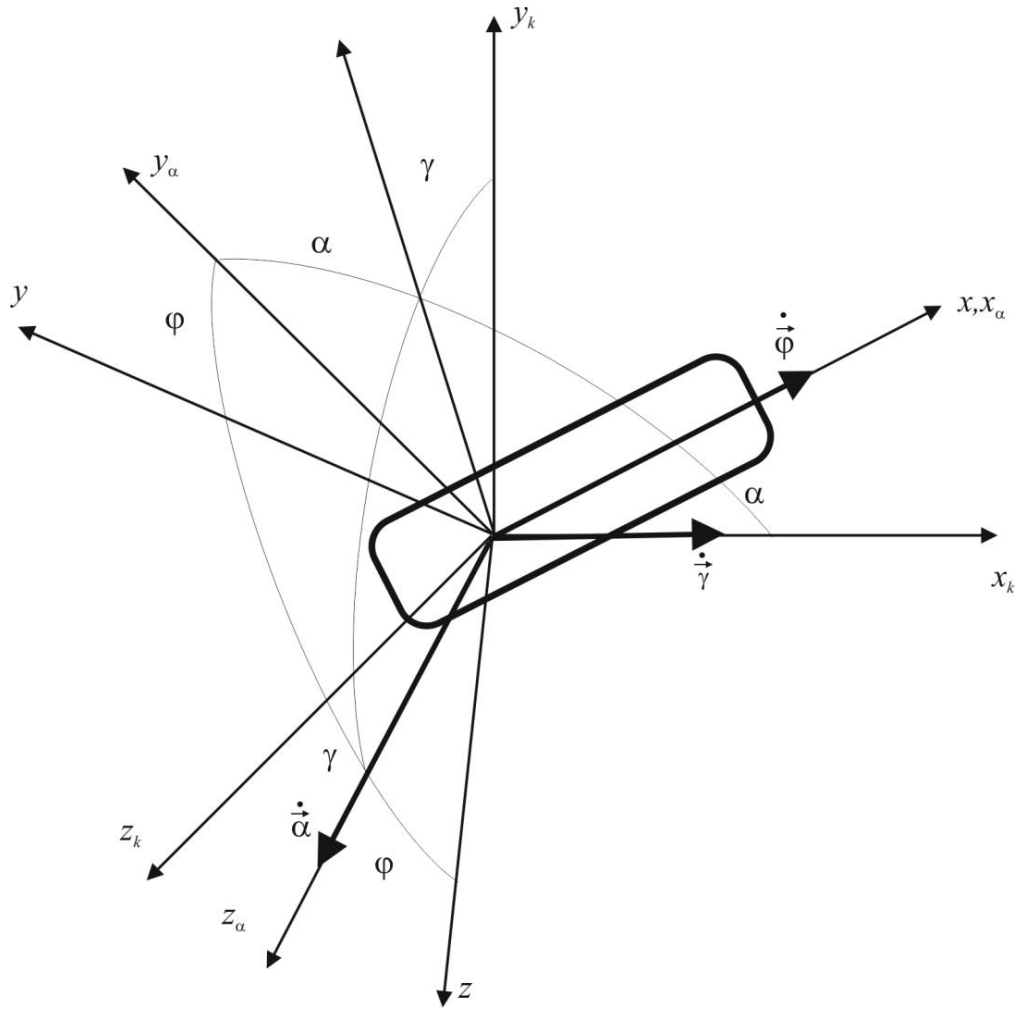

Figure 4.5 – Coordinate systems

4.3. Equation of motion

Let us consider the body moving in the incompressible inviscid flow of the air. As it follows from Bernoulli's equation (Clansy, 1975, pp.19-21), the pressure and velocity of the flow along the streamline and throughout the whole field of flow are related by the equation

$$p + \frac{\rho V^2}{2} = constant = p_0,$$

where p is the static pressure or the air flow, $\rho V^2/2$ is the dynamic component usually called dynamic pressure, and p_0 is the total (or stagnation) pressure. The static pressure of the air flow here can also be treated as the static pressure of the atmosphere at given altitude.

The aerodynamic force acting on a body that is a solid of rotation is usually written in terms of projections onto the axis of $Oxy_\alpha z_\alpha$ coordinate system.

$$R_x = c_x qS, R_y = c_{y_\alpha} qS, R_z = c_{z_\alpha} qS,$$

where $q = \rho V^2/2$ – dynamic pressure of the air flow, S – body reference area usually defined as cross-sectional area at the maximum diameter (midsection), $\rho = \rho(h)$ – density of the atmosphere (as a function of altitude), V – magnitude of oncoming air flow velocity (assuming that the flow can be considered to be unidirectional over the complete spacecraft and stabilizer system), c_x, c_{y_α}, c_{z_α} – are non-dimensional aerodynamic force coefficients (Clansy, 1975, pp. 58-62) on corresponding axis of $Oxy_\alpha z_\alpha$ coordinate system.

The total drag is the sum of the profile drag and the induced drag. The profile drag is the sum of the surface, or skin, friction drag and the form drag. As the aerodynamic forces are defined through the body reference area, they are dependent on the form and the square of the surface of the body. In other words, the body reference area defines the value of the aerodynamic force, and it is dependent on the shape of the body and on the square of its surface. Then the calculations are made for the spherical body, the body reference area is the cross-sectional area. For more complex shapes of the aircraft the value of the body reference area becomes dependent on other parameters because of the surface drag. For example, for the long cylinder then body moves in the direction of its longitudinal axis, the body reference area is usually calculated as equal to the diameter multiplied by the length of the cylinder, and for a complex shape it is the full area of the surface divided by four.

The magnitude of approaching air flow velocity V in fluid dynamics is usually represented by Mach number $M = V/c$, where c is the speed of sound in the surrounding medium. By definition, at $M = 2$ the velocity of the body is two times higher than the speed of the sound in the airflow. The Mach number depends on the conditions of the medium such as temperature and density. The Mach number determines if the flow can be treated as an incompressible flow. In an incompressible flow, the speed of sound approaches infinity, and Mach number approaches zero. The value of Mach number defines the regime of motion on the airflow:

- $M < 0.8$ is the subsonic regime,
- M between 0.8 and 1.3 is the transonic regime,
- M between 1.3 and 5 is the supersonic regime and
- $M > 5$ is the hypersonic regime.

As the speed of sound is dependent on density, temperature and other parameters of the surrounding medium, the Mach number is also dependent on them. The International Standard Atmosphere gives the value of speed of sound at altitude 80 km equal to 281 m/s.

The velocity of spacecraft during descent at given altitude is nearly 7000 m/s, and the Mach number for the spacecraft at the beginning of the descent is about 24. During the descent, the spacecraft is slowed by the influence of aerodynamic forces, and Mach number decreases. Figure 4.6 shows how the Mach number changes during the descent of a spacecraft through the atmosphere of Earth from an altitude of 80 km.

In the terms given above, tether system (or descending spacecraft) begins its motion in the atmosphere in the hypersonic regime which lasts down to an altitude of about 52 km, where it then moves in the supersonic regime, and upon reaching approximately 41 km in altitude, it continues its motion in the transonic regime. The duration of the transonic regime is comparatively short, and then, from an altitude of nearly 35 km, the motion of a tether system is subsonic until the end of its mission. In time terms, the supersonic regime lasts about 230 seconds from the beginning of the descent from Earth orbit, supersonic regime takes nearly 40 seconds, and transonic regime lasts about 20 seconds.

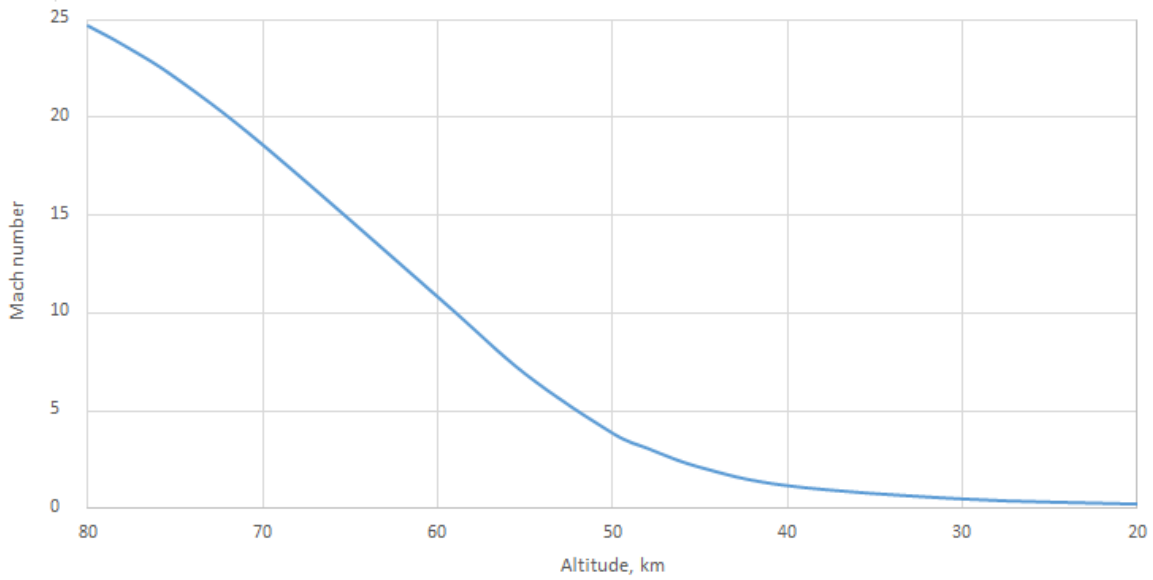

Figure 4.6 – Change of Mach number during descent

Because the body is symmetrical, the resultant of the aerodynamic forces acts in the plane of the solid angle of attack, so $c_{z_\alpha} = 0$.

The static aerodynamic moment of resultant aerodynamic forces around the centre of mass is calculated by

$$\vec{\tau}_C(\vec{R}) = \overrightarrow{\Delta r} \times \vec{R},$$

where $\overrightarrow{\Delta r}$ – radius-vector of centre-of-pressure position relative to the centre of mass for each body.

Newton's second law states (Halliday, 2011) that the net external torque acting on a system of particles is equal to the time rate of change of the total angular momentum of the system. Thus the dynamic equations of motion of each body are

$$\begin{aligned} \frac{d\vec{l}_1}{dt} &= \vec{\tau}_{C_1}(\vec{R}_1) + \vec{\tau}_{C_1}(\vec{T}_1), \\ \frac{d\vec{l}_2}{dt} &= \vec{\tau}_{C_2}(\vec{R}_2) + \vec{\tau}_{C_2}(\vec{T}_2), \end{aligned} \tag{4.2}$$

where $\vec{l}_1$ and $\vec{l}_2$ are the net total angular momenta for spacecraft and stabilizer, $\vec{\tau}_{C_1}(\vec{R}_1) = \Delta\vec{r}_1 \times \vec{R}_1$ and $\vec{\tau}_{C_2}(\vec{R}_2) = \Delta\vec{r}_2 \times \vec{R}_2$ – external torque from aerodynamic forces $\vec{R}_1$ and $\vec{R}_2$, $\vec{\tau}_{C_1}(\vec{T}_1) = \vec{r}_1 \times \vec{T}_1$ and $\vec{\tau}_{C_2}(\vec{T}_2) = \vec{r}_2 \times \vec{T}_2$ – the external torque from tether tension force, $\vec{T}_1$ and $\vec{T}_2$ – the tether tension forces, acting on the spacecraft and the aerodynamic stabilizer respectively, $\vec{T}_1 = -\vec{T}_2$, $\Delta\vec{r}_1$ and $\Delta\vec{r}_2$ – vectors of position of aerodynamic forces' centre-of-pressure relative to centre of mass of each body (Figures 4.2-4.3), vectors $\vec{r}_1$ and $\vec{r}_2$ determine the position of the tether attachment points relative to centre of mass of each body.

For bodies moving within the atmosphere, small additional moments should be added in the right hand part of the system (4.2) as the need arises. These moments would account for damping, shape asymmetry, etc.

Next, is it necessary to determine the tether tension force, $\vec{T}$. Based on Newton's Second and Third Laws, the mass of the system multiplied by acceleration of the centre of mass of the system is equal to the resultant of all external forces acting on the system, Therefore,

$$\begin{aligned} m_1 \frac{d\vec{V}_1}{dt} &= \vec{T}_1 + \bar{R}_1 + \vec{G}_1, \\ (m_1 + m_2) \frac{d\vec{V}_c}{dt} &= \bar{R}_1 + \bar{R}_2 + \vec{G}_1 + \vec{G}_2, \end{aligned} \tag{4.3}$$

where $\vec{G}_1 = m_1\vec{g}_1$ and $\vec{G}_2 = m_2\vec{g}_2$ – gravity forces acting on the spacecraft and the aerodynamic stabilizer, $\vec{V}_C$ – velocity of the centre of mass of the tether system, $\vec{V}_1 = \vec{V}_C + \vec{V}_{C1}$ – velocity of the spacecraft, $\vec{V}_{C1}$ – velocity of the centre of mass of the spacecraft relative to the centre of mass of the system, m_1 – mass of the spacecraft, m_2 – mass of the stabilizer, $\vec{g}_1$ and $\vec{g}_2$ – acceleration due to gravity for the spacecraft and the stabilizer respectively.

From the first equation of system (4.3) it is possible to find the tension of the tether:

$$\vec{T}_1 = m_1 \frac{d\vec{V}_1}{dt} - \vec{R}_1 - \vec{G}_1,$$

When, calculating velocity $\bar{V}_1$ through the system centre of mass velocity,

$$\vec{T}_1 = m_1 \frac{d\bar{V}_C}{dt} + m_1 \frac{d\bar{V}_{C1}}{dt} - \vec{R}_1 - \vec{G}_1, \tag{4.4}$$

Inserting the second equation of system (4.3) into equation (4.4), it is possible to obtain

$$\vec{T}_1 = \frac{m_1}{m_1 + m_2}\left(\vec{R}_1 + \vec{R}_2 + \vec{G}_1 + \vec{G}_2\right) + m_1 \frac{d\vec{V}_{C1}}{dt} - \vec{R}_1 - \vec{G}_1,$$

or

$$\vec{T}_1 = \frac{m_1}{m_1 + m_2}\vec{G}_2 - \frac{m_2}{m_1 + m_2}\vec{G}_1 + \frac{m_1}{m_1 + m_2}\left(\vec{R}_1 + \vec{R}_2\right) - \vec{R}_1 + m_1 \frac{d\vec{V}_{C1}}{dt}, \tag{4.5}$$

Since the variation of the acceleration due to gravity values can be ignored within the size of the mechanical system, $\vec{g}_1 = \vec{g}_2 = \vec{g}$, $\vec{G}_1 = m_1\vec{g}$, $\vec{G}_2 = m_2\vec{g}$,

$$\frac{m_1}{m_1 + m_2}\vec{G}_2 - \frac{m_2}{m_1 + m_2}\vec{G}_1 \approx 0.$$

Taking into consideration this condition the formula (4.5) becomes

$$\vec{T}_1 = \frac{m_1}{m_1 + m_2}\vec{R}_2 - \frac{m_2}{m_1 + m_2}\vec{R}_1 + m_1\vec{W}_{1C}, \tag{4.6}$$

where $\vec{W}_{1C} = d^2\vec{r}_{1C}/dt^2$ – is the acceleration of the spacecraft centre of mass relative to the system centre of mass, $\vec{r}_{1C} = \overrightarrow{CC_1}$ – is the vector connecting the system centre of mass and spacecraft centre of mass, $\overrightarrow{C_1C_2}$ – is the vector, connecting the spacecraft centre of mass and the centre of mass of the stabilizer.

It is necessary to mention here that vectors $\vec{r}_{1C}$ and $\overrightarrow{C_1C_2}$ are co-linear. Based on the definition that C_1 is the centre of mass of the spacecraft and C_2 is the centre of mass of the stabilizer, the C point divides the line segment C_1C_2 in proportion with the masses m_2 and m_1. Therefore,

$$\vec{r}_{1C} = -\overrightarrow{C_1C_2} \cdot m_2/(m_1 + m_2)$$

Let us determine the value of acceleration $\vec{W}_{1C}$. This requires differentiating the $\overrightarrow{CC_1}$ vector twice with respect to t,

$$\vec{W}_{1C} = \frac{d^2\vec{r}_{1C}}{dt^2} = \frac{d^2\overrightarrow{CC_1}}{dt^2} = -\frac{m_2}{m_1 + m_2} \cdot \frac{d^2\overrightarrow{C_1C_2}}{dt^2},$$

Calculating the position of the centre of mass of the whole system relative to the spacecraft centre of mass (Figure 4.1), we get

$$\overrightarrow{C_1C} = \frac{m_2}{m_1 + m_2} \cdot \left(\overrightarrow{C_1A} + \overrightarrow{AB} + \overrightarrow{BC_2}\right),$$

or

$$\overrightarrow{CC_1} = \frac{m_2}{m_1 + m_2} \cdot \left(\overrightarrow{AC_1} + \overrightarrow{BA} - \overrightarrow{BC_2}\right) = \frac{m_2}{m_1 + m_2} \cdot \left(-\overrightarrow{r_1} + \overrightarrow{BA} + \overrightarrow{r_2}\right),$$

where $\overrightarrow{r_1} = \overrightarrow{C_1A} = -\overrightarrow{AC_1}$, $\overrightarrow{r_2} = \overrightarrow{C_2B} = -\overrightarrow{BC_2}$.

Making designation $\overrightarrow{r_3} = \overrightarrow{BA}$ and differentiating the last formula, we find the relative acceleration

$$\overrightarrow{CC_1} = \frac{m_2}{m_1 + m_2} \cdot (-\overrightarrow{r_1} + \overrightarrow{r_3} + \overrightarrow{r_2}),$$

$$\overrightarrow{W}_{1C} = \frac{d\overrightarrow{CC_1}}{dt} = \frac{m_2}{m_1 + m_2} \cdot \left(\frac{d^2\overrightarrow{r_2}}{dt^2} - \frac{d^2\overrightarrow{r_1}}{dt^2} + \frac{d^2\overrightarrow{r_3}}{dt^2}\right),$$

$$\overrightarrow{W}_{1C} = \frac{m_2}{m_1 + m_2} \cdot \left(\frac{d^2\overrightarrow{r_2}}{dt^2} - \frac{d^2\overrightarrow{r_1}}{dt^2} + \frac{d^2\overrightarrow{r_3}}{dt^2}\right).$$

The vector $\overrightarrow{r_3}$ in the $Bx_3y_3z_3$ related to the tether coordinate system, has only one non-zero component when the tether is strained,

$$\vec{r}_3 = [x_3, 0, 0],$$

Thus, the expression for the tether tension force (4.6) can be re-written as

$$\vec{T}_1 = \frac{m_1}{m_1 + m_2}\vec{R}_2 - \frac{m_2}{m_1 + m_2}\vec{R}_1 + \frac{m_1 m_2}{m_1 + m_2} \cdot \left(\frac{d^2\vec{r}_2}{dt^2} - \frac{d^2\vec{r}_1}{dt^2} + \frac{d^2\vec{r}_3}{dt^2}\right). \qquad (4.7)$$

The derivatives of vectors $\vec{r}_{1,2,3}$ are determined here in the coordinate systems relative to each of three bodies of the system. According to the rule of differentiation of vectors in moving coordinate systems,

$$\frac{d^2\vec{r}_i}{dt^2} = \dot{\vec{\omega}}_i \times \vec{r}_i + \vec{\omega}_i \times (\vec{\omega}_i \times \vec{r}_i), \qquad i = 1, 2, 3$$

where $\vec{\omega}_i$ is the angular velocity of corresponding body, index $i = 3$ corresponds with the tether.

By virtue of the fact that the tether is strained, the tether tension force coincides in time with vector $\vec{r}_3 = \overrightarrow{BA}$. In this case the tether tension force projections on the axis of the coordinate system bound to the tether, By_3 and Bz_3 (Figures 4.1, 4.5), are equal to zero. Hence

$$T_{y_3} = 0, \quad T_{z_3} = 0 \tag{4.8}$$

Actually, the equations (4.8) are the equations for the geometric constraint for the mechanical system under consideration.

Let us make designations

$$\vec{E} = \dot{\vec{\omega}}_1 \times \vec{r}_1, \ \vec{D} = \dot{\vec{\omega}}_2 \times \vec{r}_2, \ \vec{F} = \dot{\vec{\omega}}_3 \times \vec{r}_3. \tag{4.9}$$

Taking into consideration formulae (4.9) the constraint equations for the system (4.8) will be as follows

$$\left[\frac{m_1}{m_1+m_2} \cdot \vec{R}_2 - \frac{m_2}{m_1+m_2} \cdot \vec{R}_1 + \frac{m_1 m_2}{m_1+m_2} \cdot \left(\vec{D} - \vec{E} + \vec{F}\right)\right]_{y_3} = 0,$$
$$\left[\frac{m_1}{m_1+m_2} \cdot \vec{R}_2 - \frac{m_2}{m_1+m_2} \cdot \vec{R}_1 + \frac{m_1 m_2}{m_1+m_2} \cdot \left(\vec{D} - \vec{E} + \vec{F}\right)\right]_{z_3} = 0.$$

To make further mathematical calculations more convenient, these equations are rewritten to include a vector cross product with vector describing the tether $\vec{r}_3$

$$\begin{aligned}
&\frac{m_1}{m_1+m_2} \cdot \left(\vec{r}_3 \times \vec{R}_2\right)_{y_3} - \frac{m_2}{m_1+m_2} \cdot \left(\vec{r}_3 \times \vec{R}_1\right)_{y_3} + \frac{m_1 m_2}{m_1+m_2} \cdot \left(\vec{r}_3 \times \left(\vec{D} - \vec{E} + \vec{F}\right)\right)_{y_3} = 0, \\
&\frac{m_1}{m_1+m_2} \cdot \left(\vec{r}_3 \times \vec{R}_2\right)_{z_3} - \frac{m_2}{m_1+m_2} \cdot \left(\vec{r}_3 \times \vec{R}_1\right)_{z_3} + \frac{m_1 m_2}{m_1+m_2} \cdot \left(\vec{r}_3 \times \left(\vec{D} - \vec{E} + \vec{F}\right)\right)_{z_3} = 0.
\end{aligned} \tag{4.10}$$

These equations (4.10) should be supplemented by the dynamic equations for the rotating motion of each body (4.2), which are written in the non-inertial coordinate system (Lurie, A., 2002) as

$$\begin{aligned}
&\frac{d\vec{l}_1}{dt} + \vec{\omega}_1 \times \vec{l}_1 = \Delta\vec{r}_1 \times \vec{R}_1 + \vec{r}_1 \times \vec{T}_1, \\
&\frac{d\vec{l}_2}{dt} + \vec{\omega}_2 \times \vec{l}_2 = \Delta\vec{r}_2 \times \vec{R}_2 + \vec{r}_2 \times \vec{T}_2
\end{aligned} \tag{4.11}$$

where $\vec{\omega}_1$ and $\vec{\omega}_2$ are angular velocities for each body.

If the equations of spinning motion of each body are written in the main central bound coordinate systems, then the total angular momentum projections on body-fixed coordinate axes are

$$\tau_{ix} = I_{ix}\omega_{ix}, \qquad \tau_{iy} = I_{iy}\omega_{iy}, \qquad \tau_{iz} = I_{iz}\omega_{iz}$$

where $i = 1, 2$.

Rearranging equations (4.10-4.11) by grouping together summands with multipliers $\vec{\omega}_i$ on the left hand side, and transferring the other summands to the right hand side, we obtain the following system of dynamic differential equations, describing the system spinning motion, in matrix form

$$A \cdot \dot{\overline{\omega}} = B, \tag{4.12}$$

where $A = [A_{ij}]$ – matrix of variable coefficients, depending on the angle position and angular velocity of each body, 9x9 in size,

$\dot{\overline{\omega}} = [\dot{\omega}_{x_1}, \dot{\omega}_{y_1}, \dot{\omega}_{z_1}, \dot{\omega}_{x_2}, \dot{\omega}_{y_2}, \dot{\omega}_{z_2}, \dot{\omega}_{x_3}, \dot{\omega}_{y_3}, \dot{\omega}_{z_3}]^T$ – vector of the components of angular accelerations, and $B = [B_j]$ – vector of the right hand sides of differential equations.

Formulae for components of matrices *A* and *B* are listed in the Appendix A.

The dynamic equations (4.12) obtained must be supplemented by kinematic equations, for instance, the Euler equations for two bodies and the tether, and the equations of motion of the centre of mass.

The kinematic equations for the system under consideration are written as follows:

$$\begin{aligned} \omega_{x_i} &= \dot{\varphi}_i + \dot{\gamma}_i \cos\alpha_i \\ \omega_{y_i} &= \dot{\alpha}_i \sin\varphi_i - \dot{\gamma}_i \sin\alpha_i \cos\varphi_i \qquad \text{where } i = 1, 2, 3. \\ \omega_{z_i} &= \dot{\alpha}_i \cos\varphi_i + \dot{\gamma}_i \sin\alpha_i \sin\varphi_i \end{aligned}$$

To perform numerical calculations with these equations it is necessary to solve for the derivatives $\dot{\varphi}_i$, $\dot{\gamma}_i$ and $\dot{\alpha}_i$,

$$\begin{aligned} \dot{\gamma}_i &= \frac{\omega_{z_i} \sin\varphi_i - \omega_{y_i} \cos\varphi_i}{\sin\alpha_i} \\ \dot{\alpha}_i &= \omega_{z_i} \cos\varphi_i + \omega_{y_i} \sin\varphi_i \qquad \text{where } i = 1, 2, 3 \\ \dot{\varphi}_i &= \omega_{x_i} - \dot{\gamma}_i \cos\alpha_i \end{aligned}$$

These classical kinematic equations for bodies in motion in the atmosphere should be supplemented by terms that take account of the non-inertial property of the trajectory's coordinate system (see §4.2), relative to which the Euler angles are calculated. Here

$$\begin{aligned} \dot{\gamma}_i &= \frac{\omega_{z_i} \sin\varphi_i - \omega_{y_i} \cos\varphi_i}{\sin\alpha_i}, \\ \dot{\alpha}_i &= \omega_{z_i} \cos\varphi_i + \omega_{y_i} \sin\varphi_i - \frac{(C_{yv1} S_1 + C_{yv2} S_2) q}{m_1 + m_2}, \\ \dot{\varphi}_i &= \omega_{x_i} - \dot{\gamma}_i \cos\alpha_i, \end{aligned} \tag{4.13}$$

where C_{yv1}, C_{yv2} are the lift force coefficients for the spacecraft and the stabilizer respectively.

To write down the equations of motion of the centre of mass in the atmosphere the following hypotheses were assumed:

1) The planet has an ideal spherical shape, gravitation field is radial;

2) The equatorial rotation rate of the planet and of velocity of motion of the atmosphere is small in comparison to the velocity of the tether system;

3) The centre of mass moves in one plane;

4) The aerodynamic lift force can be ignored.

On the basis of these hypotheses the equations of motion are written as

$$\begin{aligned} \frac{dV_C}{dt} &= -\frac{C_{xk} q S}{m} - g\sin\theta, \\ V_C \frac{d\theta}{dt} &= -\left(g - \frac{V_C^2}{R_\mathrm{E} + h}\right)\cos\theta, \\ \frac{dh}{dt} &= V_C \sin\theta, \end{aligned} \tag{4.14}$$

where V_C is the velocity of the centre of mass of the tether system, C_{xk} is the drag coefficient for the tether , θ is the path inclination, h is the altitude above sea level, R_E – radius of Earth, $g = g_0 \left(\frac{R_\mathrm{E}}{R_\mathrm{E}+\mathrm{h}}\right)^2$ – acceleration due to gravity at altitude h, "standard gravity" $g_0 = 9.80665$ m/s^2 is the nominal acceleration due to gravity at sea level, $\rho = \rho_0 e^{-\lambda h}$ is the atmospheric density at the altitude of h, $\lambda \approx 1/7000$ m^{-1} is the logarithmic density coefficient, S is the midsection, $q = \rho V_C^2/2$ is the dynamic pressure of the air flow.

The complete system of equations in the usual Cauchy form, of the ordinary differential equation written in scalar form, includes nine dynamic equations of motion for the system (4.12), nine kinematic Euler equations (4.13) and three equations of motion for the centre of mass of the system (4.14).

In summary, the ***basic assumptions for the modelling*** of the motion of the deployed tether system with aerodynamic stabilizer in the atmosphere, as derived in this Chapter, are that:

1. The mass of the tether is small enough that it can be considered as equal to zero.

2. The tether is inextensible, and provides a constant geometrical distance constraint between the bodies.

3. Gravity torques, acting on every body of the system and on the whole system, can be ignored.

4. The spacecraft and the aerodynamic stabilizer can be considered to be perfectly rigid bodies.

5. Both the spacecraft and the aerodynamic stabilizer can be considered to be solids of rotation in form.

6. The change of acceleration due to gravity within the size of the system is negligible.

4.4. Undisturbed motion of the tether system in the atmosphere

Let us consider the motion in ideal conditions, where both spacecraft and stabilizer are symmetrical bodies, and therefore their centres of mass are on their longitudinal axes. The mount points of the tether are also placed on these axes.

The slow change of the dynamic pressure q is one of the main factors to introduce a disturbance to the system. If the dynamic pressure is constant and the aerodynamic coefficients depend on angle of attack only, then the tether system is in the undisturbed motion in the airflow. The analysis of the undisturbed motion is necessary for research of stability of motion of the system.

The knowledge of integrals of motion (constants of motion that do not depend explicitly on time) enables the mathematical model to be tested using numerical modelling, because their values should be constant for the period that is modelled.

Let us find kinetic energy K and potential energy U of the tether system.

The kinetic energy K of this system is the sum of kinetic energies of the spacecraft and the stabilizer,

$$K = K_1 + K_2,$$

where K_1 is the kinetic energy of the spacecraft and K_1 is the kinetic energy of the stabilizer.

As it is known from König's theorem (Greenwood, 2000), the kinetic energy of a system is the sum of the energy of the linear motion of the centre of mass and the energy of rotation relative to the centre of mass.

$$K_i = K_{Ci} + \frac{m_i V_i^2}{2},$$

where K_{Ci} is the kinetic energy due to the motion of the body relative to its centre of mass, $m_i V_i^2/2$ is the kinetic energy due to a particle with the mass equal to the mass of the body m_i and moving with the velocity of the centre of mass V_i, $i = 1$ for the spacecraft and $i = 2$ for the stabilizer.

The kinetic energy of rotation of the body

$$K_{Ci} = \frac{1}{2}\left[I_{xi}\omega_{xi}^2 + I_{yi}\omega_{yi}^2 + I_{zi}\omega_{zi}^2\right],$$

where $I_{xi},\ I_{yi}\ and\ I_{zi}$ are moments of inertia (or rotational inertia) of the bodies with respect to axis $x_i,\ y_i$ and z_i of the bound coordinate system.

The other summands of the kinetic energy are

$$\sum_{i=1}^{2}\frac{m_i V_i^2}{2} = \frac{1}{2}(m_1 + m_2)V_C^2 + \frac{1}{2}m_1 V_{C1}^2 + \frac{1}{2}m_2 V_{C2}^2,$$

Considering that

$$\vec{V}_{C1} = d\overrightarrow{CC_1}/dt\,, \qquad \vec{V}_{C2} = d\overrightarrow{CC_2}/dt$$

and

$$\overrightarrow{CC_1} = \frac{m_2(\vec{r}_2 - \vec{r}_1)}{(m_1 + m_2)}, \qquad \overrightarrow{CC_2} = \frac{m_1(\vec{r}_1 - \vec{r}_2)}{(m_1 + m_2)},$$

it is possible to find the relative velocities

$$\vec{V}_{C1} = \frac{m_2}{(m_1 + m_2)}\left(\frac{d\vec{r}_2}{dt} - \frac{d\vec{r}_1}{dt}\right), \qquad \vec{V}_{C2} = -\frac{m_1}{(m_1 + m_2)}\left(\frac{d\vec{r}_1}{dt} - \frac{d\vec{r}_2}{dt}\right)$$

or

$$\vec{V}_{C1} = \frac{m_2}{(m_1 + m_2)}(\vec{\omega}_2 \times \vec{r}_2 - \vec{\omega}_1 \times \vec{r}_1),$$

$$\vec{V}_{C2} = \frac{m_1}{(m_1 + m_2)}(\vec{\omega}_1 \times \vec{r}_1 - \vec{\omega}_2 \times \vec{r}_2).$$

As a result, the kinetic energy of the system

$$K = \frac{1}{2}\sum_{i=1}^{2}\left[I_{xi}\omega_{xi}^2 + I_{yi}\omega_{yi}^2 + I_{zi}\omega_{zi}^2\right] + \frac{m_1 + m_2}{2}V_C^2 + \frac{1}{2}\frac{m_1 m_2}{m_1 + m_2}(\vec{\omega}_2 \times \vec{r}_2 - \vec{\omega}_1 \times \vec{r}_1)^2$$

The potential energy U of the system can be found if some assumptions are made. Let us consider the spacecraft and the stabilizer as spherical bodies. Upon this simplification the vectors of aerodynamic forces are co-linear with the vector of air flow. The potential energy is similar to potential energy of the simple double pendulum in the gravitational field.

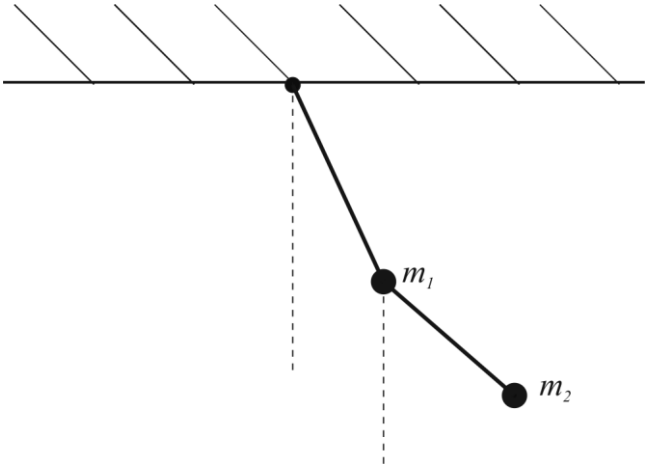

Figure 4.7 – Double pendulum

In this case, the direction of the airflow becomes comparable to the vertical line, and the analogue of the potential energy U is equal to

$$U = \frac{m_1 R_{2xk} - m_2 R_{1xk}}{m_1 + m_2}(-x_1 \cos \propto_1 + x_2 \cos \propto_2 + x_3 \cos \propto_3),$$

where the first multiplier is comparable to the gravitational force for the double pendulum and relates to the tension force, $x_i,\ i = 1, 2, 3$ are projections of vectors $\vec{r}_i$ onto the axis of the bound coordinate systems, $x_1 < 0$, $x_2 > 0$, $x_3 > 0$.

The undisturbed tether system considered is an isolated system, and its total energy E should be constant (Halliday, 1975).

$$E = K + U = const. \tag{4.15}$$

This statement allows the mathematical model of the system to be tested by means of numerical calculations. It is necessary to note that statement (4.15) is eligible for isolated systems only and cannot be used for a tether system if it is affected by disturbances or the dissipation of energy arising from heating or other causes. During the undisturbed motion, the dynamic pressure of the oncoming airflow should be constant. As the dynamic pressure by definition $q = \rho V^2/2$ (§4.3) depends on the density of the atmosphere and the velocity of the airflow, it means basically that both velocity and density of the atmosphere should be constant. Thus, the undisturbed motion of the tether system is a simplification that allows one to understand the basics of motion and test the mathematical model.

The total angular momentum of the system in the sum of total angular momenta of the bodies (Halliday, 1975),

$$\vec{l} = \vec{l}_{1C} + \vec{l}_{2C}, \tag{4.16}$$

where $\vec{l}_{1C}$ and $\vec{l}_{2C}$ are vectors of the total angular momenta of the spacecraft and the stabilizer relative to the centre of masses of the tether system. They are defined by equations

$$\vec{l}_{1C} = \vec{l}_1 + \overrightarrow{CC_1} \times m_1\vec{V}_1,$$
$$\vec{l}_{2C} = \vec{l}_2 + \overrightarrow{CC_2} \times m_2\vec{V}_2,$$

where $\vec{l}_1$ and $\vec{l}_2$ are defined relative to the centres of masses of the spacecraft and the stabilizer respectively.

With respect to the values of vectors $\overrightarrow{CC_1}$, $\overrightarrow{CC_2}$ and $\overrightarrow{C_2C_1}$ shown in the previous paragraph,

$$\vec{l} = \vec{l}_1 + \vec{l}_2 + \overrightarrow{CC_1} \times m_1\vec{V}_1 + \overrightarrow{CC_2} \times m_2\vec{V}_2,$$
$$\vec{l} = \vec{l}_1 + \vec{l}_2 + \frac{m_1m_2}{m_1+m_2}\overrightarrow{C_2C_1} \times \vec{V}_1 - \frac{m_1m_2}{m_1+m_2}\overrightarrow{C_2C_1} \times m_2\vec{V}_2,$$
$$\vec{l} = \vec{l}_1 + \vec{l}_2 + \frac{m_1m_2}{m_1+m_2}\overrightarrow{C_2C_1} \times (\vec{V}_1 - \vec{V}_2),$$
$$\vec{l} = \vec{l}_1 + \vec{l}_2 + \frac{m_1m_2}{m_1+m_2}\overrightarrow{C_2C_1} \times (\vec{V}_{C1} - \vec{V}_{C2}).$$

Using previously obtained formulae for $\vec{V}_{C1}$ and $\vec{V}_{C2}$, $\overrightarrow{CC_1}$ and $\overrightarrow{CC_2}$ it is possible to write

$$\vec{l} = \vec{l}_1 + \vec{l}_2 + \frac{m_1m_2}{m_1+m_2}(\vec{r}_2 - \vec{r}_1) \times (\vec{\omega}_2 \times \vec{r}_2 - \vec{\omega}_1 \times \vec{r}_1).$$

Therefore, the total angular momentums of the bodies can be found using the parameters of motion of the tether system. The projection of the total angular momentum of the system onto the x_k axis of the trajectory coordinate system can be found using matrices $\underset{1\leftarrow\mathrm{tr}}{L}$ and $\underset{2\leftarrow\mathrm{tr}}{L}$ (Appendix A) and equations

$$\vec{l}_{1xk} = \underset{\mathrm{tr}\leftarrow 1}{L} I_1\vec{\omega}_1, \qquad \vec{l}_{2xk} = \underset{\mathrm{tr}\leftarrow 2}{L} I_2\vec{\omega}_2.$$

For the spherical shaped bodies, the vectors of the aerodynamic forces are co-linear to the vector of the airflow. This means that the projection of the total angular momentum from aerodynamic forces onto the x_k axis of the trajectory coordinate system is equal to zero, and

$$l_{xk} = const.$$

This integral of motion is based on the vector of angular momentum of the system and exists for spherical bodies with any positions of the mounting points of the tether.

There are obvious integrals of motion concerning the undisturbed motion for both bodies. If the bodies are symmetrical and the mounting points of the tether are located on their axes of symmetry, then the angular velocity of each of the bodies is constant during the undisturbed motion.

$$\omega_{x_1} = const, \qquad \omega_{x_2} = const.$$

Thereby, there are three conclusions, listed below, concerning the motion for the tether system in the airflow.

1. If the angular velocities of the bodies are constant during the undisturbed motion, then the bodies are symmetrical and mounting points of the tether are located on their axes of symmetry.

2. The projection of the total angular momentum on the axis of the trajectory coordinate system is constant, $l_{xk} = const$.

3. The analogue of total energy is constant. Due to complexity of equations, this integral of motion is found analytically for spherical bodies only.

These integrals of motion are useful for testing the results of the numerical modelling of motion of the tether system.

Figure 4.8 shows the results of numerical calculations of the undisturbed motion of the tether system – the change of potential, kinetic and full energy of the system in conditions of constant dynamic pressure, and mass symmetry of the spherical spacecraft and stabilizer. The value of the integral of motion – the total energy – remains constant, thus validating the mathematical model of motion of the tether system.

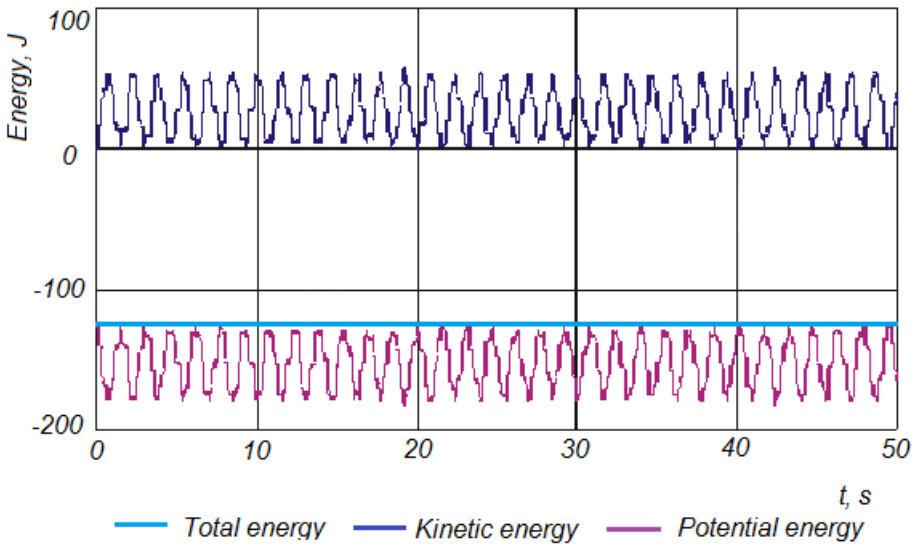

Figure 4.8 – The energy of the system

4.5 Summary

In this chapter the following results were obtained:

1. The definition of the tether system and forces acting on the tether system. The tether system is defined as a system of two bodies – a spacecraft and a stabilizer – connected by a massless tether. The assumptions and simplifications made are also described and justified.

2. The three coordinate systems used for the derivation of the equations of motion of the tether system are described.

3. The mathematical model of spatial motion has been derived. Its novelty is based on the description of spinning motion of both spacecraft and stabilizer. The model takes into consideration aerodynamic and gravity forces, tension of the tether, mass and shape asymmetry of the bodies.

4. The integrals of the undisturbed motion of the tether system were found and used for numerical testing the mathematical model of motion of the tether system.

5. THE INFLUENCE OF PARAMETERS OF THE TETHER SYSTEM ON ITS MOTION

To say that the tether system is stable means that it is able to sustain a previously defined condition of motion. The stability of the system can be said to be "static", which means the necessary condition for stability is met, or "dynamic", which can be considered to be a sufficient condition for stability. Here, the conditions of static stability are determined based on the undisturbed motion of the tether system. The tether system can be in stable motion even if either or both bodies are statically unstable. The dependence of stability on the natural frequencies of the system is assessed relative to the parameters.

The influence of parameters of the tether system under conditions of stable motion during the descent in the dense layers of the atmosphere is investigated. Here, the parameters being adjusted to obtain stable motion are the mass, the geometrical dimensions and the length of the tether.

It is found that the increase in the length of the tether, meaning the deployment process during descent, can be an additional stabilizing factor for the tether system.

5.1. The stability of motion of the tether system

The stability of motion of the rigid body generally refers to its ability to sustain a predefined condition of motion. If the net forces and moments acting on the body are equal to zero, then the body is in equilibrium. Under external forcing, the body can change its position (for example, the angle of attack) and the equilibrium condition is lost. In this context, the notion of "stability of motion" for the spacecraft means the same as the better known notion of stability of motion for aircraft (Cutler C., 2015).

To find the conditions of stability of motion for a rigid body it is necessary to determine the conditions for "static stability". These conditions should be found when the dynamic pressure of the air low is constant and there are no other disturbances, such as asymmetry of the body or dissipative forces. The constant dynamic pressure means that both the velocity and the density of the air flow must be constant.

The conditions of the static stability near the equilibrium point $\alpha_i = 0$, where $i = 1,2,3$, are necessary conditions for the stable motion of the tether system.

The condition of "dynamic stability" defines slow reducing of amplitudes of oscillations with respect to undisturbed motion. These conditions are sufficient conditions for the equilibrium condition. The achievability of these equilibrium conditions is usually dependent on the size and type of motion perturbations, such as dissipative forces.

The conditions of dynamic stability determine the rate of decrease of the amplitudes of oscillation near the unperturbed solution. Dynamic conditions can be treated as sufficient conditions for the stability of the system equilibrium, but they are too complex to be found analytically, thus making it hard to analyse the dynamic stability of the motion of the tether system.

The sufficiency of the stability conditions is usually verified by applying various perturbations, like slow variations in the system parameters, or by applying dissipative forces to the system.

Flat motion is a particular case of spatial motion when the angles $\varphi_i = 0$, $\gamma_i = 0$, and angular velocities $\omega_{x_i} = 0$, $i = 1,2,3$. The necessity of researching flat motion is based on finding the conditions of static stability of motion in the atmosphere. "Flat motion" is also called two dimensional motion, and "spatial motion" is three dimensional motion.

It is known (Yaroshevskiy, 1978) that the transition from flat motion to spatial motion, which adds gyroscopic forces, cannot destroy the stability of motion. This transition can only lead to appearance of new equilibrium points. For example, a symmetric body in addition to equilibrium point $\alpha = 0$, where α is the angle of attack, will obtain a new equilibrium point $\alpha = \pi$ if under the condition that the frequency of its rotation around the longitudinal axis is sufficiently high. It is also known that the application to the system of gyroscopic or dissipative forces will not destroy the stability of motion. Therefore, it is necessary to obtain the static conditions of stability during flat motion of the tether system. Hereinafter, the stability of equilibrium point $\alpha_i = 0$, $i = 1,2,3$ is considered.

For the case of the spacecraft without stabilizer, the condition of static stability is rather simple: the position of the centre of mass of the spacecraft must be close to the nose part than the centre-of-pressure position of the aerodynamic forces. Equivalently, the value of the projection of $\Delta\vec{r}_1$ (Figure 4.1) on the longitudinal axis of the spacecraft must be less than zero.

To obtain the conditions of static stability of the tether system, let us consider the equations of motion of the tether system (4.12-4.13) and make a linearization near the equilibrium point $\alpha_i = 0$. Choosing this point ensures that the longitudinal axes of the

spacecraft and stabilizer and the tether are co-linear with the velocity of the centre of masses of the tether system.

Then, considering $\sin\alpha_i \approx \alpha_i$, $\cos\alpha_i \approx 1$, $i = 1,2,3$ and neglecting non-linear summands,

$$P\frac{d^2\alpha}{dt^2} + Q\alpha = 0, \tag{5.1}$$

where $\alpha = [\alpha_1, \alpha_2, \alpha_3]^T$, P and Q are matrices of coefficients,

$$P = \begin{bmatrix} I_1 + m_{12}r_1^2 & m_{12}r_1r_2 & m_{12}r_1r_3 \\ m_{12}r_1r_2 & I_2 + m_{12}r_2^2 & m_{12}r_2r_3 \\ m_{12}r_1 & m_{12}r_3 & m_{12}r_3 \end{bmatrix},$$

$$Q = \begin{bmatrix} -\Delta R_x r_1 - \dfrac{m_2 r_1}{m_1+m_2}R^{\alpha}_{yk1} - \Delta x_1 R_{y1} & \dfrac{m_1 r_1}{m_1+m_2}R^{\alpha}_{yk2} & 0 \\ -\dfrac{m_2 r_2}{m_1+m_2}R^{\alpha}_{yk1} & -\Delta R_x r_2 + \dfrac{m_1 r_2}{m_1+m_2}R^{\alpha}_{yk2} - \Delta x_2 R_{y2} & 0 \\ -\dfrac{m_2}{m_1+m_2}R^{\alpha}_{yk1} & \dfrac{m_1}{m_1+m_2}R^{\alpha}_{yk2} & -\Delta R_x \end{bmatrix},$$

where $m_{12} = m_1m_2/(m_1+m_2)$,

$\Delta R_x = (m_1R_{2xk} - m_2R_{1xk})/(m_1+m_2)$, $\Delta R_y = \left(m_1R_{2yk} - m_2R_{1yk}\right)/(m_1+m_2)$,

r_3 is the length of the tether,

Δx_1 and Δx_2 are projections of vectors $\Delta\vec{r}_1$ and $\Delta\vec{r}_2$ onto the axis of symmetry of each body respectively,

R_{1xk}, R_{2xk}, R_{1yk}, R_{2yk} are projections of the aerodynamic forces $\vec{R}_1$ and $\vec{R}_2$ onto the axes of the trajectory coordinate system $Ox_ky_kz_k$,

$R^{\alpha}_{yk1} = (C_{x1} + C_{y1})qS_1$ and $R^{\alpha}_{yk2} = (C_{x2} + C_{y2})qS_2$ are partial derivatives of the aerodynamic forces with respect to angle of attack.

The analysis of the static stability reduces to the analysis of the characteristic roots (*i.e.* eigenvalues) of the dynamic system (5.1). The characteristic equation is written as

$$\det(P\lambda^2 + Q) = 0.$$

Expanding a determinant and collecting similar variables, we obtain cubic equation with respect to λ^2:

$$p_\lambda\lambda^6 + q_\lambda\lambda^4 + r_\lambda\lambda^2 + t_\lambda = 0, \tag{5.2}$$

where $p_\lambda = m_{12}I_1I_2r_2$,

$q_\lambda = -[m_{12}I_1r_2(r_2+r_3) + m_{12}I_2r_1(r_1+r_3) + I_1I_2]\Delta R_x$,

$$r_\lambda = I_1 \Delta R_x \left(\Delta R_x r_2 - \frac{m_1}{m_1 + m_2} r_2 R^\alpha_{yk2} - \Delta x_2 R_{y2} \right) +$$
$$+ I_2 \Delta R_x \left(\Delta R_x r_1 + \frac{m_2}{m_1 + m_2} r_1 R^\alpha_{yk1} - \Delta x_1 R_{y1} \right) +$$
$$+ m_{12} \Delta R_x^2 r_1 (r_1 r_2 + r_2^2 + r_2 r_3),$$
$$t_\lambda = r_1 r_2 (\Delta R_x)^2 \cdot \left(\Delta R^\alpha_y - \Delta R_x \right),$$
$$\Delta R^\alpha_y = \left(m_1 R^\alpha_{2yk} - m_2 R^\alpha_{1yk} \right) / (m_1 + m_2).$$

To define natural frequencies of the tether systems, the characteristic equation (5.2) can be re-written as

$$\lambda^6 + \frac{q_\lambda}{p_\lambda}\lambda^4 + \frac{r_\lambda}{p_\lambda}\lambda^2 + \frac{t_\lambda}{p_\lambda} = (\lambda^2 + \omega_1^2)(\lambda^2 + \omega_2^2)(\lambda^2 + \omega_3^2) = 0, \qquad (5.3)$$

where $\omega_1, \omega_2, \omega_3$ are the natural frequencies of the tether system.

Then the angles of attack are small, the parameter $\Delta R^\alpha_y - \Delta R_x$ is

$$\Delta R^\alpha_y - \Delta R_x = \frac{m_1 q S_2 C_{y2}}{m_1 + m_2} - \frac{m_2 q S_1 C_{y1}}{m_1 + m_2}.$$

The motion of the system is statically stable if all the roots of the characteristic equation are purely imaginary numbers (Gantmacher, 1959), and this happens if and only if the cubic equation with respect to λ^2 (5.2) has three real roots, all of which are less than zero. If the system is statically stable, then the characteristic equation allows to determine the frequencies of small oscillations of the mechanical system during the flat motion.

The analysis of the equation (5.2) shows that if $\Delta R_x = 0$, then all the roots of the characteristic equation (eigenvalues) are degenerately equal to zero, and for symmetrical bodies there are two necessary condition of static stability.

The first necessary condition of static stability is

$$\Delta R_x < 0.$$

The second necessary condition of static stability is

$$\Delta R^\alpha_y < \Delta R_x,$$

because when $\Delta R^\alpha_y = \Delta R_x$, two roots of the characteristic equation equal to zero.

When both bodies of the tether system are spherical, these necessary conditions are equal to each other.

It is possible to show the area of static stability of the tether system using the Vyshnegradsky's diagram (Lurie, A., 2002) by reducing the characteristic equation to the form

$$\mu^3 + A\mu^2 + B\mu + 1 = 0,$$

where $\mu = \sqrt[3]{p_\lambda / t_\lambda}$, $A = q_\lambda / \sqrt[3]{t_\lambda p_\lambda^2}$, $B = r_\lambda / \sqrt[3]{p_\lambda t_\lambda^2}$.

The area of stability in Cartesian coordinates (A, B) can be shown as corresponding to real roots area (Figure 5.1). This area is determined by inequality

$$f(A,B) = \left(\frac{B}{3} - \frac{A^2}{9}\right)^3 + \left(\frac{AB-3}{6} - \frac{A^3}{27}\right)^2 < 0.$$

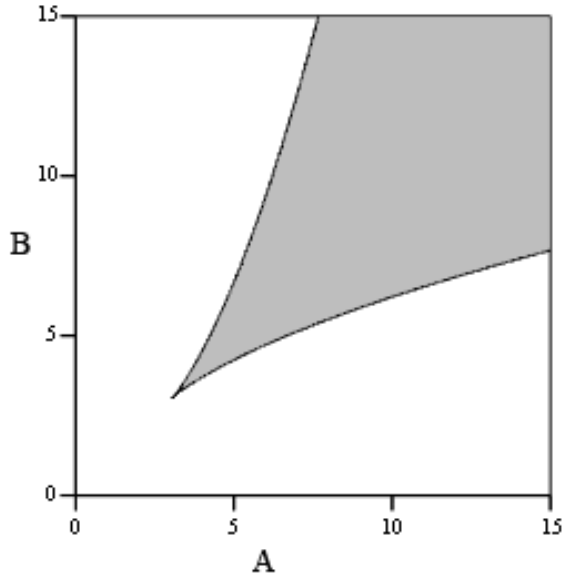

Figure 5.1 – The area of stability (grey)

Figure 5.2 depicts the typical change of function $f(A, B)$ with respect to the mass of the stabilizer. When the value of $f(A, B)$ becomes greater than zero, the system loses its stability. The area to the right from the dot line is the area of stable motion while motion in the area left to the dot line is unstable.

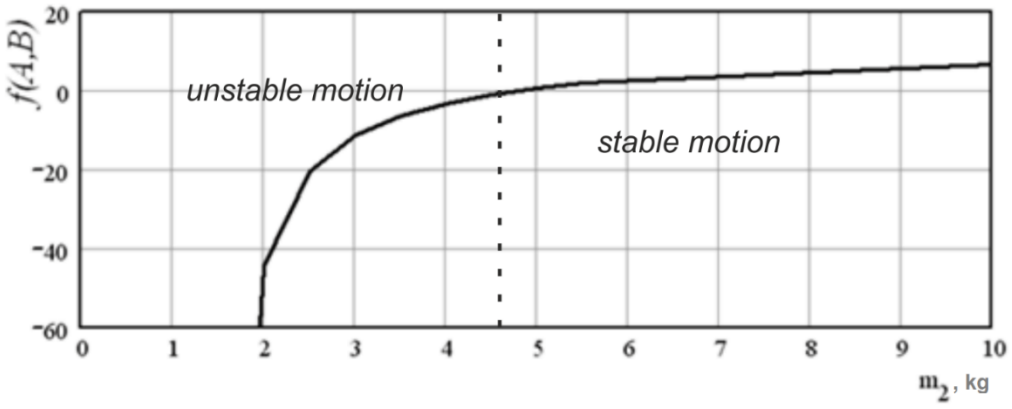

Figure 5.2 – The increase of the mass of the stabilizer affects the stability

5.2. The dependence of stability and frequencies on the parameters

As it has been shown above, it is possible to determine the static stability or instability of the system with the given spacecraft and stabilizer parameters and their aerodynamic characteristics.

It is always important to know how the stability conditions (or the system frequencies) depend on the parameters of the system. If the parameters and aerodynamic characteristics of the spacecraft are given, then the problem of the choice of parameters is reduced to the choice of the characteristics of the stabilizer and the length of the tether. The stabilizer here is characterized by its mass and inertia characteristics, and its reference area.

The influence of the mass and reference area of the stabilizer and the length of the tether on the frequencies of the system is obtained below, under the condition of static stability of the system.

By way of example, in this section, the case of two bodies of rotation shaped as cones with spherically rounded apexes is considered. The shape of the bodies is shown in Figure 5.3.

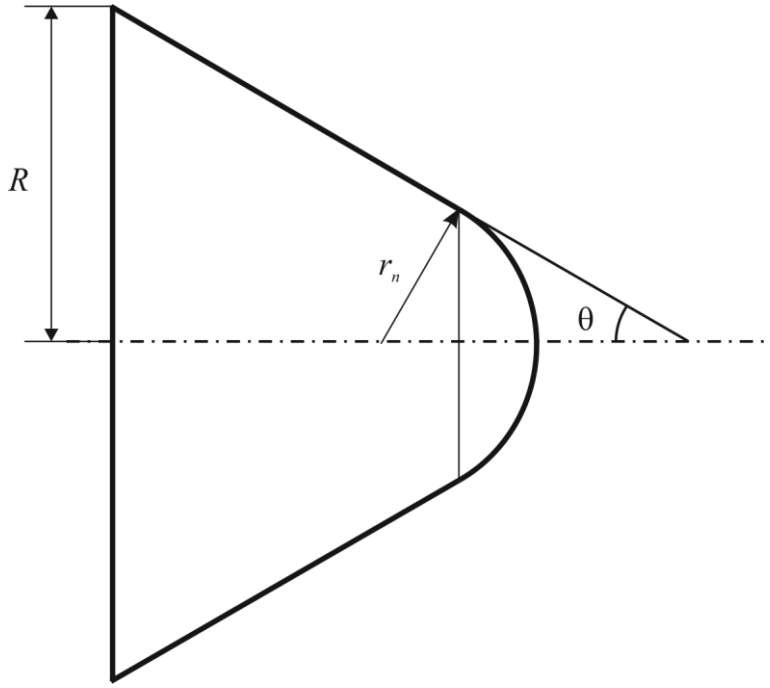

Figure 5.3 – The cone with rounded apex

The aerodynamic characteristics of the bodies were calculated (see Appendix B) using the approximate Newton theory (Anderson, 1989). The approximate Newton theory gives results with quite acceptable accuracy for Mach numbers greater than four and for flight in the denser part of the atmosphere where altitude is less than 110 km.

The dependence of the stability of motion on the length of the tether is the most simple to demonstrate. The change of the length of the tether does not lead to loss of stability. This means that the stability is defined by parameters of the spacecraft and the stabilizer only. Typical dependencies of the frequencies on the length of the tether are shown in Figure 5.4. Other parameters of the system were selected and remain constant during the calculations for this Figure and for Figures 5.4, 5.5 and 5.6.

As the length of the tether increases, each of the frequencies decreases monotonically. Upon the increase of the length of the tether, the frequencies tend to horizontal asymptotes, so that further increase in the length of the tether does not lead to any significant change of frequencies. If the length of the tether tends to zero, one of the frequencies rises asymptotically. These dependencies are typical and common for any shapes of the spacecraft and the stabilizer.

For the statically neutral bodies, $\Delta x_1 = \Delta x_2 = 0$, the stability or instability of the system cannot be changed by any variation in the length of the tether.

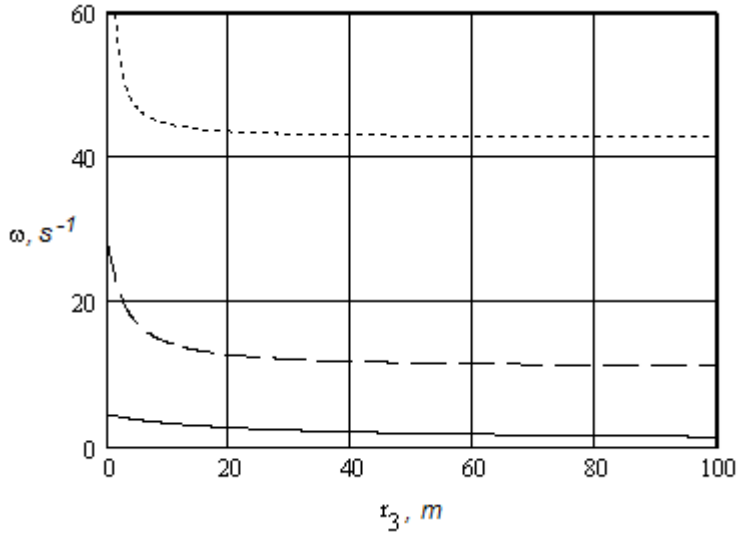

Figure 5.4 – Frequencies depending on the length of the tether

Figure 5.5 shows the dependence of the system natural frequencies on the mass of the second body. These dependencies are typical for the case where both the spacecraft and stabilizer are bodies of rotation other than spheres. The figures for the system frequencies are obtained for a constant value of the dynamic pressure of the air flow. The frequencies are proportional to $\sqrt{q}$ and can easily be recalculated for other values of dynamic pressure of the air flow. A characteristic of the system frequency dependence on the mass of stabilizer is the loss of static stability as the mass increases, and this loss of stability occurs at the point of coincidence of the two frequencies as it is shown on Figure 5.5.

Figure 5.6 depicts how the system frequencies changes when the reference area of the stabilizer increases. The loss of static stability in the variation of the scale coefficient occurs for sufficiently small dimensions of the second body.

When both the spacecraft and stabilizer are spherical bodies, these dependencies of stability on the parameters of the system become much more simple to demonstrate. For example, when the mass of the stabilizer m_2 increases, or the dimensions of the stabilizer decrease, a loss of stability occurs when the curves of all three frequencies of the system meet at one point $\omega_i = 0$, *i.e.* when the eigenvalues (frequencies) become degenerate.

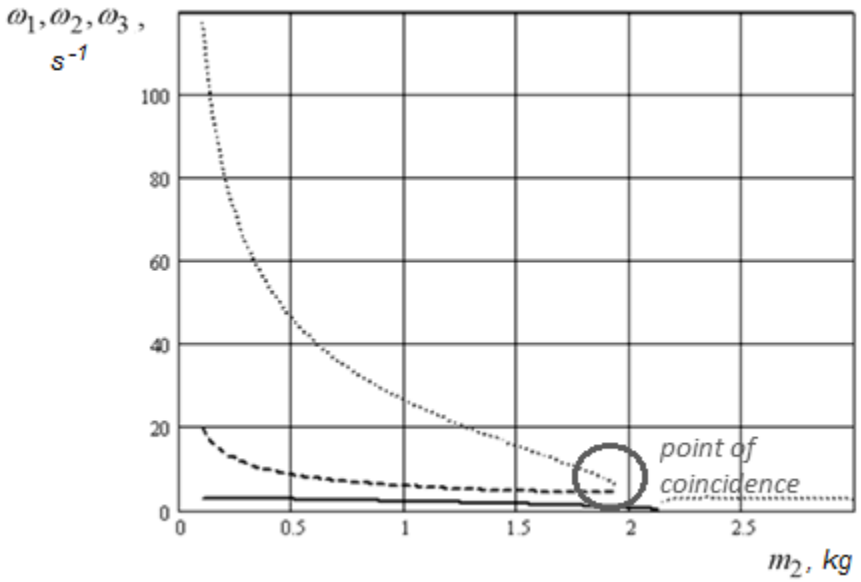

Figure 5.5 – Frequencies depending on the mass of the stabilizer

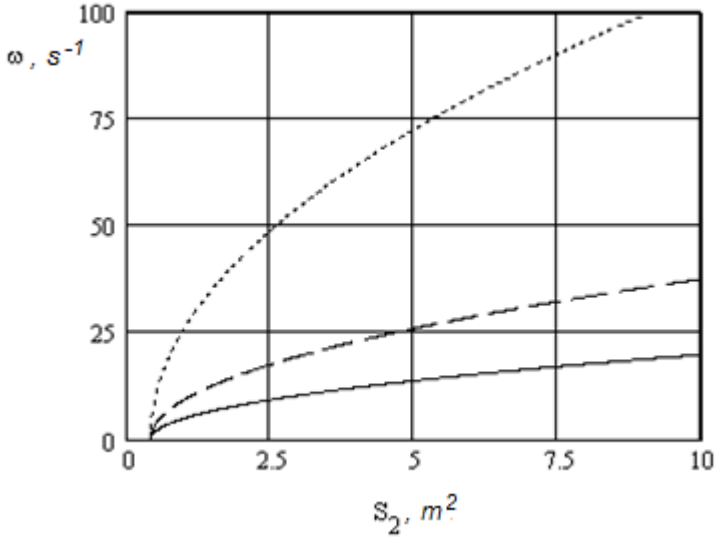

Figure 5.6 – Frequencies depending on reference area

If the bodies are not statically neutral, then the dependence of system frequency on the parameters of the second body is more complicated. On the one hand, even when both bodies are statically unstable, the tether system as a whole can be statically stable. The example of such a system is a tether system consisting of two cones. On the other hand, a tether system consisting of two statically stable bodies can still be statically unstable with an unlucky choice of the parameters.

If the first body is statically stable, in a certain range of the tether lengths, the system becomes statically unstable, and the loss of stability occurs as two frequencies of the system coincide. As the length of the tether continues to increase, the system becomes stable again.

Numerical calculations of the motion of system in the instability regions confirm the existence of regions of static instability. Thus, the static stability of the motion of the system in the atmosphere is determined by the consistent choice of parameters of the entire system by using the above static stability conditions rather than by the characteristics of separate bodies.

5.3. The tension of the tether

One of the most important practical parameters of motion of the system is the value of tension force.

The tension of the tether can be found using the system of dynamic equations (4.12), kinematic equations (4.13) and the equations of motion of the centre of mass (4.14).

The value of tension force was determined above by equation (4.7)

$$\vec{T}_1 = \frac{m_1}{m_1+m_2}\vec{R}_2 - \frac{m_2}{m_1+m_2}\vec{R}_1 + \frac{m_1 m_2}{m_1+m_2}\cdot\left(\frac{d^2\vec{r}_2}{dt^2} - \frac{d^2\vec{r}_1}{dt^2} + \frac{d^2\vec{r}_3}{dt^2}\right),$$

where derivatives of vectors $\vec{r}_i$ are determined by equations

$$\frac{d^2\vec{r}_i}{dt^2} = \dot{\vec{\omega}}_i \times \vec{r}_i + \vec{\omega}_i \times (\vec{\omega}_i \times \vec{r}_i), \qquad i = 1,2,3,$$

where $\vec{\omega}_i$ are the angular velocities of the spacecraft, the stabilizer and the tether respectively.

The equation for the tension of the tether shows that the tension force has two components. The first component is defined by aerodynamic forces acting on the tether system and masses of the spacecraft and the stabilizer. The second component depends not only on masses, but also on angular velocities of the bodies, while the values of angular velocities can be estimated using the values of natural frequencies of the tether system.

It is not possible to find the value of the tension force analytically, but it can be calculated numerically using (4.7). On this basis, the effect of the tether system parameters on the tension of the tether can be analysed.

The following results of calculations were obtained for the descent of a light spacecraft. Here, both the spacecraft and stabilizer are cones. The parameters of the tether

system are listed in the Table 5.1. The mass of the spacecraft and its conical shape refer to the initial mass and geometry of a light capsule in early design of YES2 landing module. The dependencies obtained subsequently are typical for tether systems consisting of two cones.

Table 5.1 – The parameters of the tether system

The parameter	Variable	Value
Mass of the spacecraft	m_1	10 kg
Mass of the stabilizer	m_2	2 kg
Length of the tether	r_3	10 m
Reference area of the spacecraft	S_1	0.275 m^2
Reference area of the stabilizer	S_2	0.2 m^2
Aerodynamic force coefficients for the spacecraft	C_{x1}	-1
	C_{y1}	2
Aerodynamic force coefficients for the stabilizer	C_{x2}	-1
	C_{y2}	2

The results of numerical calculations are shown in Figures 5.7-5.8. All these results are typical for any combination of shape and mass. Figure 5.7 depicts the dependence of full tension force on time during the descent, while Figure 5.8 illustrates how the components of tension force vary during descent. Figure 5.8 shows that the component depending on angular velocities is about four times smaller than the component depending on aerodynamic forces.

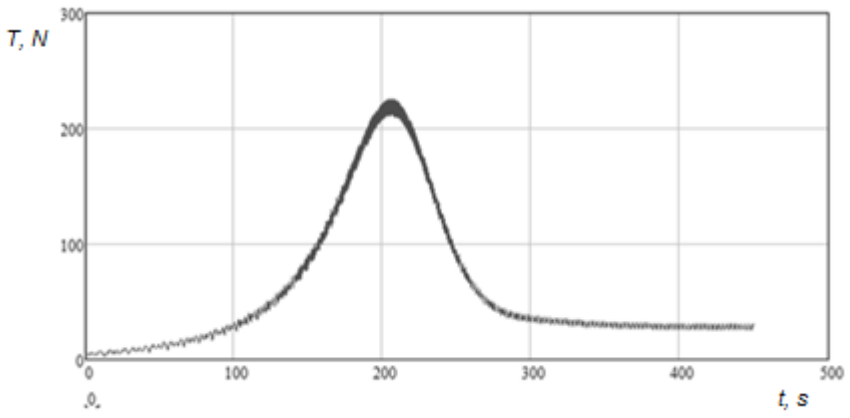

Figure 5.7 – The typical dependence of tether tension on time

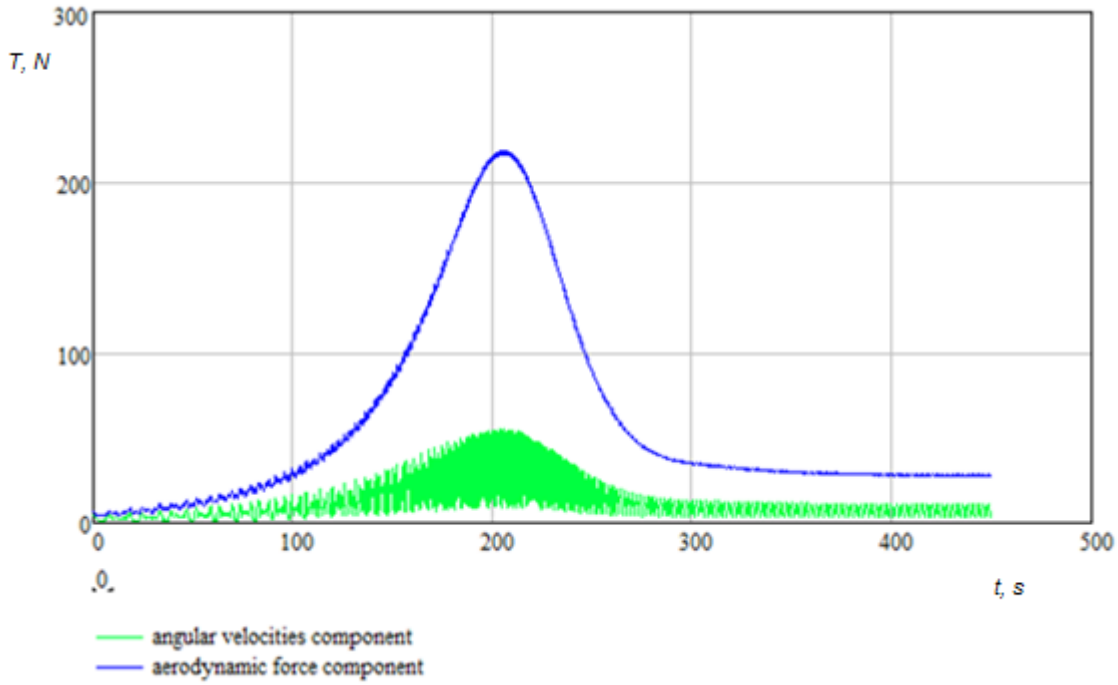

Figure 5.8 – The components of tether tension during descent

Next, consider how the maximal tension force depends on the parameters of the stabilizer and the length of the tether for different shapes of spacecraft and stabilizer. The Figures 5.9-5.11 were built based on a series of calculations for the following combinations of shapes of spacecraft and stabilizer respectively: sphere and sphere, cylinder and sphere, cylinder and cone. The mathematical model described in the previous and current chapter is used for these calculations. The system parameters are given in Table 5.1. Figures 5.9-5.11 show consistently the dependence of tension force on the mass of the stabilizer, the reference area of the stabilizer, and the length of the tether, respectively. The end of the curve indicates loss of stability in the tether system. The stability of motion is treated as lost when the value of the angle of attack of the spacecraft, or the value of the angle of attack of the stabilizer, during the modelling exceeds a value of 90 degrees, or when the tension of the tether becomes less than zero, in which case, the spacecraft and the stabilizer continue separate motions from each other.

Inspection of these figures indicates that the maximal tension of the tether has only a slight dependence on the length of the tether, for any combination of spacecraft and the stabilizer shape: the dependence of the tension on the mass of the stabilizer is much more significant. The geometric dimensions of the stabilizer, measured by its reference area, have

the most effect on the tension of the tether, and usage of a stabilizer with larger dimensions leads to sharp increase in the tension force.

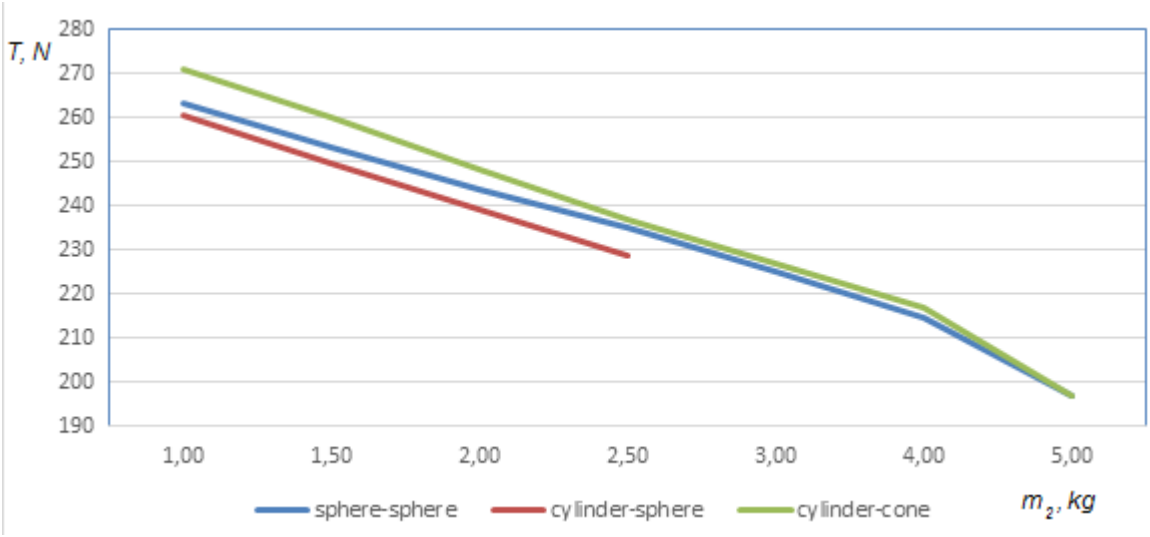

Figure 5.9 – The dependence of maximal tether tension on the mass of the stabilizer

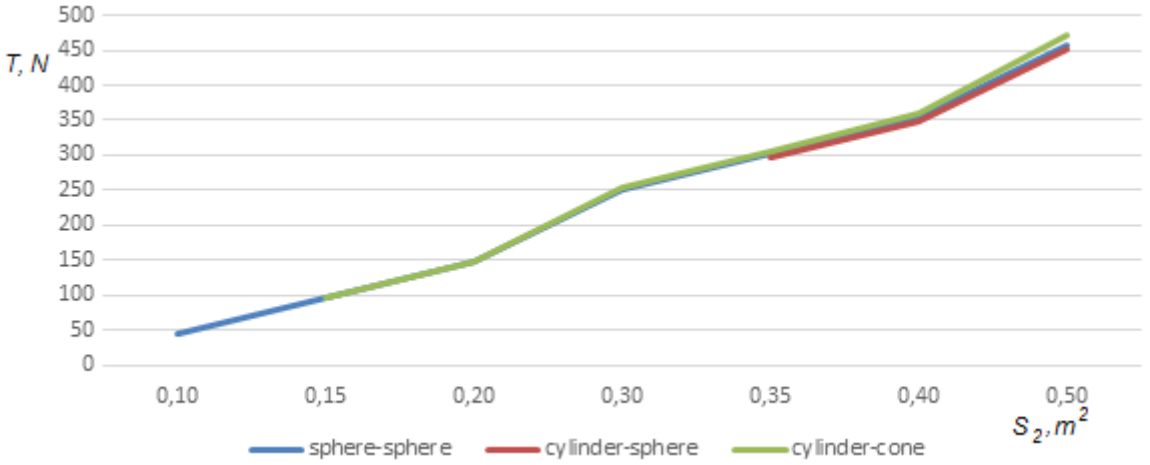

Figure 5.10 – The dependence of maximal tether tension on the reference area of the stabilizer

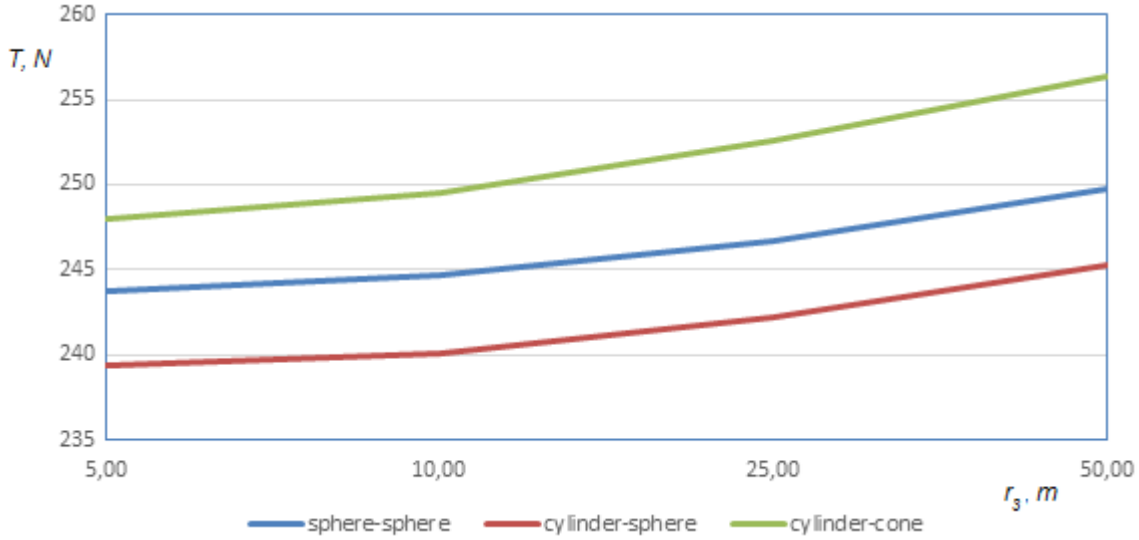

Figure 5.11 – The dependence of maximal tether tension on the length of the tether

The Figures 5.12-5.15 show the parameters of motion of the centre of mass of the system. These dependencies are typical for all combinations of parameters of the spacecraft and the stabilizer. During the first 500 seconds of descent the velocity of the centre of mass decreases from its initial value of 7842 to 49.6 metres per second as it is shown in Figure 5.12, and the altitude changes from initial value of 100 kilometres down to 16 kilometres (Figure 5.13). The trajectory of the centre of masses of the system is shown in Figure 5.14, there the X-axis depicts the path traversed by the centre of masses, and the Y-axis is the altitude.

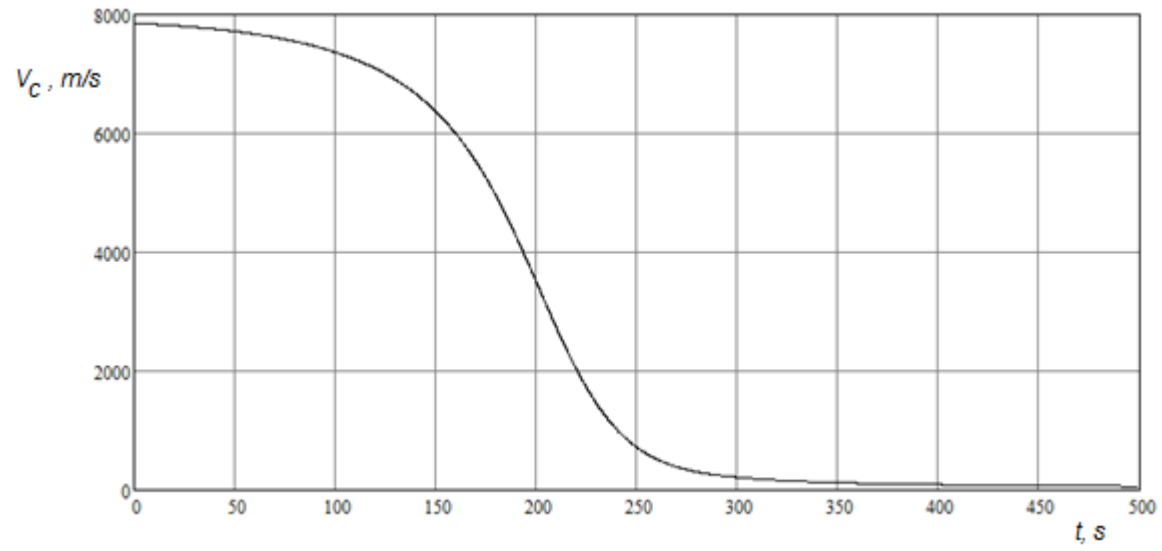

Figure 5.12 – The dependence of velocity of centre of masses on time

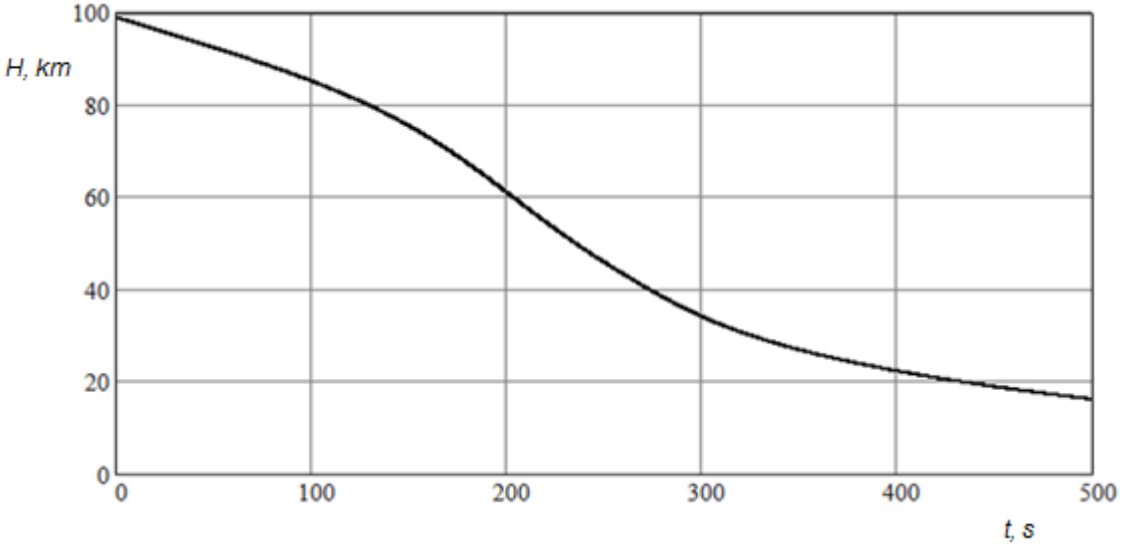

Figure 5.13 – The dependence of altitude on time

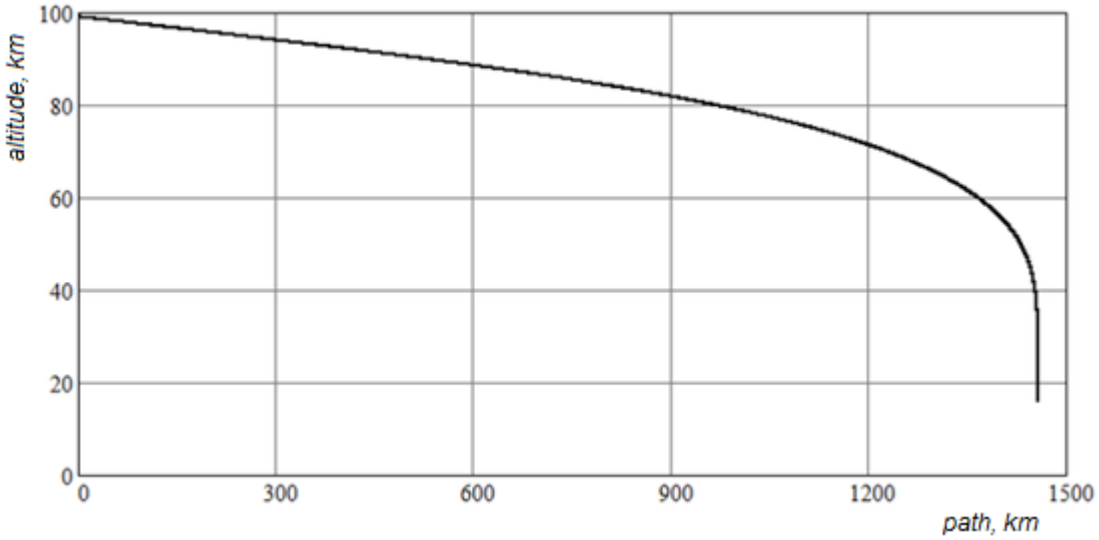

Figure 5.14 – The trajectory of centre of mass

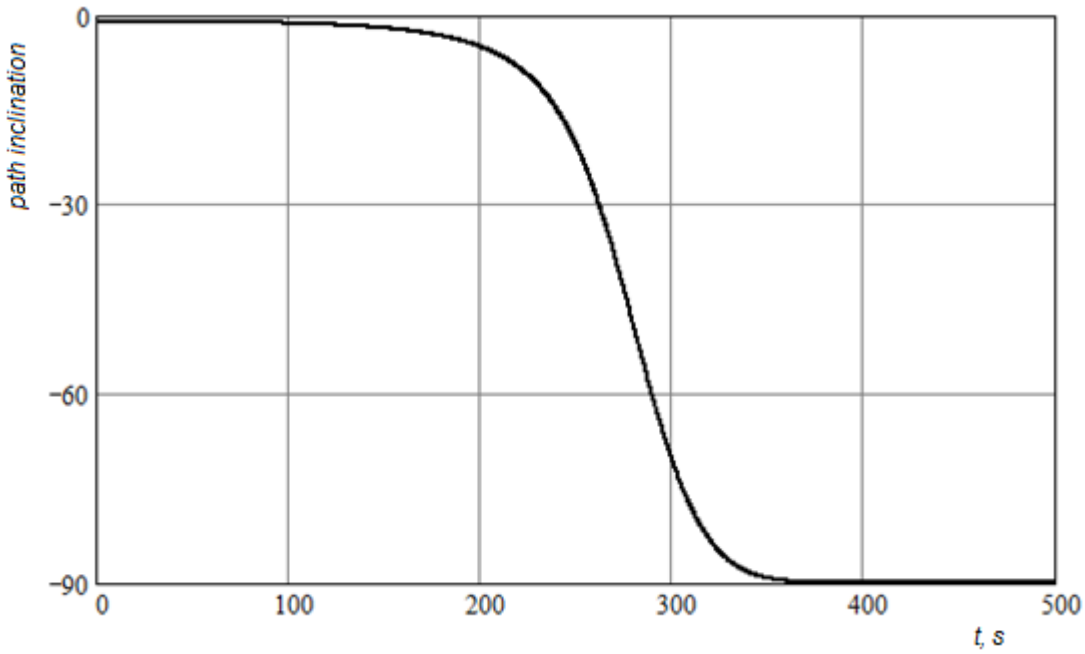

Figure 5.15 – Path inclination

5.4. How to choose the parameters of the tether system

The choice of parameters of the tether system assumes compliance with a number of practical criteria, including a consideration of the production costs of spacecraft and the total mass of the system. In the context of a spacecraft, the mass criteria is the dominant driver for design decision because any additional launch weight would mean a significant increase in total cost of the space flight. Therefore, the research in this chapter is focused on the choice of parameters based on the minimization of the mass of the aerodynamic stabilizer. The parameters being chosen here are the mass, the geometrical dimensions of the stabilizer, and the length of the tether. It is considered that the dimensions of the stabilizer can be changed without changing its shape, thus keeping its geometrical proportions, thus only a single dimension scaling parameter is needed.

It is necessary to take into consideration that there are several types of limitation on the parameters of motion of the tether system.

Firstly, there are limitations on the values of angles of attack. These limitations are closely related to the conditions of the stability of the tether system.

Secondly, there are limitations on the angular velocities. These limitations are checked to ensure that the system meets the requirements for the angles of attack. High angular velocities lead to significant local accelerations, and, as a result, to the destruction of the

system. The values of the angular velocities depend on the natural frequencies of the system, so it is expected that the limitations on angular velocities are satisfied when the natural frequencies are within their limits.

The third limitation is the limitation on the value of the tension of the tether. Should the value of tension force exceed the tether material allowable, the tether will fail and the tether system will be destroyed.

The fourth limitation type is related to the motion of centre of mass of the tether system. Such limitations include the maximal acceleration of the centre of mass, the maximal value of heat flux, and other such limits. These limitations are not related to the parameters of the tether system itself but are determined by the deployment and operational environment. In this case, the critical environment is that of entry into the high-density layers of the atmosphere at altitudes about 100-110 km above the sea level. The parameters of entry include the entry velocity and flight path angle. These limitations are considered out of scope for this thesis.

If a check for any group of limitations fails, when it is inacceptable solution.

As discussed above, it is possible to define the task of choosing the parameters of the tether system. A choice of parameters for the aerodynamic stabilizer, and for the length of the tether, is/should be based on the minimization of the mass of the stabilizer, while considering the limitations of rotary motion within the tether system and tension of the tether.

The values of the natural frequencies of the system are of great importance during the design process. On this basis, it is possible to define an inverse problem: to set up the natural frequencies of the system and to determine the parameters of the tether system basing on these values. As the selected parameters let us take the mass of the stabilizer m_2, its reference area S_2, and the tether length r_3.

To identify the design properties listed, the terms in the brackets in equation (5.3) should be considered. From these the further non-linear algebraic equation system can be obtained, relative to the parameters selected:

$$\begin{aligned}
\frac{q_\lambda}{p_\lambda} &= f_1(m_2, S_2, r_3) = \omega_1^2 + \omega_2^2 + \omega_3^2, \\
\frac{r_\lambda}{p_\lambda} &= f_2(m_2, S_2, r_3) = \omega_1^2\omega_2^2 + \omega_1^2\omega_3^2 + \omega_2^2\omega_3^2, \\
\frac{t_\lambda}{p_\lambda} &= f_3(m_2, S_2, r_3) = \omega_1^2\omega_2^2\omega_3^2,
\end{aligned} \tag{5.4}$$

where $f_i(m_2, S_2, r_3),\ i = 1, 2, 3$ are the functions determined by Equations (5.4).

By solving this system of equations with given natural frequencies, usually it is possible to determine the parameters of the mechanical system. Unfortunately, for a set of frequencies arbitrarily selected during the design process, it is not always possible to find an acceptable solution, because of the nonlinearity of the system (5.4). The following two-stage algorithm overcomes this problem and provides the ability to find an acceptable set of parameters:

1) The admissible values of design parameters m_2, S_2, r_3 are set. As a full set of parameters of the tether system is known, it is possible to calculate the natural frequencies $\omega_1, \omega_2, \omega_3$. This stage solves the direct task.

2) The natural frequencies of the system are set to lower values. The system (5.4) is solved repeatedly, and the values of the design parameters of tether system are iterated. Therefore, this stage solves the inverse task. During this stage, it is necessary to pay attention to the fulfilment of certain restrictions imposed on the selected parameters based on additional conditions. For example, the mass of the aerodynamic stabilizer should not exceed a certain value, the tether should not be too long, and the stabilizer dimensions should not be too big.

As it will be shown below, the values of the natural frequencies have a noteworthy influence on the angular velocities of the system. By using this algorithm, it is usually possible to reduce the initial frequencies of the system by several times thus decreasing angular velocities.

It should be noted that the natural frequencies of the system change during descent in the atmosphere, since they depend on the dynamic air pressure q, and hence on the altitude of flight; however, when realizing the algorithm, the altitude or the dynamic air pressure can be set in an arbitrary way, since the decrease in frequencies at a given altitude leads to the decrease of the system frequencies along the entire descent.

As an example of application of this algorithm, the descent of a tether system consisting of a cylinder shaped spacecraft and a spherical stabilizer is considered here. The key parameters of the system are shown in Table 5.2. These parameters are fixed during the selection process. The parameters for selection are listed in Table 5.3. They include parameters of the stabilizer and the length of the tether. These parameters are chosen to find how to reduce the angular velocities for a landing module with a commonly used cylindrical shape. Here, the design limitation on the minimum mass of the stabilizer is set to 1 kg.

Table 5.2 – The key parameters of the tether system and their values

The parameter	Variable	Value
Mass of the spacecraft	m_1	10 kg
Reference area of the spacecraft	S_1	0.2 m^2
Aerodynamic force coefficients for the spacecraft	C_{x1}	-1
	C_{y1}	5
Aerodynamic force coefficients for the stabilizer	C_{x2}	-1
	C_{y2}	1

Table 5.3 – The parameter values selected

The parameter	Variable	Value
Mass of the stabilizer	m_2	1.5 kg
Reference area of the stabilizer	S_1	0.1 m^2
Length of the tether	r_3	15 m

These parameters correspond to the values of frequencies equal to $\omega_1 = 2$ 1/s, 59.4 1/s and 5 1/s, calculated at dynamic pressure of the air flow $q = 1000$ m/s^2.

During implementation of the algorithm for the choice of parameters, the inverse task was solved several times, and, as a result, the modified/updated parameters $m_2 = 1$ kg, $S_2 = 0.2$ m^2, $r_3 = 10$ m were found. The values for frequencies for these systems are lower than for the initial system, $\omega_1 = 0.1$ s^{-1}, $\omega_1 = 34$ s^{-1}, $\omega_1 = 19$ s^{-1}. A further reduction in frequencies would be possible only by increasing the mass of the stabilizer at the design stage, but even this increase is possible only up to critical value, which for the tether system considered is equal to 1.9 kg. Should the mass of the stabilizer exceed this critical value, the condition of stability would be lost and the motion would become unstable.

Figures 5.16-5.19 show how the angles of attack of the spacecraft, the stabilizer, the tether, and the tension of the tether changed after the modification of the parameters. The angular velocity values are lowered significantly, and the maximal value of the tension force of the tether is reduced by more than 17 percent (from 226.2 N to 186.9 N).

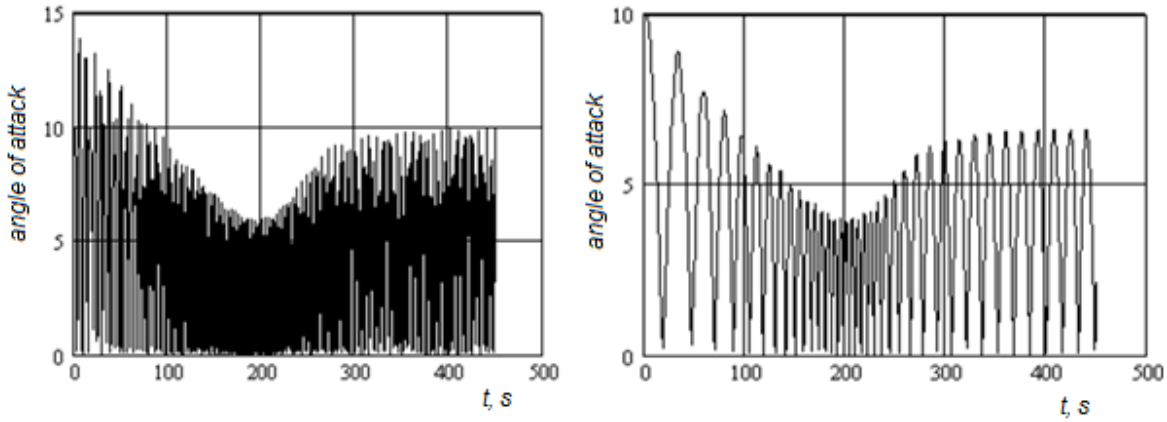

Figure 5.16 – Angle of attack of the spacecraft before and after the corrections

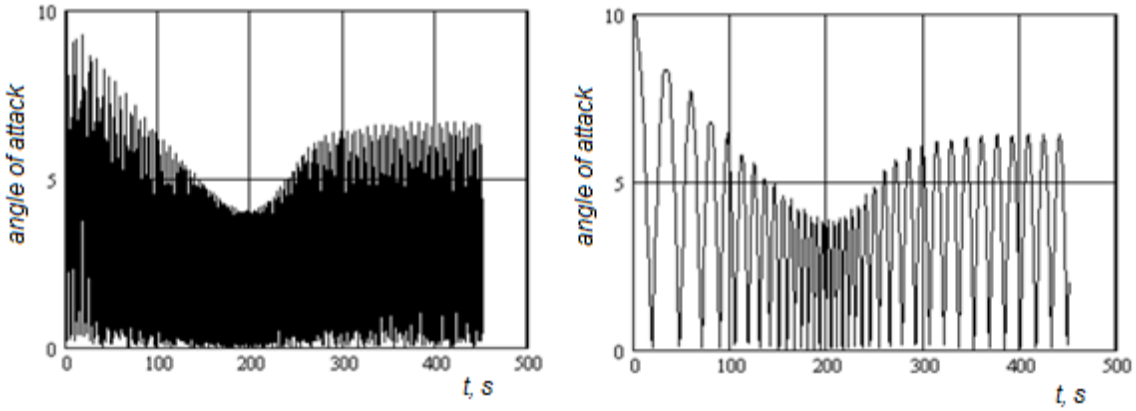

Figure 5.17 – Angle of attack of the stabilizer before and after the corrections

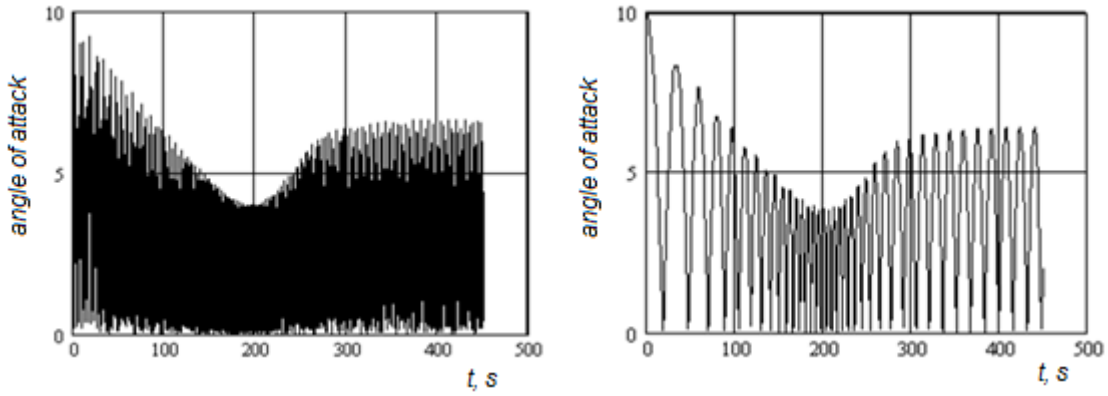

Figure 5.18 – Angle of attack of the tether before and after the corrections

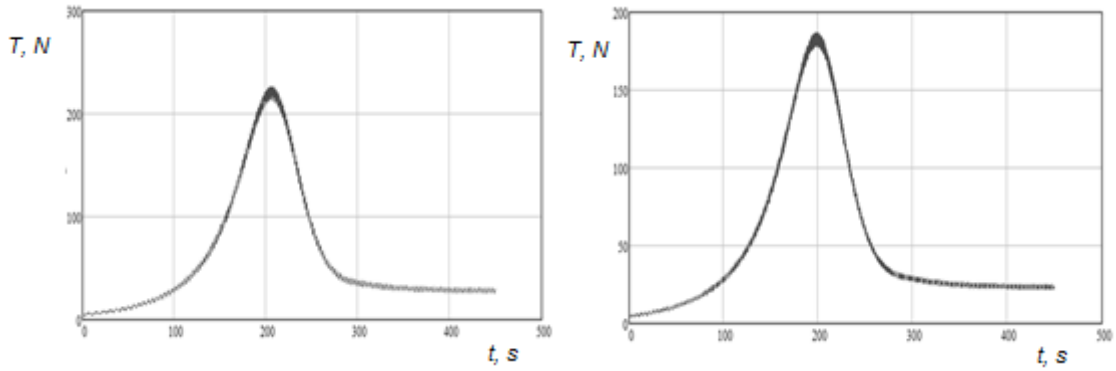

Figure 5.19 – Tension of the tether before and after the corrections

5.5. Impact of the deployment of the tether on the stability

During the analysis of the stability of motion of the tether system in the atmosphere it was assumed that the tether length is constant. On the other hand, the study of the tether system behaviour when the tether length varies is a key topic of interest for this thesis. The tether length variation can take place, for instance, during the deployment process of the tether system, or it can be used as an additional stabilizing factor during the motion through the dense layers of the atmosphere. In either case, it is necessary to assess the impact of the change of tether length on the stability of motion of the system in the atmosphere.

It is possible to assess the tether length variation by evaluating the derivative of spacecraft to stabilizer position vector $\vec{r_3} = \{x_3, 0, 0\}$ with respect to time, taking into consideration the variation of its length

$$\frac{d^2\vec{r}_3}{dt^2} = \dot{\vec{\omega}}_3 \times \vec{r}_3 + \vec{\omega}_3 \times (\vec{\omega}_3 \times \vec{r}_3) + 2\left(\vec{\omega}_3 \times \frac{\tilde{d}\vec{r}_3}{dt}\right) + \frac{\tilde{d}^2 r_3}{dt^2},$$

where $\tilde{d}\vec{r}_3/dt$, $\tilde{d}^2 r_3/dt^2$ are local derivatives of vector $\vec{r}_3$ in the coordinate system bound to the tether. After inserting this value into Equation (4.7), it is possible to obtain the variation of tether tension by means of variating its length:

$$\Delta\vec{T}_1 = \frac{m_1 m_2}{m_1 + m_2} \cdot \left[\frac{\tilde{d}^2\vec{r}_3}{dt^2} + 2\left(\vec{\omega}_3 \times \frac{\tilde{d}\vec{r}_3}{dt}\right)\right] \tag{5.5}$$

In this case additional summands will appear in right hand sides if vector B in the dynamic equations of motion of the system (4.12). These additional summands are listed in Appendix A.

Now consider the variation of the tether length. The dynamic equations for the flat motion of the tether system with respect to the change of the length of the tether can be written as:

$$(I_1 + m_{12}r_1^2)\frac{d\omega_1}{dt} + m_{12}r_1r_2\frac{d\omega_2}{dt}\cos(\alpha_1 - \alpha_2) + m_{12}r_1r_3(t)\frac{d\omega_3}{dt}\cos(\alpha_1 - \alpha_3) =$$
$$= \Delta R_x r_1 \sin\alpha_1 - \Delta R_y r_1 \cos\varphi_1 + m_{12}r_1r_2\omega_2^2 \sin(\alpha_2 - \alpha_1) +$$
$$+m_{12}r_1r_3(t)\omega_3^2 \sin(\alpha_3 - \alpha_1) +$$
$$+r_1 m_{12}\left[\frac{d^2r_3}{dt^2}\sin(\alpha_1 - \alpha_3) - \frac{dr_3}{dt}\omega_3\cos(\alpha_1 - \alpha_3)\right],$$

$$(I_2 + m_{12}r_2^2)\frac{d\omega_2}{dt} + m_{12}r_1r_2\frac{d\omega_1}{dt}\cos(\alpha_1 - \alpha_2) + m_{12}r_2r_3(t)\frac{d\omega_3}{dt}\cos(\alpha_3 - \alpha_2) =$$
$$= \Delta R_x r_2 \sin\alpha_2 - \Delta R_y r_2 \cos\alpha_2 + m_{12}r_1r_2\omega_1^2 \sin(\alpha_1 - \alpha_2) +$$
$$+m_{12}r_2r_3(t)\omega_3^2 \sin(\alpha_3 - \alpha_2) +$$
$$+r_2 m_{12}\left[\frac{d^2r_3}{dt^2}\sin(\alpha_2 - \alpha_3) - \frac{dr_3}{dt}\omega_3\cos(\alpha_2 - \alpha_3)\right],$$

$$m_{12}r_2\frac{d\omega_2}{dt}\cos(\alpha_2 - \alpha_3) + m_{12}r_1\frac{d\omega_1}{dt}\cos(\alpha_1 - \alpha_3) + m_{12}r_3(t)\frac{d\omega_3}{dt} =$$
$$= \Delta R_x \sin\alpha_3 - \Delta R_y \cos\alpha_3 + m_{12}r_1\omega_1^2 \sin(\alpha_1 - \alpha_3) +$$
$$+m_{12}r_2\omega_2^2 \sin(\alpha_2 - \alpha_3) - m_{12}\omega_3\frac{dr_3}{dt}.$$

During the motion of the tether system in the atmosphere, the deployment of the tether should be possible under the action of aerodynamic forces only. Therefore, only models corresponding to increasing the tether length, $dr_3/dt \geq 0$, are considered below. The study of the impact of the variation of the tether length was made by the numerical calculations using different model of deployment.

The descent of the system in the atmosphere was modelled from an altitude of 100 km and with a predicted duration of approximately 500 sec. Three different models for the change of tether length are considered here: a linear model, an arctangent model, and a cubic model.

The linear model means that length of the tether varies linearly with time, so that the rate of change of the length of the tether is constant during the descent process (Figure 5.20a).

The arctangent model corresponds to the case when the rate of change of the length of the tether dr_3/dt possesses maximum value in the area of maximum dynamic pressure of the airflow (Figure 5.21a).

The cubic model of the tether length increase refers to the case where the rate of change of the length of the tether is greater at the beginning of the descent and before landing than in the intermediate stages (Figure 5.22a).

The results for each model of the change of tether length are compared with results for the tether of constant length, which is taken to be equal to trajectory average for each given model.

The results of modelling are shown in Figures 5.20-5.22. Numerical calculations show that the amplitudes of the oscillations of the angles of attack decrease during the descent, for the spacecraft, the stabilizer, and the tether. This means that the increase of tether length always plays a more steadying role in comparison with motion with the tether of constant length.

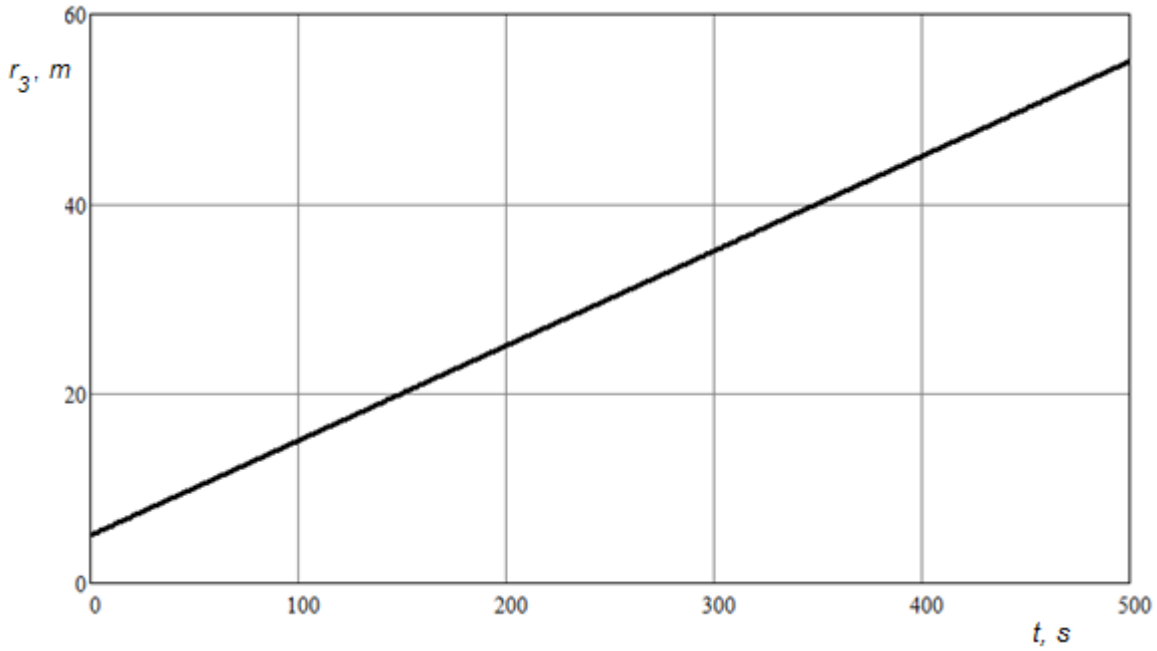

Figure 5.20a – Tether length variation (linear model)

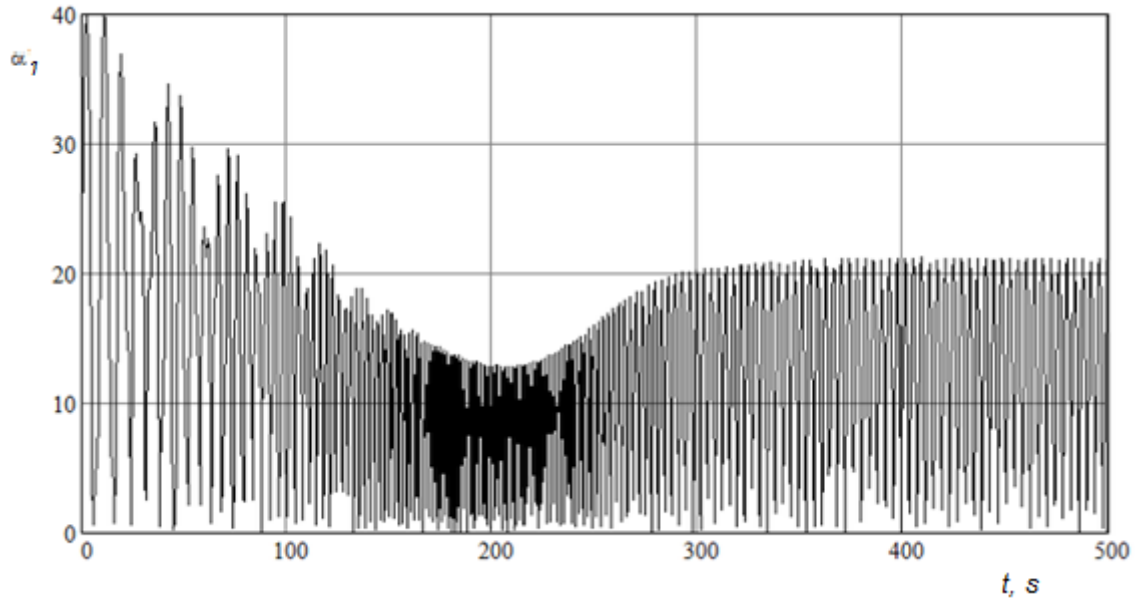

Figure 5.20b – Calculation with constant tether length (linear model)

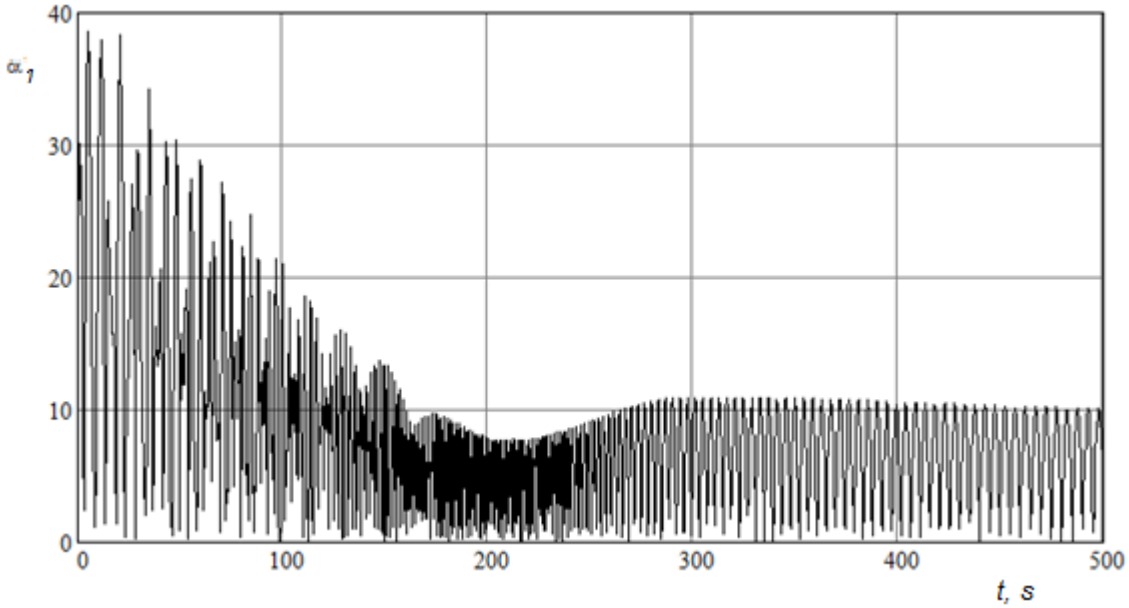

Figure 5.20c – Angle of attack for the system with increasing tether length (linear model)

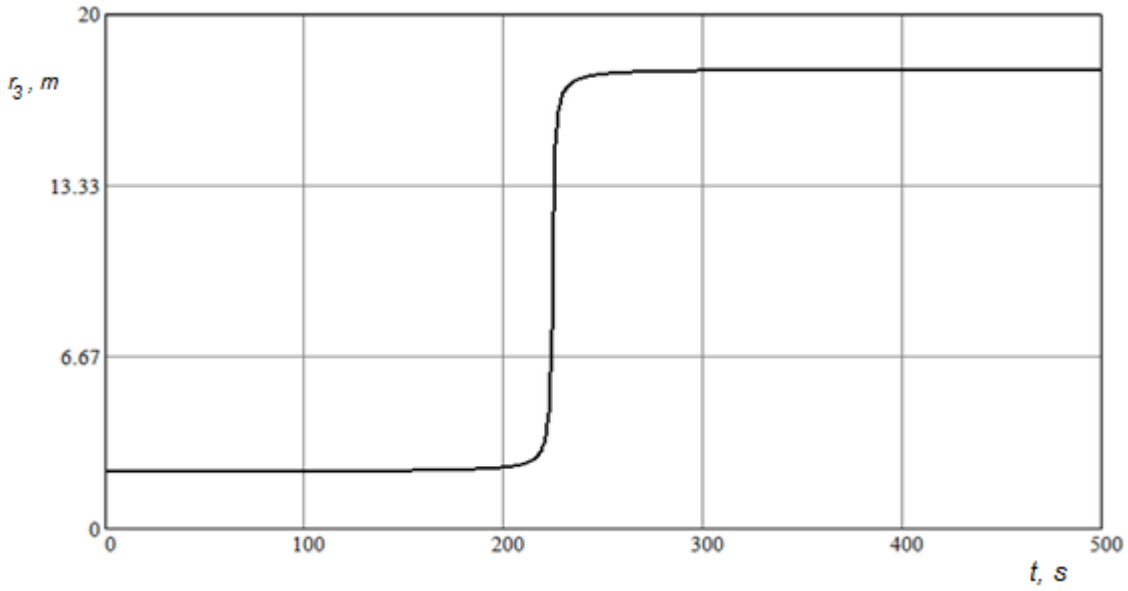

Figure 5.21a – Tether length variation (arctangent model)

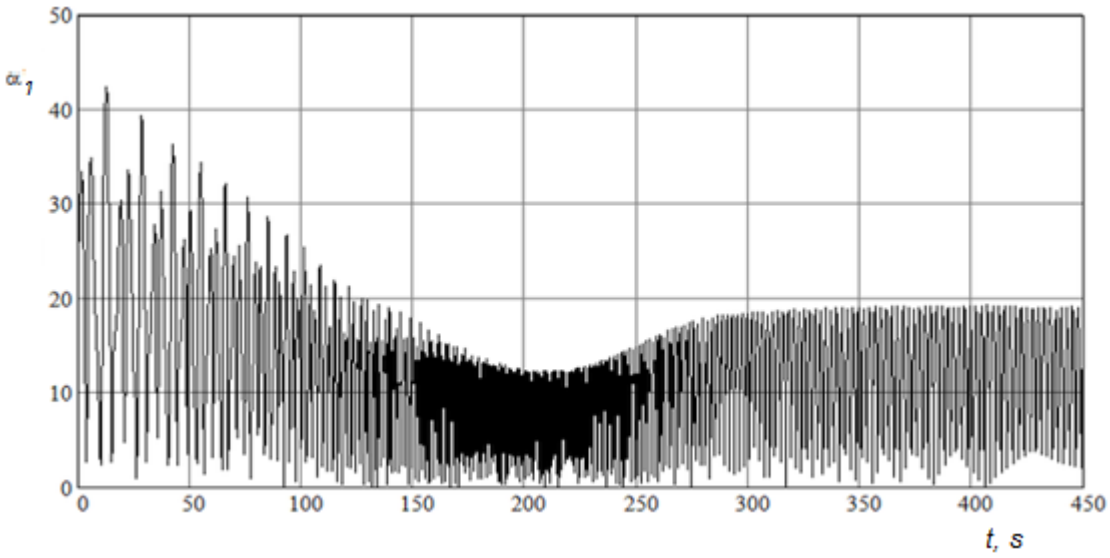

Figure 5.21b – Angle of attack for the system with constant tether length (arctangent model)

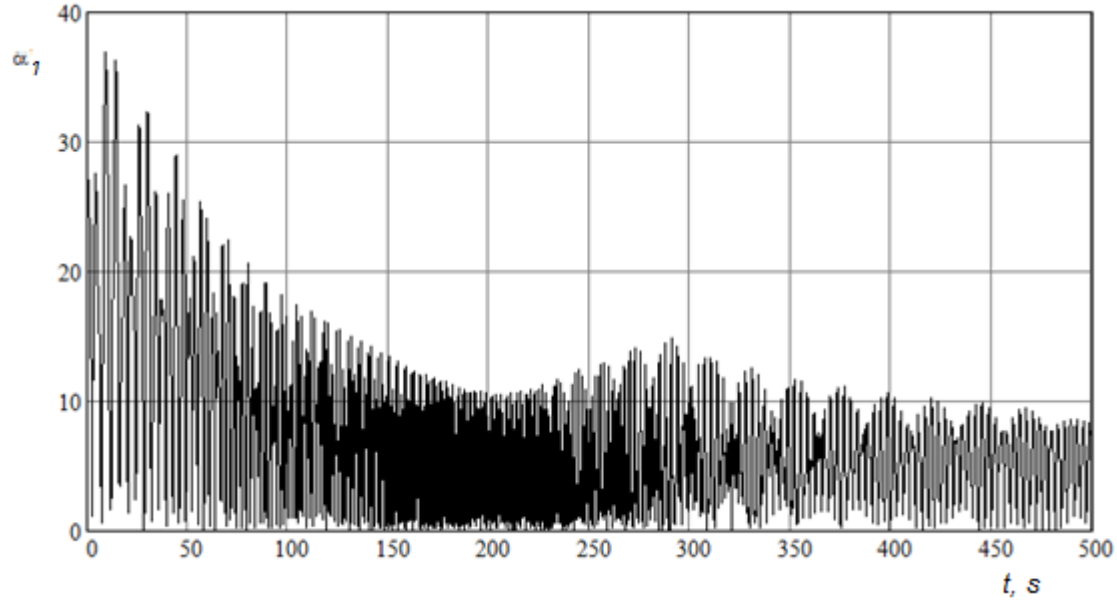

Figure 5.21c – Angle of attack for the system with increasing tether length (arctangent model)

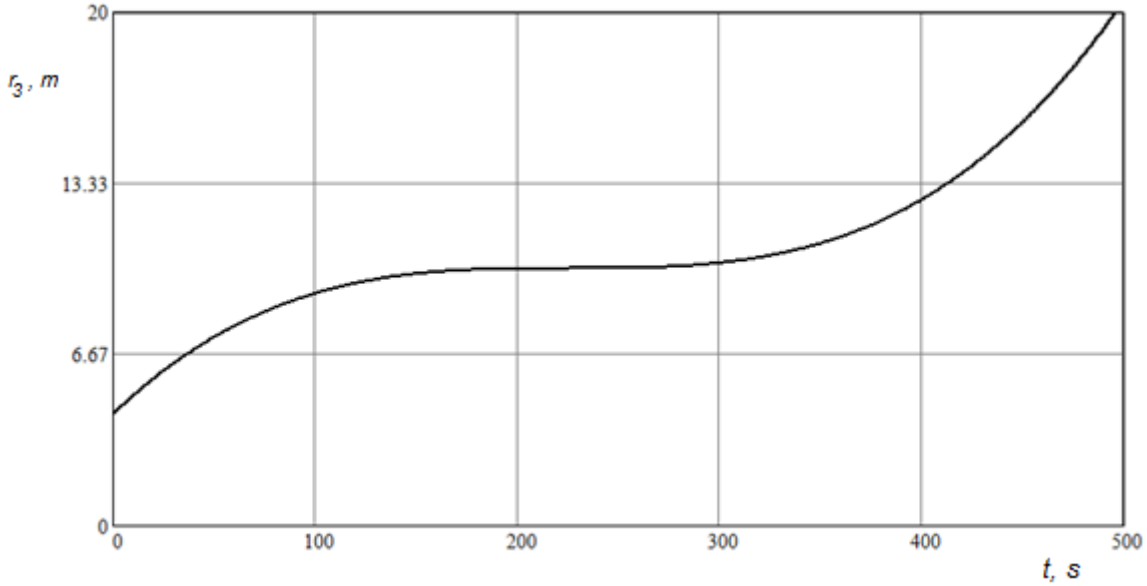

Figure 5.22a – Tether length variation (cubic model)

When the length of the tether increases sharply (arctangent model), the dramatic decrease of the angle-of-attack of the stabilizer and of the tether may appear as it is shown in Figures 5.22 and 5.23. This stems from the fact that the mass of the stabilizer is about three times smaller than the spacecraft mass for this tether system.

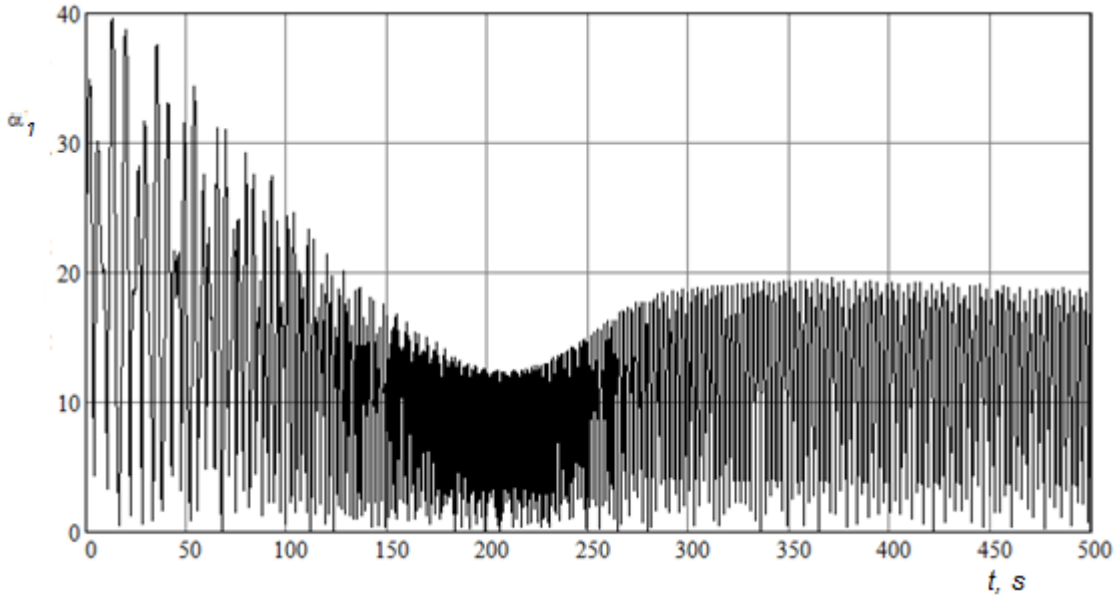

Figure 5.22b – Angle of attack for the system with constant tether length (cubic model)

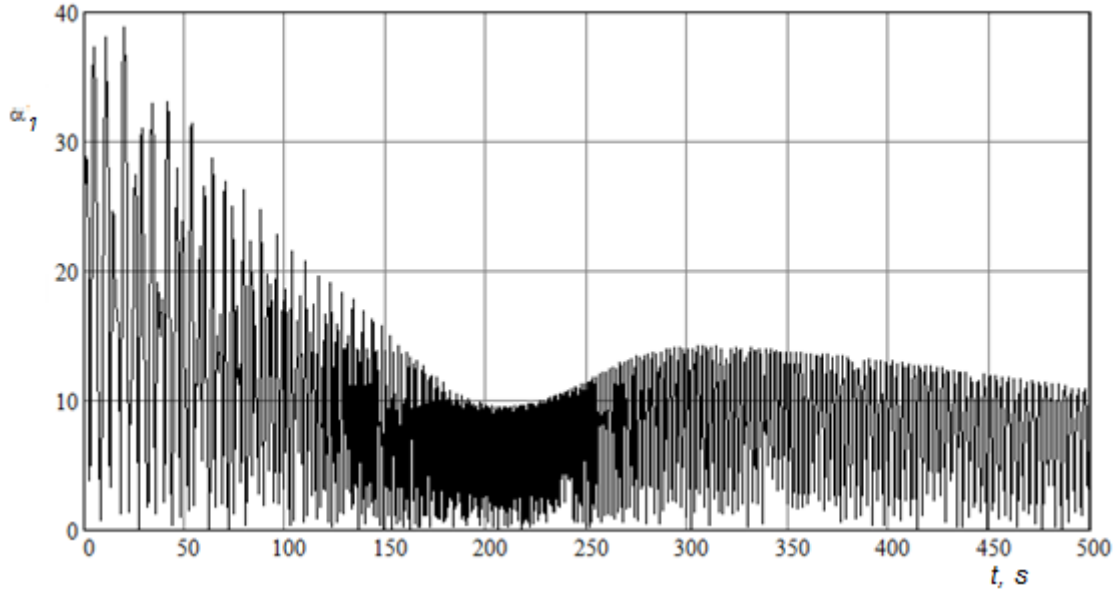

Figure 5.22c – Angle of attack for the system with increasing tether length (cubic model)

As can be seen from the above, the increase of the tether length during the descent always leads to stabilization of the system motion. There is a corresponding decrease in the oscillation amplitudes of angles of attack of the spacecraft, the stabilizer and the tether. Therefore, the increase of the tether length during the descent can be an additional stabilizing factor that improves the stability properties of the tether system.

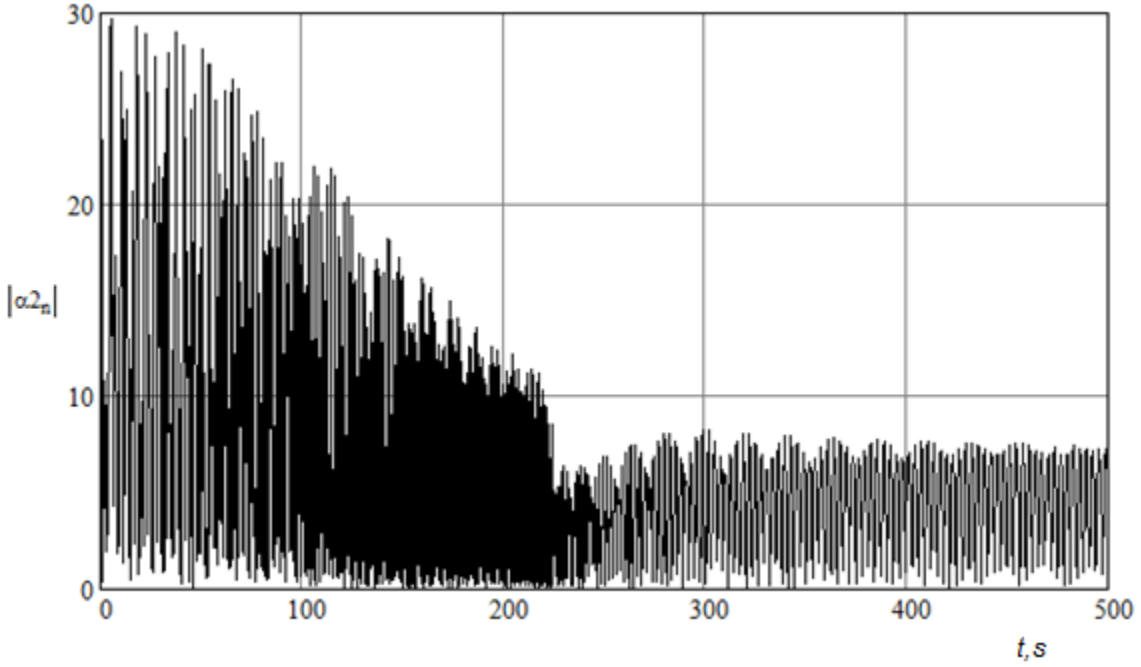

Figure 5.23 – The angle of attack of the stabilizer

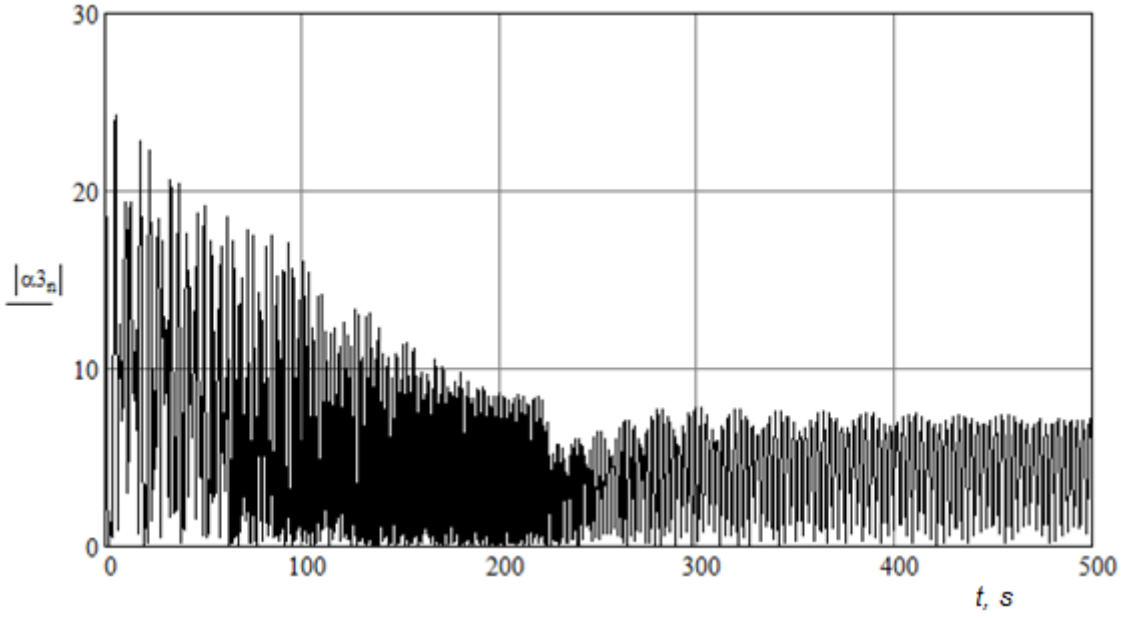

Figure 5.24 – The angle of attack of the tether

5.6. Summary

1. The concept of stability for the motion of the tether system is defined in terms of the parameters of the system: mass, stabilizer shape and dimensions, and tether length.
2. The dependencies of stability and natural frequencies on the parameters of the system are determined. The natural frequencies decrease with increased stabilizer mass, but upon reaching a critical value of mass the system loses its stability.
   Increasing the length of the tether has no significant effect on the values of the frequencies: the frequencies converge asymptotically to the limit values.
3. The tension of the tether depends most significantly on the geometrical dimensions of the stabilizer, while length of the tether has only a slight influence on this force.
4. For design purposes the parameters of the stabilizer and tether length must meet the requirements for the parameters of motion of the tether system in the atmosphere. The mass of the stabilizer should be minimized during this process.
   The proposed algorithm for choosing the parameters is based on solving the inverse problem, where the parameters are defined on the basis of frequencies. This algorithm enables a significant reduction of the frequencies in most cases.
5. The increase of the tether length during the descent always leads to a more stable motion of the tether system. This leads to a reduction in the amplitudes of oscillations of angles of attack for the spacecraft, the stabilizer, and the tether. Therefore, the deployment of a tether during descent can increase the stability of the system.

6. DEPLOYMENT OF AN AERODYNAMIC TETHER SYSTEM

This chapter is focused on the deployment of the tether system, taking account of aerodynamic effects. The deployment process is based on the aerodynamic forces acting on bodies. The initial condition for the deployment model is that of a spacecraft with a rigidly connected stabilizer in a circular orbit about the planet. As has been demonstrated in the previous chapter, when one of the bodies in the tether system – the stabilizer – has a significantly higher ballistic coefficient, the tension of the tether should be sufficiently high to enable the deployment of the tether system. After the separation of the rigid connection between the spacecraft and stabilizer, their further motions are then controlled by the tether release mechanism. The tether release mechanism unreels the tether and controls the rate at which the tether is unreeled, but by its construction is not able to pull the tether back in. Different methods of deployment and system dynamics are investigated. These investigations enable the analysis of the motion of systems comprising a lightweight and relatively short tether, and those with a longer tether.

6.1. The mathematical model of the deployment

As it has been shown in the previous chapters, by changing the parameters of the stabilizer it is possible to obtain stable motion. As before, the stable motion means the pre-defined orientation of the tether system. In this context, stable motion is defined such that the angles between the longitudinal axis of bodies and tether do not exceed 90 degrees. The same restrictions are applied to the angles of attack of the bodies and the tether – they should also be less than 90 degrees.

The parameters for the body moving through the air of the upper atmosphere include the mass, the reference area and the drag coefficient. It is possible to define the ballistic coefficient of the rigid body as the combinations of these parameters, $\sigma = C_{xv}S/m$, where C_{xv} is the drag coefficient, S is the reference area, and m is mass. Thus, through the design of the tether system, the stabilizer has a significantly higher ballistic coefficient in comparison with the spacecraft.

This chapter is focused on the deployment process and on the motion of the tether system during deployment. The initial condition for the mathematical model is in a circular orbit at an altitude of about 250 km prior to the separation of the spacecraft and stabilizer.

The mathematical model takes into consideration the extensibility of the tether so that the influence of deployment method on the motion of the system can be estimated. The mass and geometrical asymmetries of the spacecraft and the stabilizer, which are modelled as rigid bodies, are also taken into consideration. The aerodynamic deceleration during the descent from planetary orbit is included within the mathematical model.

The separation of bodies starts with a comparatively low relative velocity $\vec{V}_r$. After the separation of the rigid connection between the spacecraft and stabilizer, their further motion is then controlled by the tether release mechanism. The tether release mechanism unreels the tether, but is not able to pull the tether back in to simplify the construction of the release mechanism and reduce its mass, therefore the equations of motion of the system include a monotonic deceleration term representing the tether release mechanism. Specific features of the regulation system such as discrete work, design tolerances, etc., are not taken into consideration. The tether itself works in tension only.

The deployment of the stabilizer body is controlled through the deceleration of the tether. The deceleration control device is situated on the spacecraft.

The mathematical model describes the process of deployment as well as further motion of the tethered system, and includes a perturbation analysis.

The aerodynamic resistance of the tether and its mass characteristics are both taken into consideration in the calculation. Different methods of deployment are investigated, and assessed using mathematical system dynamics techniques. These investigations have enabled the comparison of the motion of systems comprising a light-weight and relatively short tether with those with a longer tether.

The mathematical model of the motion during deployment uses the geocentric coordinate system $Oxyz$, which is bound to the plane of the orbit of the centre of mass of the tether system. The plane of the orbit is defined at the moment of separation of the stabilizer from the spacecraft. The Ox axis is directed to the ascending node of the orbit, the Oz axis is parallel to the vector of total angular momentum of the centre of mass of the system.

The spacecraft and stabilizer are rigid bodies of finite length, which are connected by the tether (Figure 6.2). Coordinate systems associated with bodies $Cx_iy_iz_i$ are used to define the moments of inertia for each of the bodies.

The stability is considered lost when the angles ψ_i between longitudinal axis $C_i x_i$ and vector $\vec{r}_{ab}$ become higher than $\pi/2$, or when the angles of attack α_i become higher than $\pi/2$. The ideal orientation of the tether system means that the longitudinal axes $C_i x_i$ and the tether are co-linear with the vector of the velocity of the centre of mass of the tether system. Thus, the angle between the vector of the tether and the vector of velocity of the centre of mass defines the orientation of the spacecraft.

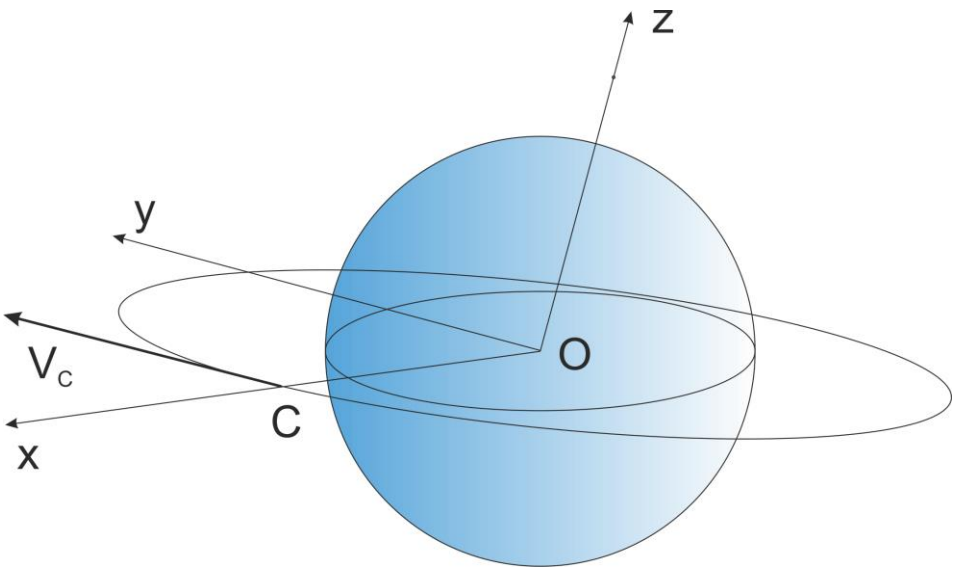

Figure 6.1 – Coordinate system

The equations of motion of this system include the equations for the motion of the centres of mass

$$m_i \frac{d^2 r_i}{dt^2} = \vec{g}_e(r_i) + \vec{T}_i + \vec{R}_i \tag{6.1}$$

and the non-linear equations of rotational motion of the bodies in the form of Euler's dynamic equations (Peraire, 2009)

$$\begin{aligned} I_{xi}\frac{d\omega_{xi}}{dt} + \omega_{yi}\omega_{zi}(I_{zi} - I_{yi}) &= l_{xi}, \\ I_{yi}\frac{d\omega_{yi}}{dt} + \omega_{xi}\omega_{zi}(I_{xi} - I_{zi}) &= l_{yi}, \\ I_{zi}\frac{d\omega_{zi}}{dt} + \omega_{xi}\omega_{yi}(I_{yi} - I_{xi}) &= l_{zi}, \end{aligned} \tag{6.2}$$

where indexes $i = 1$ and $i = 2$ refer to the spacecraft and the stabilizer respectively, m_i are masses and r_i are radius-vectors of centres of masses for both bodies, $\vec{g}_e(r_i)$ and $\vec{R}_i$ are gravitational and aerodynamic forces, t is the elapsed time during tether deployment starting

from the instant of separation, $\vec{T}_i$ is the tension force of the tether, $\vec{T}_1 = -\vec{T}_2$, I_{xi}, I_{yi}, and I_{zi} are the moments of inertia in bound to the bodies coordinate systems $Cx_iy_iz_i$; ω_{xi}, ω_{yi}, ω_{zi} are components of angular velocities of the bodies; and l_{xi}, l_{yi}, l_{zi} are components of the net total angular momentum that act on each of the bodies.

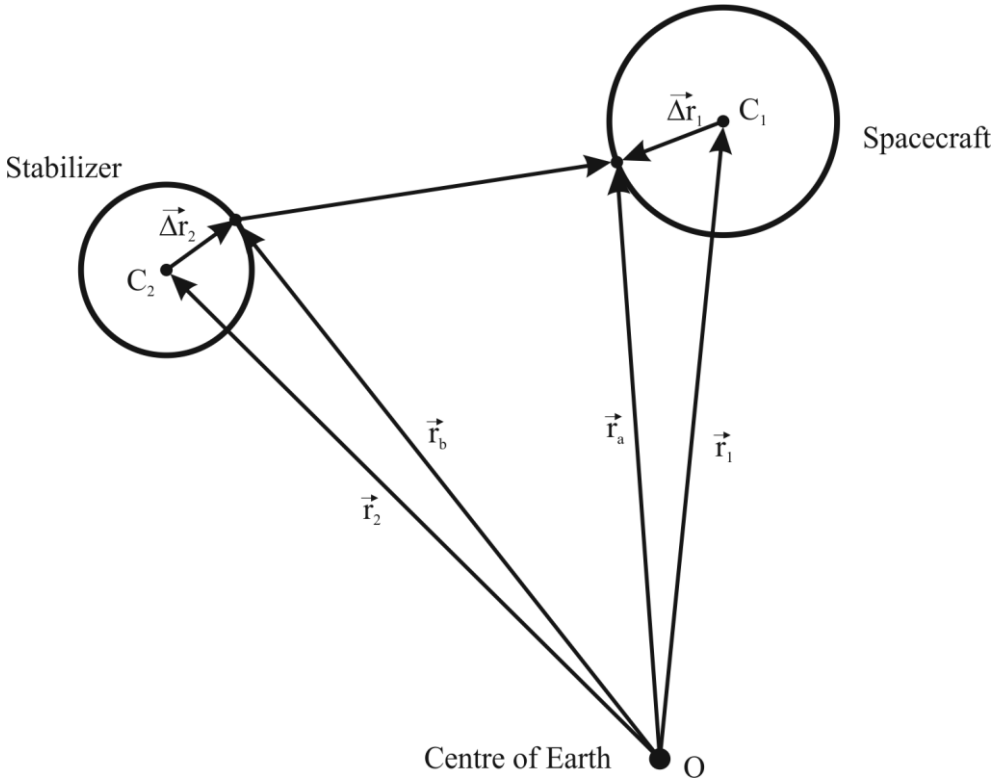

Figure 6.2 – Tether system on the orbit of the planet

In the modelling of the motion of the system, the torques from aerodynamic forces and torques arising from the tension forces are taken into consideration. The torques from gravity forces have not been included because they can be shown to be negligibly small (Zabolotnov, 2012). The tension force is defined by Hooke's law for one-sided mechanical connection.

$$\vec{T}_2 = T\frac{\vec{r}_{ab}}{r_{ab}},$$

where $\vec{r}_{ab} = \vec{r}_a - \vec{r}_b$ (as shown in figure 6.2), $\vec{r}_a$ and $\vec{r}_b$ are radius vectors for the tether attachment points. The value of T is equal to zero when r_{ab} is less than the length L_{ND} of non-deformed tether, and $T = k\,(\mathrm{r_{ab}} - L_{\mathrm{ND}})/L_{\mathrm{ND}}$ when $\mathrm{r_{ab}} \geq L_{\mathrm{ND}}$, where k is the spring constant of the tether.

If the tether is not strained, both bodies are moving freely under the action of aerodynamic forces. For modelling purposes, it is presumed that the motion takes place in low density gas and the hypothesis of diffuse reflection of gas molecules is applicable (Maxwell, 1867). Based on this hypothesis, vectors of the aerodynamic forces are co-linear with the vectors of velocities of the bodies defined relative to the atmosphere

$$\vec{R}_i = -\frac{C_i S_i \rho V_i \vec{V}_i}{2}, \tag{6.3}$$

where C_i are drag coefficients, $\rho = \rho(h)$ is the density of the atmosphere and is function of the altitude h, $S_i = S_i(\alpha_i)$ is the square of projection of the body onto the plane which is perpendicular to the velocity vector $\vec{V}_i$, α_i is the angle of attack during the spatial motion, $i = 1, 2$. If the bodies are spherical, S_i is constant.

The velocities $\vec{V}_i$, calculated relative to the atmosphere, can be found using the equation

$$\vec{V}_i = \frac{d\vec{r}_i}{dt} - \vec{\omega}_{\text{Earth}} \times \vec{r}_i,$$

where $\vec{\omega}_{\text{Earth}}$ is the angular velocity of rotation of the Earth.

The gravity forces are defined by Newton's law

$$\vec{g}_e(r_i) = -G\frac{M_E m_i}{|r_i|^2}\vec{r}_i,$$

where G is the gravity constant, M_E is the mass of the Earth.

The dynamics of the tether regulating mechanism are taken into account for modelling of the deployment process, as follows

$$m_u \frac{d^2 r_3}{dt^2} = T - F_{\text{control}}(t), \tag{6.4}$$

where r_3 is the length of the tether, the constant coefficient m_u describes the inertness of the mechanism, $F_{\text{control}}(t)$ is the control force. Then the release of the tether is unguided, the control decelerating force is constant, positive and close to zero. For the guided deployment, the tether release mechanism works on deceleration only, $dr_3/dt \geq 0$. The control force is also greater than zero, $F_{\text{control}}(t) \geq F_{\text{min}} > 0$, where F_{min} is the minimum deceleration force that the tether release mechanism can provide.

The equations of motion of the system should be supplemented by kinematic equations. Here, the Euler angles are used for both bodies in the coordinate systems associated with vectors $\vec{V_i}$ and $\vec{r_i}$. The unit vectors for these systems of coordinates are

$$\vec{e}_{1i} = \vec{V}_i/V_i \,, \vec{e}_{3i} = \vec{V}_i \times \vec{r}_i/\left|\vec{V}_i \times \vec{r}_i\right|, \vec{e}_{2i} = \vec{e}_{3i} \times \vec{e}_{1i}. \tag{6.5}$$

The kinematics equations for Euler angles are

$$\omega_{xi} = \dot{\varphi}_i + \dot{\gamma}_i \cos\alpha_i + \Delta\omega_{xi},$$
$$\omega_{yi} = \dot{\alpha}_i \sin\varphi_i - \dot{\gamma}_i \sin\alpha_i \cos\varphi_i + \Delta\omega_{yi},$$
$$\omega_{zi} = \dot{\alpha}_i \cos\varphi_i + \dot{\gamma}_i \sin\alpha_i \sin\varphi_i + \Delta\omega_{zi},$$

where, $\Delta\omega_{xi}$, $\Delta\omega_{yi}$, and $\Delta\omega_{zi}$ are the corrections to the angular velocities due to the rotation of coordinate systems (6.5),

$$\begin{pmatrix} \Delta\omega_{xi} \\ \Delta\omega_{yi} \\ \Delta\omega_{zi} \end{pmatrix} = L_i^T \begin{pmatrix} 0 \\ 0 \\ \omega_{vi} \end{pmatrix}$$

where $\omega_{vi} = V_i/r_i \, sin\vartheta_i$, $\vartheta_i = \text{acos}\left(\frac{\vec{r}_i \cdot \vec{V}_i}{r_i V_i}\right)$, $L_i = L_{\varphi i} L_{\alpha i} L_{\gamma i}$,

$$L_{\varphi i} = \begin{pmatrix} 1 & 0 & 0 \\ 0 & \cos\varphi_i & \sin\varphi_i \\ 0 & -\sin\varphi_i & \cos\varphi_i \end{pmatrix}, L_{\alpha i} = \begin{pmatrix} \cos\alpha_i & \sin\alpha_i & 0 \\ -\sin\alpha_i & \cos\alpha_i & 0 \\ 0 & 0 & 1 \end{pmatrix}, L_{\gamma i} = \begin{pmatrix} 1 & 0 & 0 \\ 0 & \cos\gamma_i & \sin\gamma_i \\ 0 & -\sin\gamma_i & \cos\gamma_i \end{pmatrix}.$$

After the separation of the stabilizer from the spacecraft, it is necessary to recalculate their velocities using the conservation of linear momentum law (Halliday, 2011)

$$\vec{V}_1 = \vec{V}_C - \frac{m_2}{m_1 + m_2}\vec{V}_2,$$
$$\vec{V}_2 = \vec{V}_C + \vec{V}_r,$$

where $\vec{V}_C$ is the velocity of the centre of mass of the tether system, $\vec{V}_1$ and $\vec{V}_2$ are velocities of the spacecraft and the stabilizer after the separation in geocentric coordinate system.

6.2. Deployment without feedback

The simplest method of the deployment is the *"Release of the tether with a minimal decelerating force until the tether is completely unreeled"*. In this case, $F_{\text{control}}(t) =$

$F_{\text{control}} = F_{\text{min}} = const$. This means that the deployment process is unguided and is provided passively by the difference in ballistic coefficients of spacecraft and stabilizer.

The following calculations are made for the deployment of the tether system starting from the altitude equal to 250 km. The parameters of the tether system are shown in Table 6.1. For these calculations both bodies were assumed to be spherical and statically stable, and the distance between the centre of mass and the centre of aerodynamic pressure was taken equal to 1% of the radius for both the spacecraft and stabilizer as an example of perturbation.

The ballistic coefficient for the spacecraft $\sigma_1 = C_1 S_1 / m_1 = 0.094$, for the stabilizer $\sigma_2 = C_2 S_2 / m_2 = 1.51$.

The results of the modelling show that it is not possible to assure the stability of the angular motion of the bodies even when the tether system has an ideal orientation at the moment of separation. As it stated above, the stability is considered lost when the angle of the longitudinal axis of any of the bodies and the tether exceeds $\pi/2$. The loss of stability occurs as a result of a non-zero value for the tether release rate at the end of deployment. Therefore, when the maximum length of the tether is reached, a shock load is applied within the tether system, and the tether sags periodically. During these moments, the stabilizing effect of tether tension force disappears.

Table 6.1 – Parameters of the tether system

Parameter	**Symbol**	**Value**
Radius of the spacecraft		0.5 m
Radius of the stabilizer		2 m
Drag coefficient of the spacecraft	C_1	2.4
Drag coefficient of the spacecraft	C_2	2.4
Mass of the spacecraft	m_1	200 kg
Mass of the stabilizer	m_2	20 kg
Velocity of separation	V_r	2 m/s
Inertness of the mechanism	m_u	0.2 kg
Control force (constant)	F_{control}	0.01 N
Full (final) length of the tether		2 km

To show how the tether system moves on the orbit during the deployment, it is useful to use the dimensionless time $\tau = t/\mathrm{T}_{\mathrm{orbit}}$, where $\mathrm{T}_{\mathrm{orbit}}$ is the orbit period on the initial orbit. When the dimensionless time τ increases from 0 to 1, it means that the tether system has made one full turn around the planet. The change of altitude during the descent is shown in Figure 6.3. The altitude decreases during the mission, but change in the altitude is not linear because, during the deployment, the second body moves relative to the spacecraft, and in an opposite direction to the direction of flight, thus changing the aerodynamic force. As a result, some oscillations occur in the motion.

Figure 6.4 depicts the dependence of tension of the tether T on dimensionless time τ. As the deployment process is finished, the severe change in tension leads to the sharp increase in the angle of attack of the stabilizer shown in Figure 6.5.

The sharp change in the values of the angle of attack in Figure 6.5 is a result of numerical modelling. As the angle of attack increases sharply, it value calculated numerically reaches the value of π, but since this is calculated from inverse trigonometric functions, the value for the angle of attack in Figure 6.5 does not exceed the value of π. As a result, this figure has physical meaning for angle of attack values of at most.

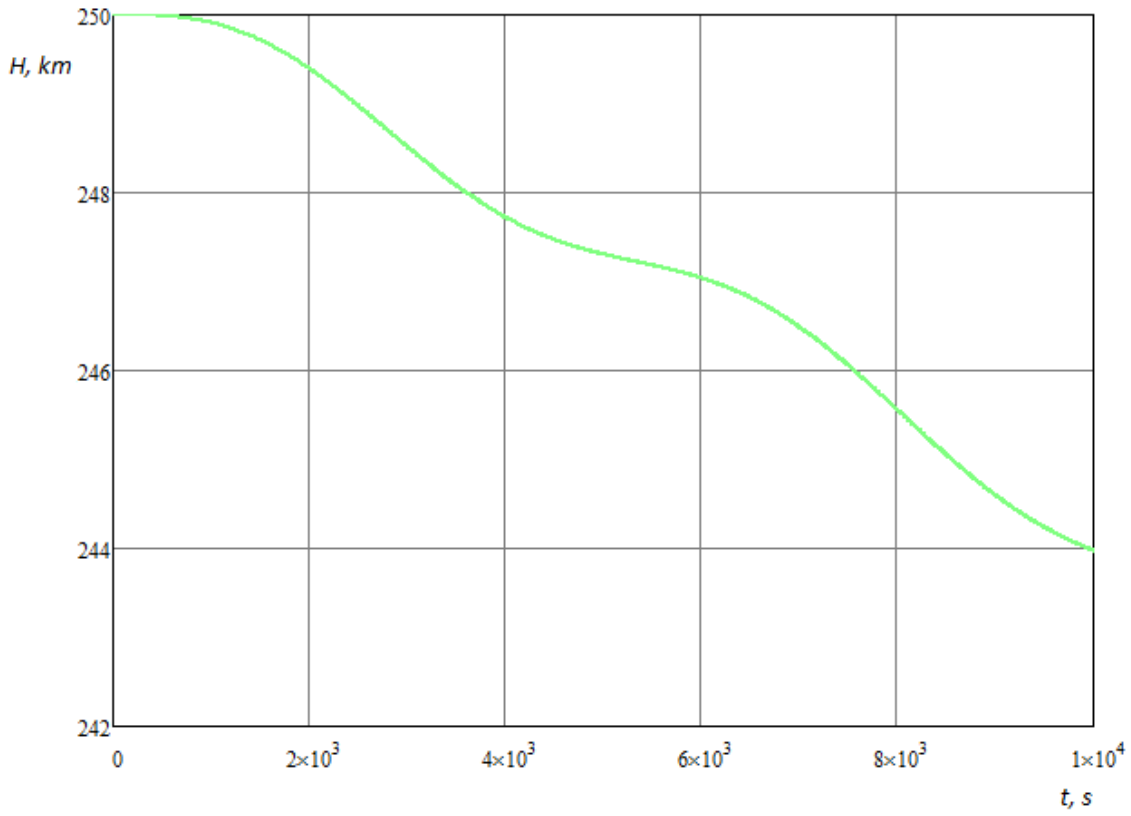

Figure 6.3 – Altitude of the centre of mass

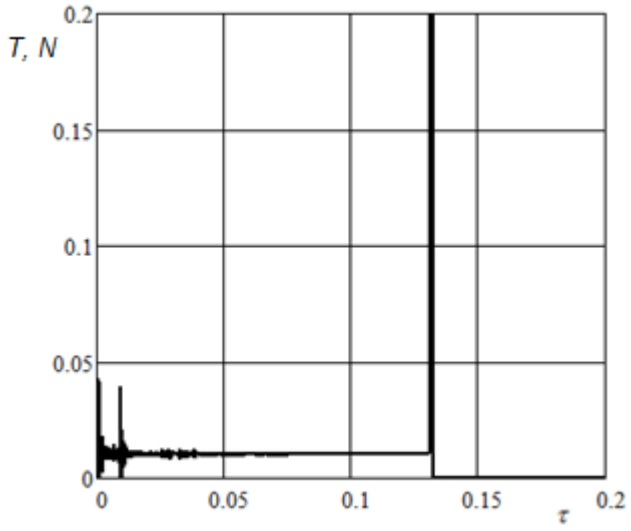

Figure 6.4 – Tension of the tether during the deployment and after it

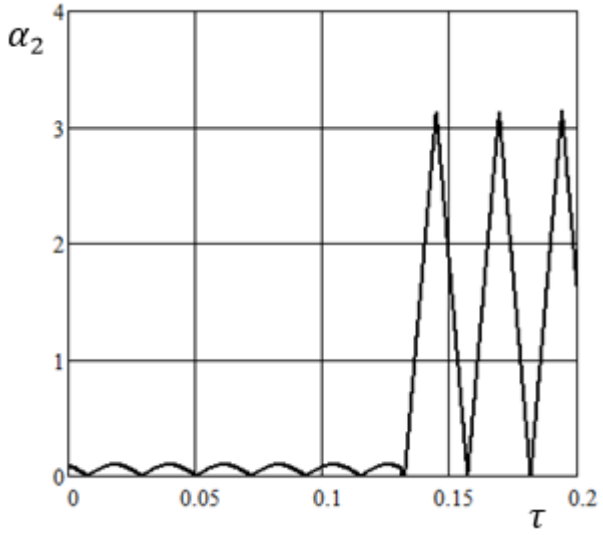

Figure 6.5 – The angle of attack of the stabilizer during the deployment and after it

Here, after the end of the deployment process the angle of attack of the tether becomes higher than $\pi/2$ because of the effect of the gravity. The torque from the gravity force at this altitude is comparable with the torque created by the aerodynamic forces. The torque created by the gravity force compels the tether to move toward the vertical direction thus increasing the angle of attack of the tether. However, during the further motion of the tether system, the altitude decreases, and the influence of the atmosphere causes a decrease of the angle of attack of the tether. Upon reaching the denser layers of the atmosphere, at the

altitudes 100-110 km, the amplitudes of the oscillations of angle of attack of the tether is less than 6 degrees for the specified parameters of the tether system.

6.3. Deployment with a decreasing rate of change of tether length

6.3.1. Continuous deceleration

The condition of stability at the end of deployment can be reached if the rate of change of tether length can be made to equal zero at the end of deployment. This can be done by choosing the value of $F_{\text{control}}(t)$ to meet the specified condition. Here, it is necessary to solve a one-parameter boundary-value problem; however, as a result of this numerical modelling some disadvantages in this method of deployment were discovered.

When the tether is sufficiently long, the boundary-value problem can be solved, and the stability of motion can be obtained by increasing only the value of the initial velocity of separation. For example, to obtain stable motion for the tether system with the parameters listed in Table 6.1, the velocity of separation must be increased to 4.15 m/s. Nevertheless, the value of the velocity of separation is limited by the properties of the separation mechanism, and this increase is not always possible. Here, the decelerating force $F_{\text{control}} = 0.15$ N.

Next, it is necessary to take into consideration the possibility of errors during separation. These errors could arise from tolerance variations at the moment of separation. These errors could occur only in the value of the velocity of separation or, more generally, in the direction of separation. The direction of the separation is defined by the vector of separation $\vec{V_r}$ (§6.1).Should these errors occur, shock loads will propagate in the tether at the moment of the end of deployment, just as is the case of the separation with constant decelerating force.

6.3.2. Length rate of change control

Another condition for the stoppage of tether release is based on setting to zero the rate of change of the length of the tether instead of finishing the deployment at the moment when tether is fully unreeled. This allows a greater range of values of permissible parameter variation during separation.

The variation in velocity of separation resulting from error is defined here as the difference between the actual, time dependent, deployment velocity and its pre-defined program value. Should it be less than zero, the perturbation is negative, and for greater than

zero differences it is possible to talk about the positive perturbation. The perturbation can occur due to manufacturing error, changes in temperature regime or other reasons.

Figure 6.6 shows the dependences of the length of the tether on dimensionless time for tether systems with the parameters listed in Table 6.1, having a negative perturbation of 0.5 m/s in the separation velocity. This error leads to reduction of the final length of the tether of approximately 0.5 km. The tether is held under tension during almost the entire process of the deployment: a sag is possible only at the very beginning of deployment and after the end of deployment, and these perturbations do not lead to a loss of stability. The motion of the system is stable for this example, and the angles of attack are shown in Figure 6.7, and the tether tension is shown in Figure 6.8. Thus, a negative perturbation in separation velocity leads to a decrease in the final deployed length of tether but does not lead to the loss of stability.

For positive perturbations in separation velocity, there is a critical value arising when the value of the decelerating force F_{control} becomes too low to reach the deployment stoppage condition. Instead, the process of deployment terminates when the tether is completely unreeled – in other words, the as-supplied tether is insufficiently long. As a result, the condition that the value of the rate of change of the length of the tether is zero is not met, causing the shock loads. To reduce the negative effect from positive perturbations, it is possible to supply a longer tether into the spacecraft, but practically this solution does not seems to be always possible because of manufacturing restrictions.

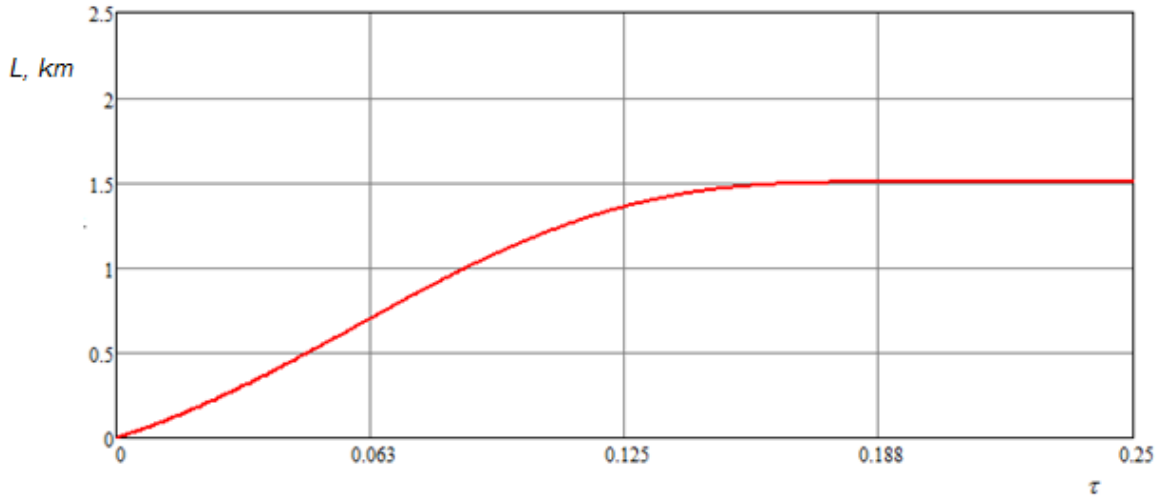

Figure 6.6 – Length of the tether during deployment

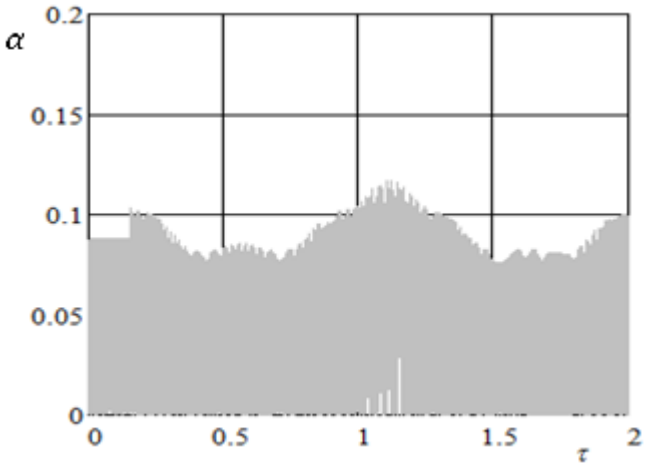

Figure 6.7 – Angle of attack of the stabilizer during deployment

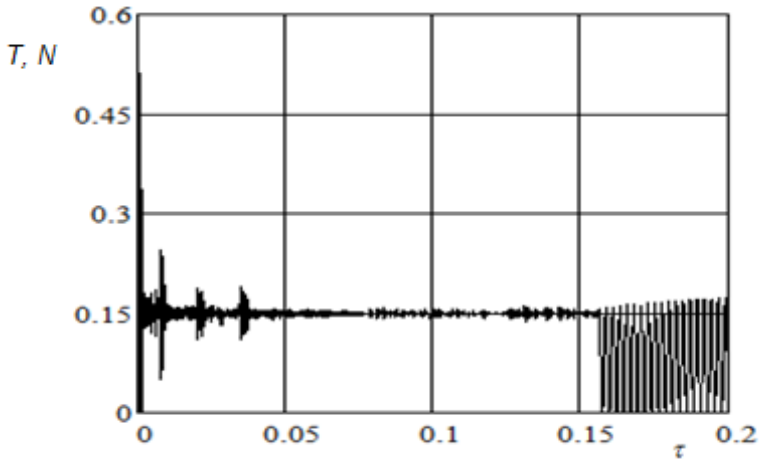

Figure 6.8 – Tension of the tether during deployment

When the errors occur in the direction of the vector of velocity of separation $\vec{V}_r$, the influence of them is determined by the value of the projection of the vector of error $\vec{V}_{\text{er}}$ onto the radius-vector of the centre of mass of the system relative to the centre of the Earth. In general, a positive value of the projection means that the error reduces the value of velocity of separation. Should the value of this projection be greater than zero, the final length of the tether will be reduced because of the early achievement of the deployment finishing condition. Should the value of the projection be less than zero, the condition cannot be achieved before the final length of the tether is reached thus causing the shock loads at the end of deployment.

6.3.3. Dynamic Deployment Law

This dynamic deployment law with constant decelerating force can be improved by mitigating the limitations of the final tether length and by using the ***program dynamic method***, which includes regions of both acceleration and deceleration.

$$F_{\text{control}} = \begin{cases} F_{\min}: & t < t_1 \\ F_{\min} + (F_{\max} - F_{\min}) \sin^2\{k_p(t - t_1)\}: & t_1 \le t \le t_2 \\ F_{\max}: & t > t_2 \end{cases} \qquad (6.6)$$

where $t_1 = t_p + \frac{\pi}{4k_p}$, $t_2 = t_p - \frac{\pi}{4k_p}$, $t_p, k_p > 0$, $F_{\min}$ and $F_{\max}$ are parameters of the method. The value of the control force switches on the bases of time. Parameter k_p defines the smoothness of switching of the value of the control force, and with its infinite increase, t_1 becomes equal to t_2 and the program described in Equation (6.6) becomes discrete.

The following calculations were made for the tether system with parameters listed in Table 6.1. The final length of the tether here is set to 5 km, the rate of change of the length of the tether is set to zero at the end of deployment, $F_{\min} = 0.01$ N, $k_p = 0.02$, $V_r = 2$ m/s. The parameters of the program dynamic method were found by solving the boundary problem, $t_p/T_0 = 0.161$, $F_{\max} = 0.312$ N.

The typical dependency of the length of the tether on dimensionless time is shown in Figure 6.9. After the end of the deployment the oscillations of tether tension take place as it is shown in Figure 6.10, thus leading to loss of the stability of motion of the bodies. Figure 6.11 illustrates this by the sharp increase of angles of attack of the bodies.

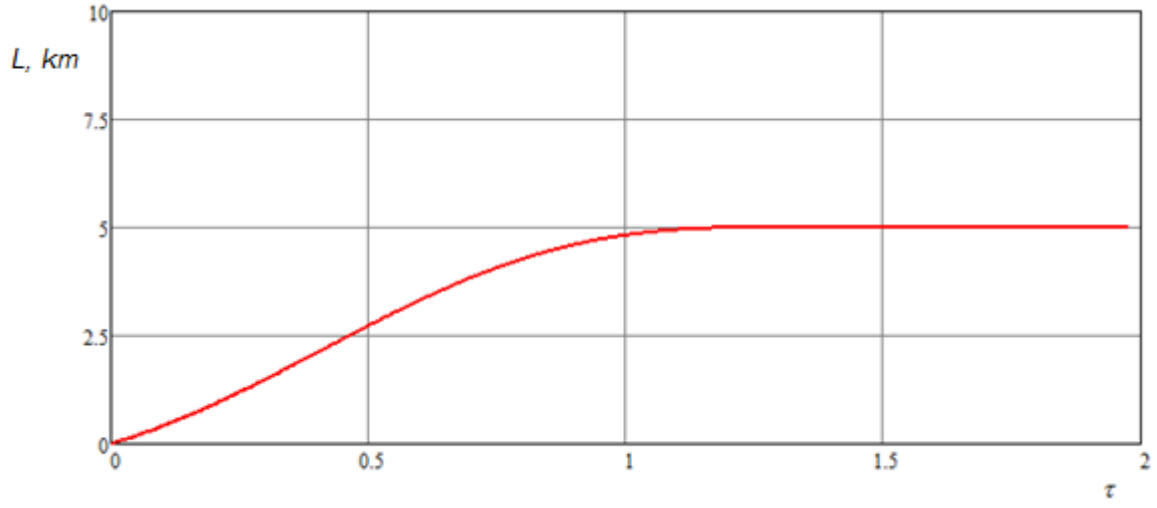

Figure 6.9 – Length of the tether during deployment

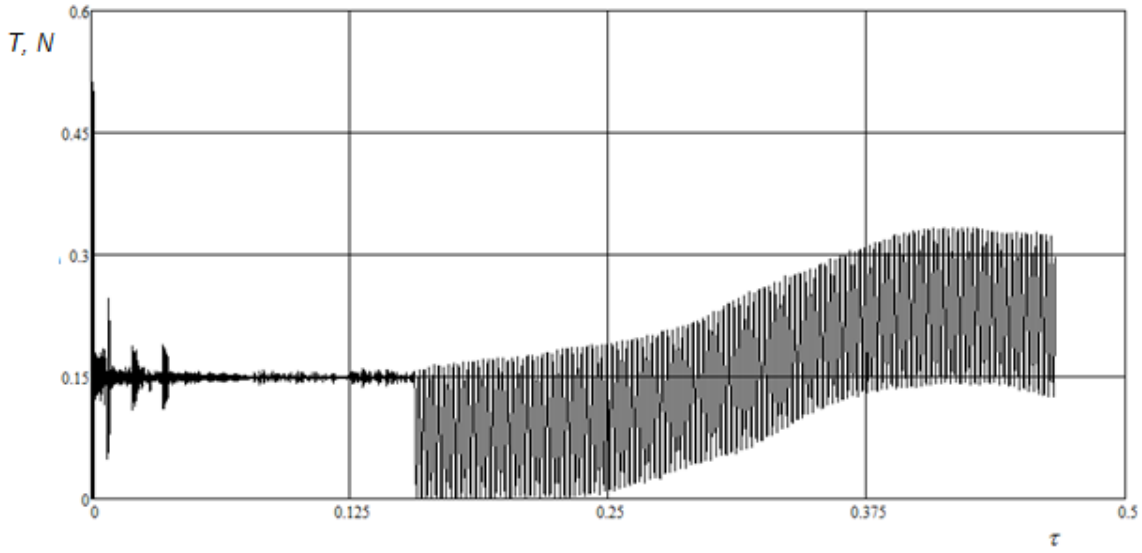

Figure 6.10 – Tension of the tether during deployment

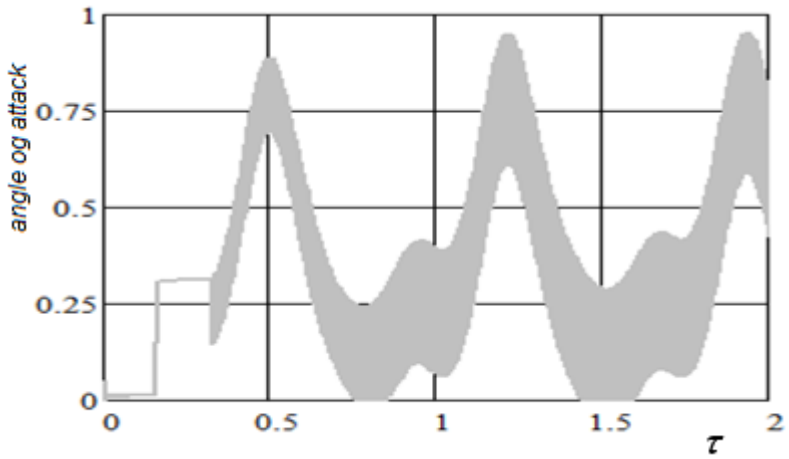

Figure 6.11 – Angles of attack during deployment

In theory, this deployment method allows for a smoother application of deceleration at the end of deployment by including a minimal deceleration force in the list of the selected parameters in the boundary problem. Such a method is impractical because for any positive perturbation in the separation velocity leads to a failure to reach the terminal condition of zero rate of change of tether length before the tether is completely unreeled.

The deployment methods employing a constant control force and the program dynamic method have similar properties, meaning that the effect of the perturbation in the separation velocity vector of the same.

6.4. Feedback methods of deployment

A dynamic method with constant decelerating force and a programmable change of control force can be improved by making use of the ***feedback principle***. In this instance, the following form of regulating force can be applied

$$F_{\text{control}} = F_n(t) + p_L\left[L - L_p(t)\right] + p_V\left[\dot{L} - \dot{L}_p(t)\right] \tag{6.7}$$

where $L_p(t)$ and $\dot{L}_p(t)$ are pre-defined program dependencies of tether length and the rate of change of length with respect to time; p_L, p_V are feedback coefficients; L and $\dot{L}$ are perturbed length and the rate of change of length of the tether, which meets the condition (6.4); $F_n(t)$ is the decelerating force.

This principle of regulating the length and the rate of its change (6.7) was used during the real orbital tether experiment "YES2" and in other research, for example, (Kruijff, M., 2011, Williams, P., 2006, Zabolotnov, Y.M., 2015).

To calculate the control force (6.6) it is necessary to find the values of $F_n(t)$, $\dot{L}_p(t)$, and $L_p(t)$ by numerical solution of the system of equations (6.1, 6.2, 6.4). Thus, it is required to first form a table with values of specified functions. Intermediate values of these functions should be found by interpolation. On the other hand, it is possible to use a more simple principle based on the ***kinematic control method***, which is defined as

$$\dot{L}_p(\tau) = V_{\max}\cos^2(\omega\tau + \nu) \tag{6.8}$$

where V_{max}, ω, ν are parameters.

Boundary conditions are imposed through the solution of the system of non-linear equations

$$\dot{L}_p\left(t_{fin}\right) = 0, \qquad \frac{d\dot{L}_p}{d\tau}(t_{\text{fin}}) = 0, \qquad \dot{L}_p(0) = V_r, \qquad \int_0^{t_{fin}} \dot{L}_p(t)dt = L_{\text{fin}}. \tag{6.9}$$

Parameters t_{fin}, $V_{\max}$, ω, ν are found by solving the system of equations (6.9).

Due to the periodicity of Equation (6.8), the system of equations (6.9) has more than one solution. Consider the solution where $\dot{L}_p(\tau)$ illustrates the method of deployment with areas of both acceleration and deceleration.

The following results are obtained for modelling a deployment of a tether system where the mass of the spacecraft is equal to 200 kg, the mass of the stabilizer is 12 kg, the initial altitude $H = 250$ km, Young's modulus for the tether material is $2.5 \cdot 10^{10}$ Pa, and

the diameter of the tether is $0.6 \cdot 10^{-3}$ m. A spacecraft with such a mass as this would be a spacecraft of the small class, such as AIST-2d, for which the base mass without scientific equipment is close to the value mentioned above. The characteristics of the tether refer to the Dyneema fibre (Van Der Heide, E.J., 2003). The initial velocity of the separation $V_r = 2$ m/s. For the tether system with final length of the tether equal to 15 km, the kinematic deployment method parameters are $V_{\max} = 3.5$ m/s, $\omega = 0.000325$, $\nu = 2.43$, $t_{\text{fin}} = 7040$ s.

The dependencies of program function $\dot{L}_p(t)$ and $L_p(t)$ on time are shown at Figures 6.12 and 6.13. Figure 6.14 illustrates how the perturbations arising from errors during the separation influence the rate of change of length of the deployed tether. The error in direction of velocity of separation was taken equal to 10 degrees with less than zero value of projection onto the radius-vector of centre of mass of the system. The value of error is 1 m/s and the feedback coefficients are $p_L = 0.2$ and $p_L = 7.8$.

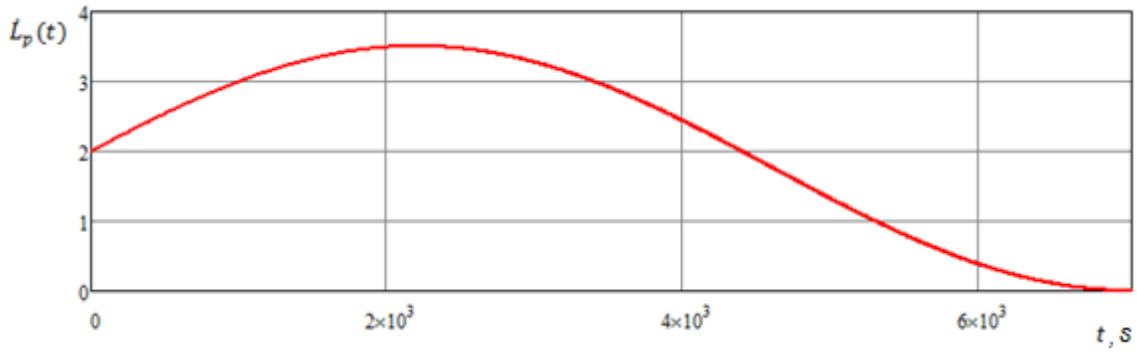

Figure 6.12 – Program function $\dot{L}_p(t)$

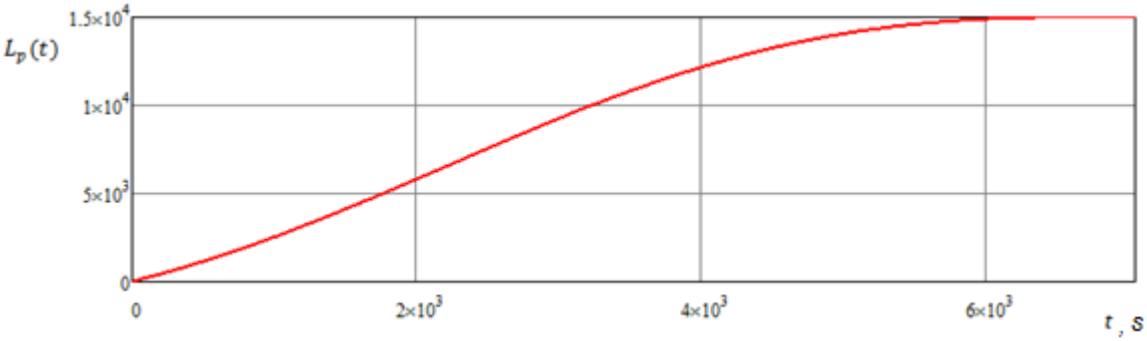

Figure 6.13 – Program function $L_p(t)$

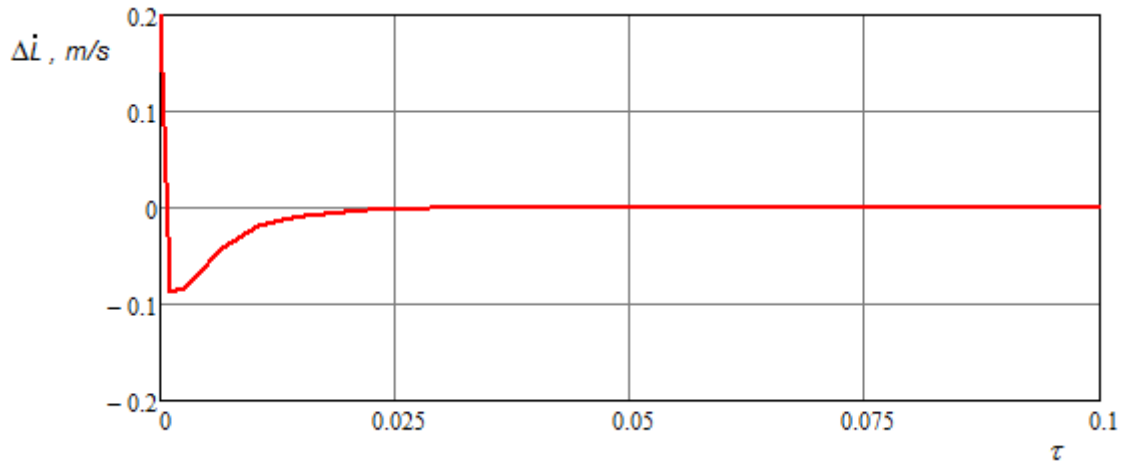

Figure 6.14 – Influence of perturbation on the rate of change of length

The tension force oscillates during the first seconds of deployment due to shock loads caused by the control force. These oscillations are shown in Figure 6.15. The value of the tension force reached here (7.09 N) is the maximum tension during further deployment process for the systems with specified length of the tether and for the systems with a shorter tether as well.

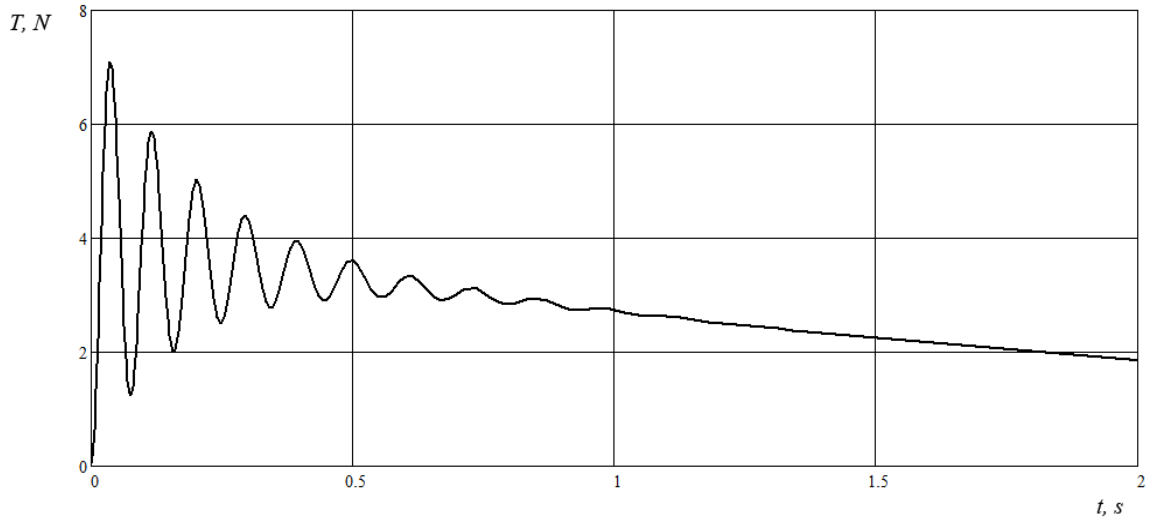

Figure 6.15 – Tension force during the beginning of the deployment

Figure 6.16 depicts how the angles between the longitudinal axes $C_i x_i$ and vector $\vec{r}_{ab}$ (the tether) for both spacecraft and stabilizer changes during the deployment. Numerical modelling shows that the motion during deployment remains stable.

Figure 6.17 illustrates the trajectories of relative motion of spacecraft and the stabilizer during the deployment. During the deployment, the velocity of the stabilizer relative to the atmosphere reduces faster than velocity of the spacecraft because of the difference in their ballistic coefficients. A decrease in the velocity of any body moving in the orbit of a planet leads to a decrease in the altitude of that orbit and to an the increase of the angular velocity of rotation of that body around the planet. As a result, the stabilizer crosses the virtual vertical line drawn through the centre of mass of the system. Next, while in the lower orbit, the aerodynamic force acting on the stabilizer becomes higher as a result of the higher density of the atmosphere, so the velocity of the stabilizer suffers greater deceleration than the spacecraft in its higher orbit. Thus, the oscillation in the relative positions of these two bodies occurs during the deployment process as it is shown in Figure 6.17. It is necessary to mention that as the whole tether system descends deeper into the dense layers of the atmosphere this effect reduces, and then the stabilizer follows the spacecraft relative to the vertical line. This result corresponds with the results obtained in other researches on deployment of tether systems (Ishkov, 2006).

The values of feedback coefficient are chosen under the condition of non-periodic process while the task of finding the optimal values of the coefficients was not taken into consideration here.

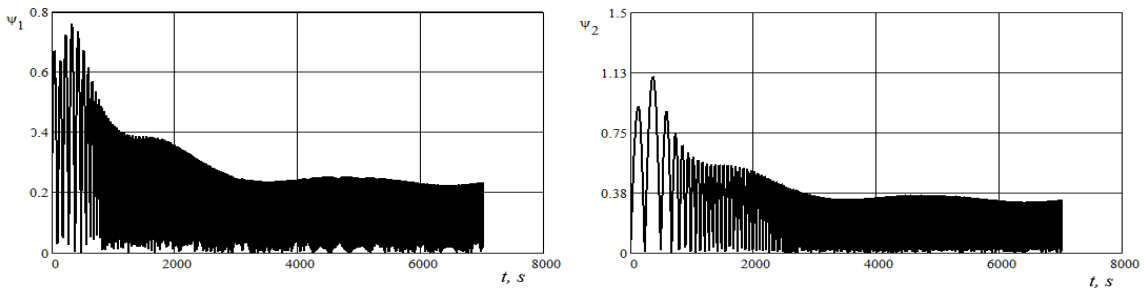

Figure 6.16 – Angles between the longitudinal axes of bodies and the tether

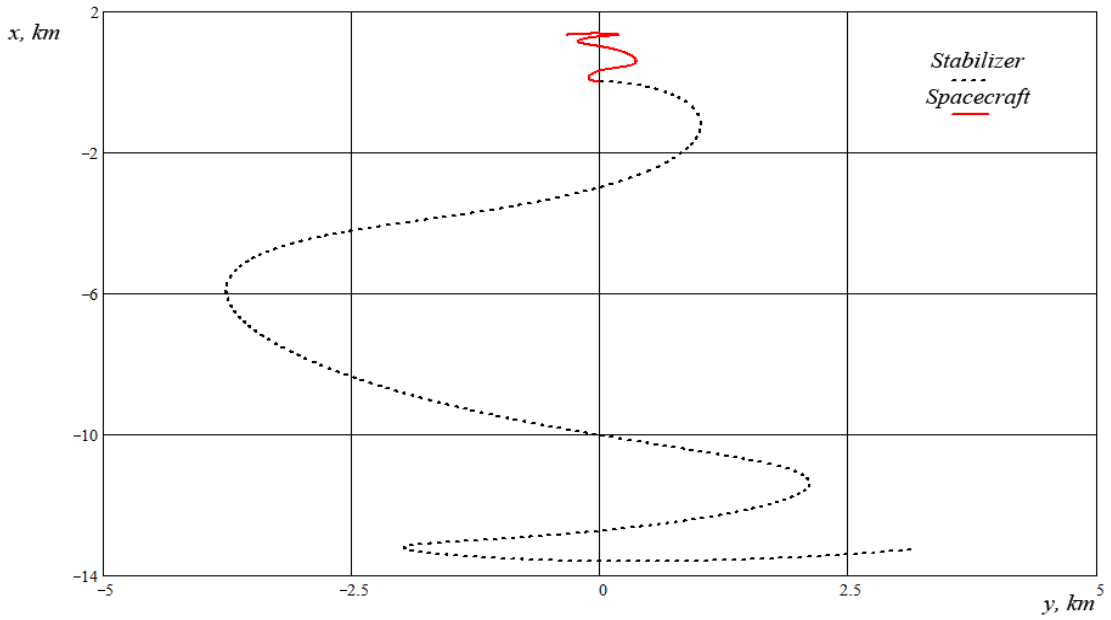

Figure 6.17 – Trajectories of the bodies

It was found that the equation for regulating force (6.7) can be simplified by setting the decelerating force equal to zero, $F_n(t) = 0$. This simplification has only a small influence on the process of regulation of the tether release (Figure 6.14). Here, the tether is strained, the oscillations of the tension after the end of deployment are close to periodic and do not lead to the instability of motion.

The analysis of the different methods of deployment shows that the motion of the tether system for the specified cases is almost independent from the static stability of the spacecraft and stabilizer. This means that the external torque arising from the tension of the tether has a major influence on the motion of the tether system during deployment.

Both of the bodies of the tether system may have static and dynamic asymmetry. The static asymmetry is the distance from the centre of mass of the body to the longitudinal axis of the body. The dynamic asymmetry is the difference between moments of inertia I_{yi} and I_{zi}. The relative value of static asymmetry is defined using the diameters of the bodies and the relative value of dynamic asymmetry is the arithmetic mean of I_{yi} and I_{zi}.

It was found that small static or dynamic asymmetry of the bodies does not have a significant influence on the motion of the system. On the other hand, there is a dependence of the angle of attack of the tether on the ballistic coefficient of the stabilizer. The higher the ballistic coefficient of the stabilizer, the lower the maximal values of angle of attack of the tether.

6.5. Summary

1. The dynamics of the system are independent of its static stability, which is based on the distance between the centre of mass of the stabilizer and the centre of the aerodynamic pressure. From this it is possible to conclude that the torque arising from the tension force has a major influence on the system dynamics.
2. The unguided deployment of the tether system with constant and low decelerating force always leads to the shock loads at the end of the deployment process and, as a result, to the oscillations of the tension of the tether. These shock loads are accompanied by the sag of the tether and lead to the instability of motion of the tether system after the deployment.
3. The dynamic control methods of deployment allow to reach predefined condition of motion of the tether system. The usage of systems of regulations of release of the tether allow to provide the smooth deceleration at the end of deployment thus providing the stability of motion of the tether system. The stability can be reached even then there are perturbations in the initial conditions of the separations.

7. MODELLING TETHER SYSTEM AS A SYSTEM WITH DISTRIBUTED PARAMETERS

The multi-point model of the tether system is based on the model obtained in Chapter 6 and splits the tether into a number of parts. The multi-point model of tether describes the series of separations of material points from the spacecraft. These material points describe the stabilizer and the nodes on the tether. The aerodynamic forces acting on the tether are taken into consideration.

The advantage of the described model is that it makes possible to calculate numerically elastic deformations and curvature of the tether.

The comparison of the two-point and multi-point model shows that the values of the tension force calculated by the multi-point model is higher because of the change in mass after adding each node and the influence of aerodynamic forces acting on the tether. This allows to make a more accurate estimation of tension force. The values of angles between the longitudinal axes of bodies and the tether are lower if compared with the two-point model for the same reasons.

7.1. The multi-point model of the tether system

For the modelling purposes in the previous chapter the tether was represented as an inflexible rod – a one-dimensional stretchable mechanical connection without mass. The model built in Chapter 6 does not take into consideration the mass of the tether, and the tether is supposed to be straight, thus making impossible to take into consideration the elastic deformation and flexure of the tether itself.

To model the flexure of the tether it is necessary to split the tether into a number of parts. The higher the number of parts of the tether, the better the resolution of the model solution. Such a result would show the flexure of the tether system as a set of material points, or nodes, along the length of the tether. The anticipated non-straight line of nodes would indicate the tether response to constant or slow-time varying forces such as the gravity field and the aerodynamic forces. Therefore, the multi-point representation of the deployed tether system consists of n nodes, including two nodes for describing the rigid bodies, the spacecraft and the stabilizer, and $n-2$ intermediate nodes defining the tether.

For modelling purposes (for more accurate modelling), the full length of the tether is divided into parts according to the number of intermediate nodes on the tether. Starting from the beginning of deployment, as the tether unreels and the length of the tether reaches $l_{\text{full}}/(n-1)$, where l_{full} is the full length of the non-stretched tether, the new intermediate material point (node) is inserted into the mathematical model of the system (Figure 7.2). The 10-node mathematical model of the tether system includes the following nodes: the spacecraft, 8 intermediate nodes and the stabilizer. The tether for this example is represented by 9 parts, and the lengths of the parts of the tether are equal under the condition that they are not stretched elastically.

In other words, the tether is represented numerically, specifying a discretization of the tether into a series of material points (nodes) with elastic connections

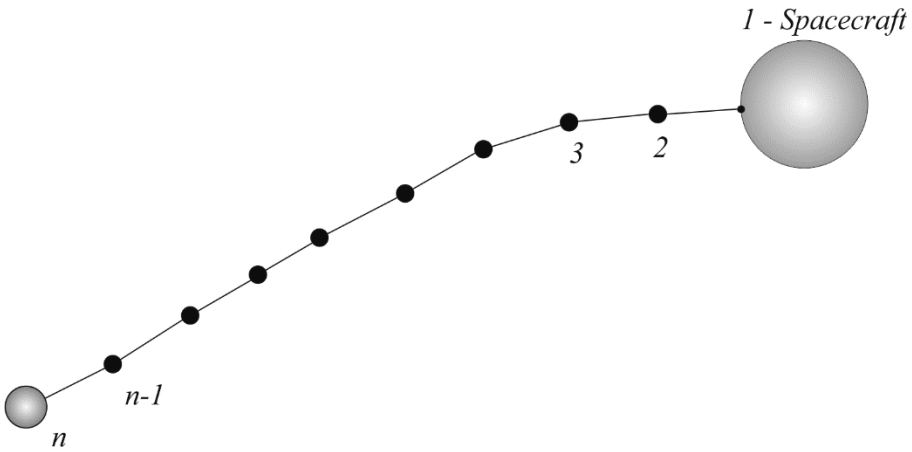

Figure 7.1 – The multi-point model of the tether system

For every intermediate node, the value of the tension of the tether should be equal from both sides, and at the moment during the deployment that the node was created this value should have been equal to the tension of the tether at this point just before the node was inserted. The vector of velocity of the new node is defined based on the velocities of the neighbouring nodes using proportions. The velocity of the spacecraft after inserting the new node is corrected using the law of conservation of momentum. It is supposed that the tether does not have internal dissipative forces like friction.

The multi-point model of tether describes a series of separations of material points from the spacecraft. These material points describe the stabilizer and the nodes on the tether. As the length of the non-stretched tether coming from the unreeling device reaches a pre-defined value equal to the distance between nodes on the tether, the next material point

separates from the spacecraft. This new material point is added between spacecraft and previous node on the tether, or, if this were the first node on the tether, between spacecraft and stabilizer. The scheme of adding each new node is shown in Figure 7.2.

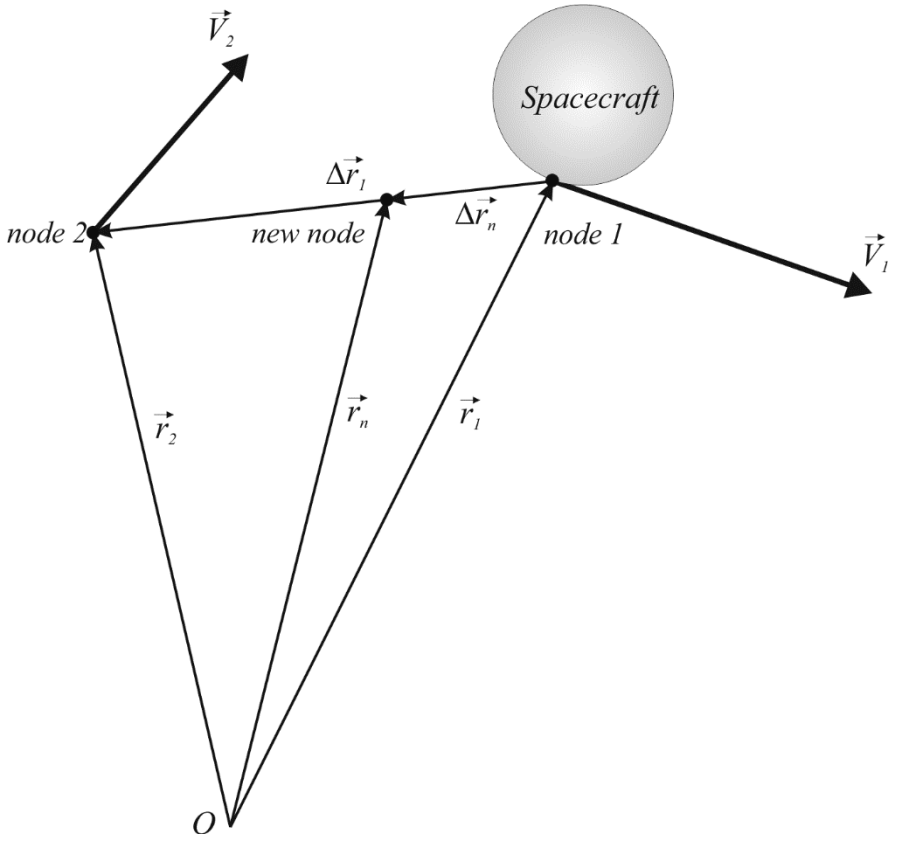

Figure 7.2 – New node on the tether

In compliance with Figure 6.2, vectors $\vec{r}_1$ and $\vec{V}_1$ describe the position and the velocity of the unreeling device placed on the spacecraft, $\vec{r}_2$ and $\vec{V}_2$ refer to the position and the velocity of the previous node on the tether, and $\vec{r}_{\text{new}}$ and $\vec{V}_{\text{new}}$ are position and velocity of the new node. The positions and velocities of nodes are defined here relative to the centre of Earth O.

Basing on Figure 7.2, the position $\Delta\vec{r}_1$ and velocity $\Delta\vec{V}_1$ of previous node relative to the spacecraft are

$$\Delta\vec{r}_1 = \vec{r}_2 - \vec{r}_1,\ \Delta\vec{V}_1 = \vec{V}_2 - \vec{V}_1.$$

The position of new node relative to the mounting point on the spacecraft

$$\Delta\vec{r}_{\text{new}} = \Delta\vec{r}_1 - \frac{\Delta\vec{r}_1}{|\Delta\vec{r}_1|} \cdot L_{\text{new}},$$

where L_{new} is the distance from the first node to the new node.

The velocity of new node relative to the mounting point on the spacecraft

$$\Delta\vec{V}_{\text{new}} = \Delta\vec{V}^{n}_{\text{new}} + \Delta\vec{V}^{\tau}_{\text{new}},$$

where $\Delta\vec{V}^{n}_{\text{new}}$ is the projection of the vector $\Delta\vec{V}_{\text{new}}$ onto the vector describing the tether and $\Delta\vec{V}^{\tau}_{\text{new}}$ is the projection of the same vector onto the axis, perpendicular to the tether. These components are defined as

$$\Delta\vec{V}^{n}_{\text{new}} = \Delta\vec{V}_{\text{new}} - \Delta\vec{V}^{\tau}_{\text{new}}, \qquad \Delta\vec{V}^{\tau}_{\text{new}} = \frac{\Delta\vec{r}_1}{|\Delta\vec{r}_1|}\left|\Delta\vec{V}_1\right|\cos\beta_1,$$

where β_1 is the angle between vectors $\Delta\vec{r}_1$ and $\Delta\vec{V}_1$.

As a result, the position and the velocity of new node are

$$\vec{r}_{\text{new}} = \vec{r}_1 + \Delta\vec{r}_{\text{new}}, \qquad \vec{V}_{\text{new}} = \vec{V}_1 + \Delta\vec{V}_{\text{new}}.$$

Each node in the mathematical model of the deployment of tether system is described by six additional differential equations.

The intermediate nodes and the spacecraft and the stabilizer are affected by the gravitational force from Earth $\vec{g}_{ei}$, tension forces acting in the direction of previous and next nodes $\vec{T}_{i-1}$ and $\vec{T}_{i+1}$, and aerodynamic force $\vec{R}_i$ (Figure 7.3). Other forces such as gravitational forces from the Moon and other space objects, the solar wind, etc. can be neglected (Aslanov, V., 2015). Here it is necessary to mention that there is only one tension force acting on the spacecraft and one – acting on the stabilizer.

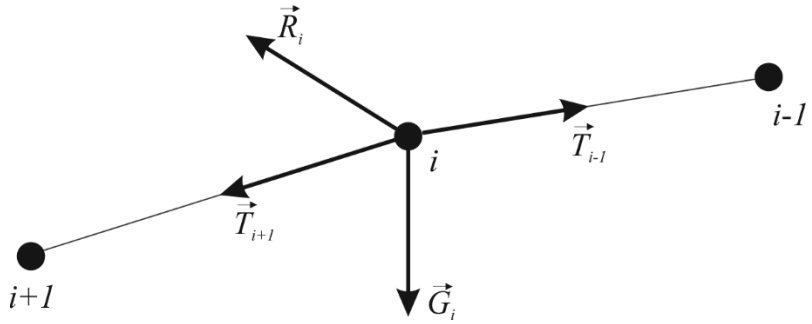

Figure 7.3 – Forces acting on an intermediate node

7.2. Consideration of parameters for the model

The definition of "short" or "long" tether can be made based on the relative size of the tether mass and the forces acting on it, and the masses of the spacecraft and stabilizer, and the forces acting on them. The aerodynamic forces acting on a tether are dependent on its length and diameter. If the aerodynamic cross-sectional area of the tether, i.e. the length of the tether multiplied by the diameter of the tether (to be more accurate, the area of the longitudinal midsection of the tether), is comparable with the reference area of the stabilizer, this means that the tether is "long".

The aerodynamic force acting on each part of the tether is calculated for the cylinder with a diameter equal to diameter of the tether and length equal to the distance between nodes. Therefore, the aerodynamic force acting on the node is the average value of aerodynamic forces acting on the neighbouring parts of the tether. For the spacecraft and the stabilizer, there is only one neighbouring part of the tether, and half of the value of the appropriate aerodynamic force is added to the aerodynamic force acting on the body.

The mass of the tether can be calculated by its density multiplied by the cross-sectional area and by the full length. The cross-sectional area of the tether is $S_{\text{tether}} = \pi d^2/4$, where d is the diameter of the tether. For a tether made from Dyneema® fibre, $d = 0.6 \cdot 10^{-3}$ m, density $\rho = 975$ kg/m^3 (Bouwmeester, J. G. H., 2008), so, according to these values, each kilometre of deployed tether has a mass of 0.276 kg.

It is necessary to take into consideration that before the beginning of the deployment the tether is situated on the spacecraft, and the mass of the spacecraft decreases during the deployment as the tether unreels. The mass of the second body remains the same as in the beginning of the deployment process. Therefore, it is important to compare the mass of the tether with the mass of the spacecraft, not stabilizer. It is also necessary to take into consideration that for a long tether the difference in gravity acceleration for the spacecraft and the stabilizer cannot be neglected.

When the length of the tether is 5 km, its mass is less than 0.7% of the mass of the spacecraft, so in most cases the mass of the tether can be neglected, but for a long tether the mass should be taken into consideration: for example, the mass of the 50 km tether would be almost 7% of the mass of spacecraft and can exceed the mass of the stabilizer.

When a new node is inserted into the mathematical model of the tether system, the mass of the spacecraft is reduced by the mass of the section of the tether.

The following calculations are made for a small spacecraft with mass equal to 200 kg and a light stabilizer with mass equal to 2 kg. The parameters of spacecraft are similar to the parameters used for simulation in §6.4. Other initial parameters of the motion of the modelled tether system are shown in Table 7.1. The deployment process is controlled by the "kinematic control method" (Equation 6.8).

Table 7.1 – Parameters of the tether system

Parameter	**Symbol**	**Value**
Radius of the spacecraft		0.5 m
Radius of the stabilizer		2 m
Drag coefficient of the spacecraft	C_1	2.4
Drag coefficient of the spacecraft	C_2	2.4
Mass of the spacecraft	m_1	200 kg
Mass of the stabilizer	m_2	2 kg
Inertness of the mechanism	m_u	0.2 kg
Young's modulus for the tether material		$2.5 \cdot 10^{10}$ Pa
Diameter of the tether	d	$0.6 \cdot 10^{-3}$ m
Initial altitude	h	250 km

For the tether system with parameters specified in Table 7.1, and the full length of the tether equal to 30 km, deployment starts with initial velocity of separation $\mathrm{V_r} = 6\ \mathrm{m/s}$. The parameters of the deployment process are defined by numerical solution of Equations (6.9), and deployment ends at $\mathrm{t_k} = 11555$ seconds. Figures 7.4 and 7.5 illustrate how the length of the tether and the rate of change of the length of the tether changes during deployment.

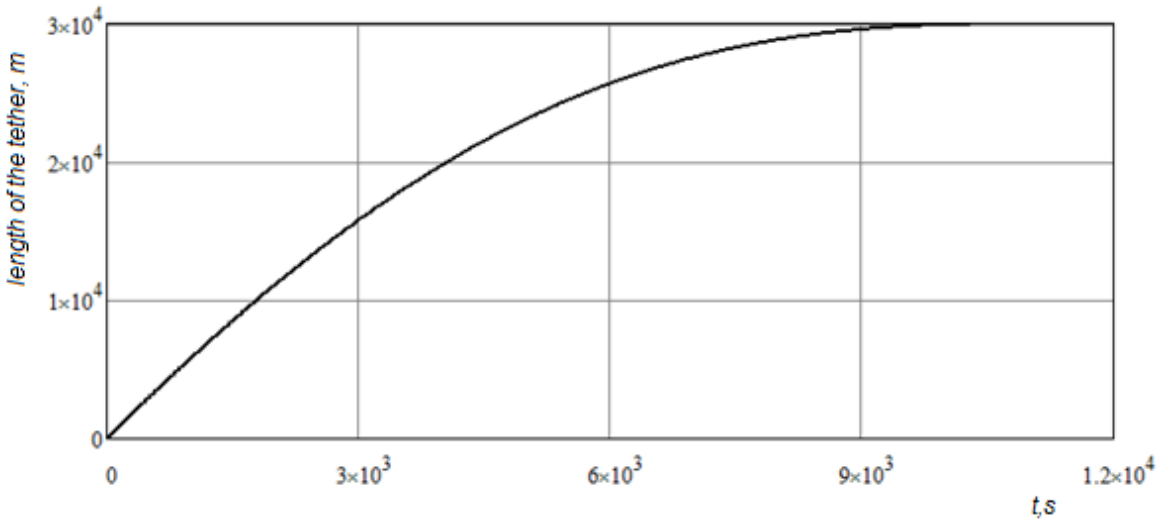

Figure 7.4 – Length of the tether during deployment

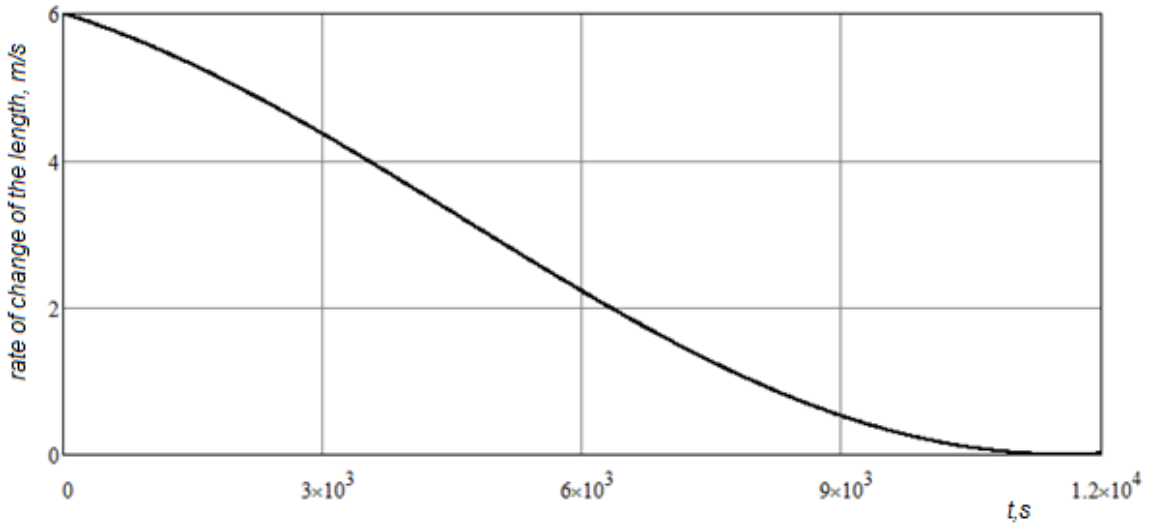

Figure 7.5 – Rate of change of the length of the tether during deployment

7.3. Multi-point and two-point model result comparison for deployment of a tether system and in the absence of atmosphere

For testing the mathematical model and understanding the generalized parameters of motion of the tether system it is useful to make calculations with some simplifications in mathematical model.

Firstly, consider the deployment of the tether system in the gravity field in the absence of atmosphere. These conditions of deployment mean that no aerodynamic force acts on the nodes, but the tether is stretchable.

The change of angle between the longitudinal axis of the spacecraft and the tether is shown in Figure 7.6 obtained for two-point model. There is a visible rise in the angle after 1800 seconds from the start of deployment process, and this growth in angle leads to the temporary increase in the tension of the tether shown in Figure 7.7.

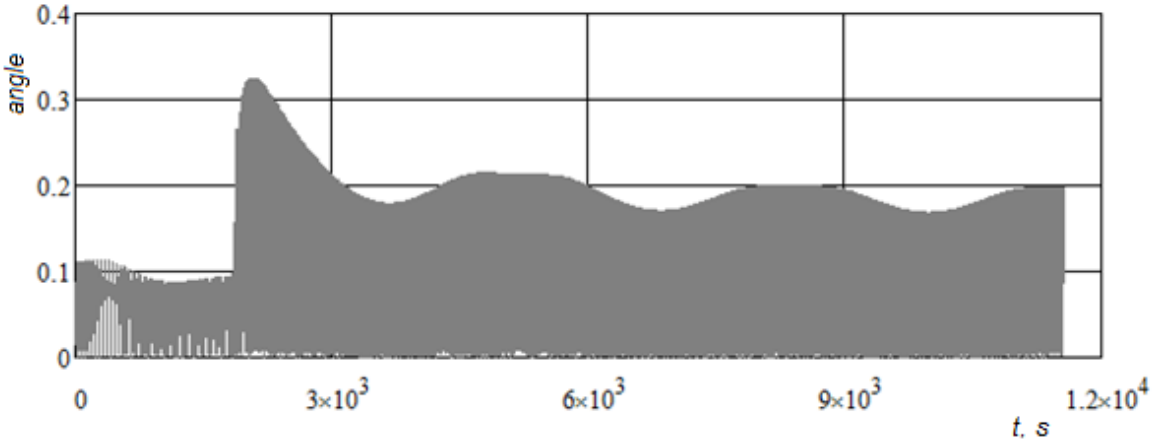

Figure 7.6 – Angle between the longitudinal axis of the spacecraft and the tether

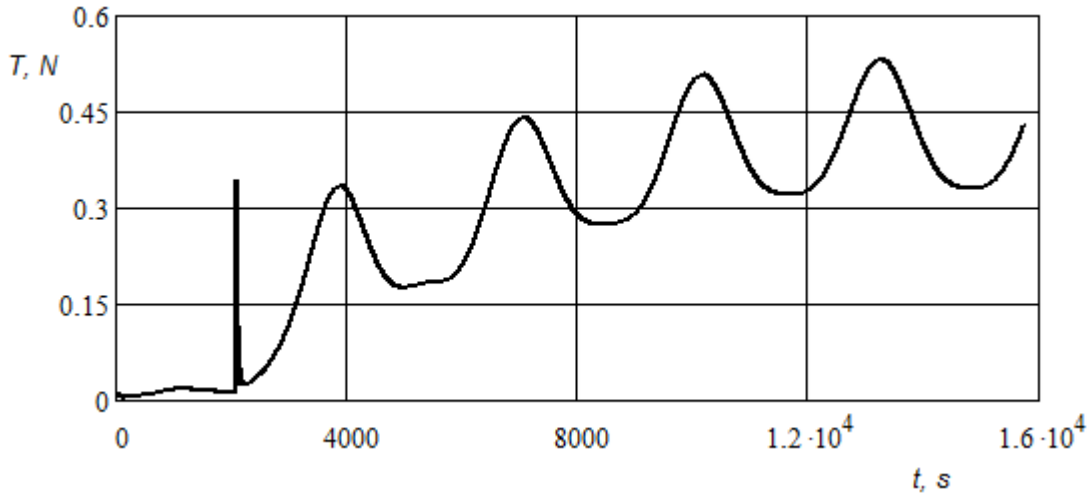

Figure 7.7 – Tension of the tether calculated using two-point model

Figures 7.8 and 7.9 compare the change of tension of the tether during the deployment for two-point model (shown by solid black line) and multi-point model. As it can be seen in Figure 7.8, at around 1825 seconds from the beginning of the deployment process, a shock load seems to occur for both models.

It is necessary to pay attention to a visible difference in values of tension of the tether for these two models. This difference occurs for the following reason: in the two-point model

the tension force is defined only by one mass – the mass of the stabilizer – and in two-point there is a change in mass after adding each node.

The multipoint model is based on a series of separations, and as a result, there is a small shock load after each separation as it is shown in Figure 7.9. The oscillation in the tension force decreases on a time basis.

Figure 7.10 shows how the tether is oriented relative to the spacecraft and its shape. The vertical line connects the spacecraft with the centre of the planet. Each line depicts the position of nodes and the shape of the tether after inserting the new node. It is clear that in the absence of the atmosphere the spacecraft remains on the initial circular orbit with altitude equal to 250 km, and the stabilizer, as a result of its lower velocity (because the separation is in the direction opposite to the direction of flight) goes to the lower orbit. As there is no drag from the atmosphere, and the orbit period is lower at a lower orbit, the stabilizer initially outpaces the spacecraft. Under this specified condition, the tether remains straight during the motion of the tether system.

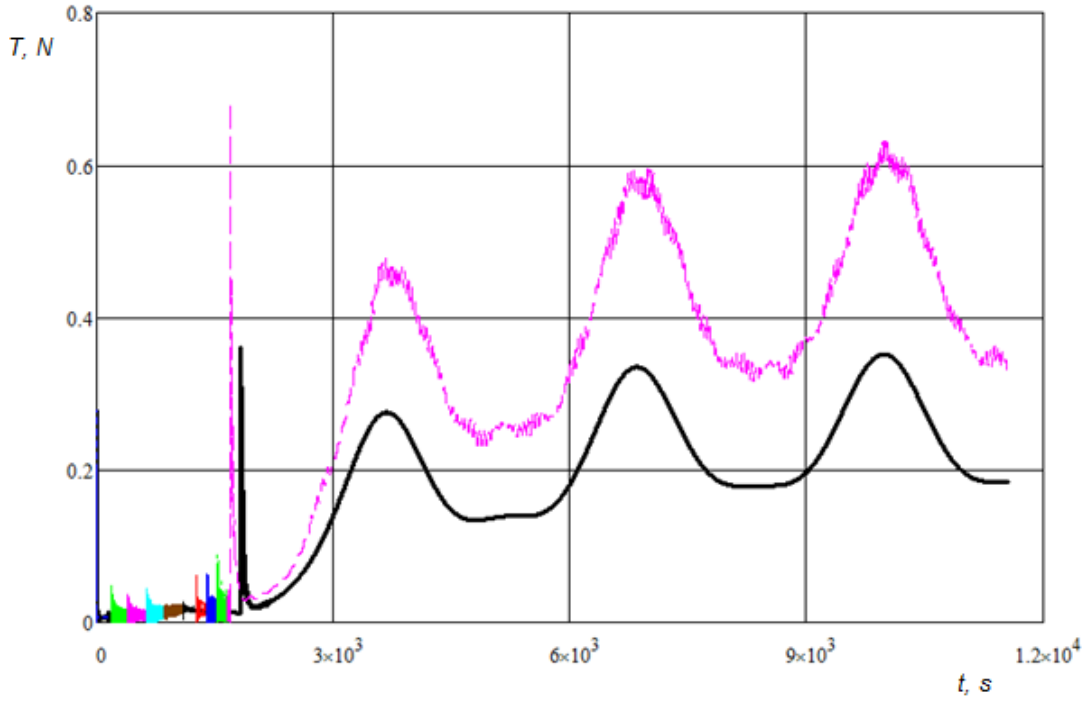

Figure 7.8 – Comparison of tension of the tether

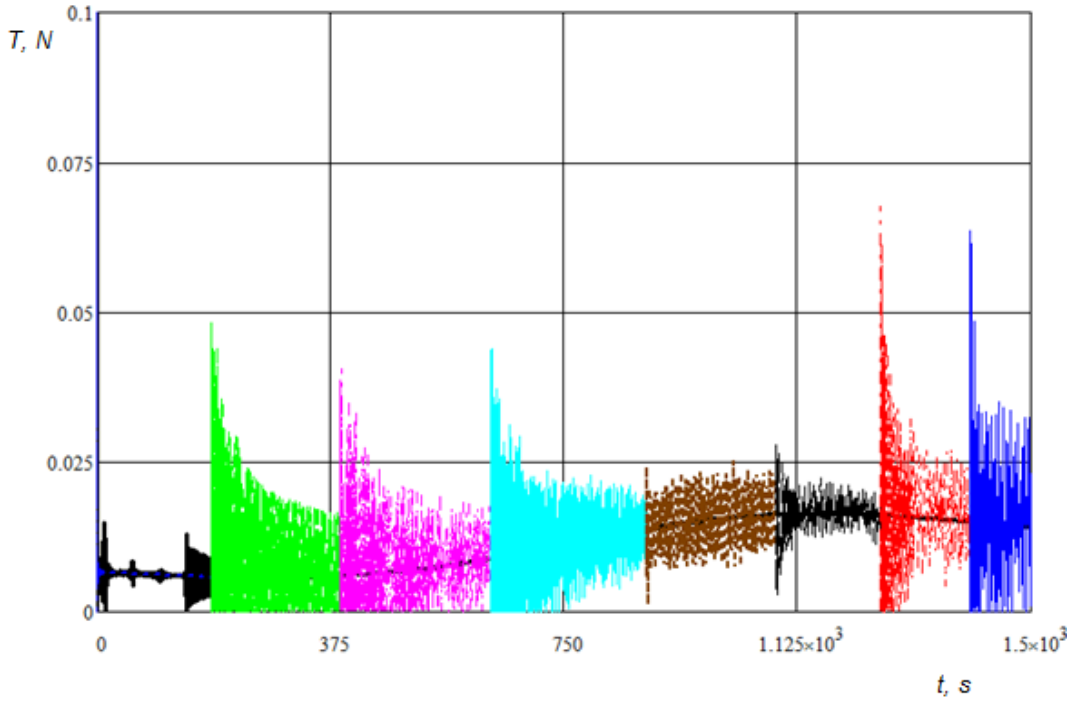

Figure 7.9 – Tension of the tether calculated using multipoint model

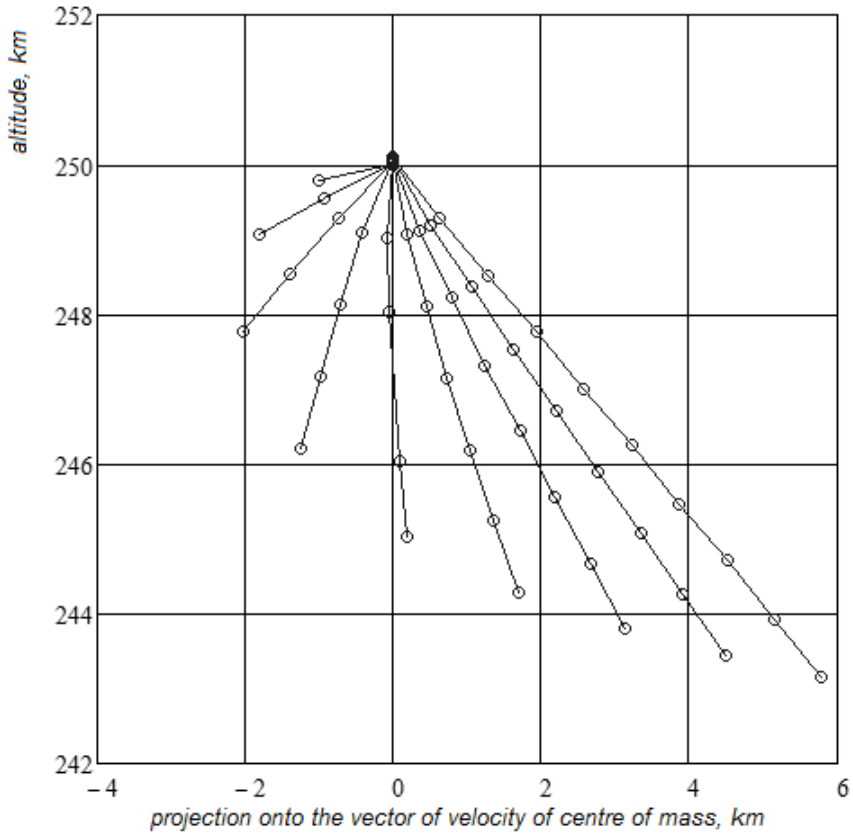

Figure 7.10 – Shape of the tether

It is necessary to mention that both the two-point and multi-point models were obtained for the aerodynamic tether system where atmosphere is an important part, and they were not expected to be used for modelling the motion around the planets without an atmosphere.

7.4. Modelling the elastic tether

The advantage of the multi-point model is that it allows the elastic deformations and curvature of the tether to be calculated numerically.

The following calculations are made for the tether system with parameters listed in Table 7.1 and in the paragraph following the specified Table. The presence of the atmosphere results in aerodynamic forces acting on spacecraft, stabilizer and the tether.

Figure 7.11 shows the change of the angles between the longitudinal axis of the spacecraft and the tether, and the change of the corresponding angle for the stabilizer is shown in Figure 7.12. The graph compares the results obtained using the multi-point model (shown in colour) with the two-point model (shown in black). In the graph of the multi-point results, the addition of a new node to the tether system during deployment is indicated by a change in the plotting colour. Because the values of the tether system orientation angles decrease, the motion of the tether system is stable.

The angles calculated using the multi-point model have slightly smaller values, which arise as a consequence of the fact that the aerodynamic forces acting on the tether are now included in the model: the two-point model neglected the aerodynamics of the tether. Therefore, the aerodynamic forces acting on the tether have a stabilizing effect during the motion of the tether system.

Figure 7.13 depicts the change of the tension of the tether during deployment. As it was noted above, there are shock loads after each new node is added into the tether. These are non-physical shocks, and related only to numerical effects in the node adding algorithm. Ideally, the node adding algorithm should be modified to avoid this.

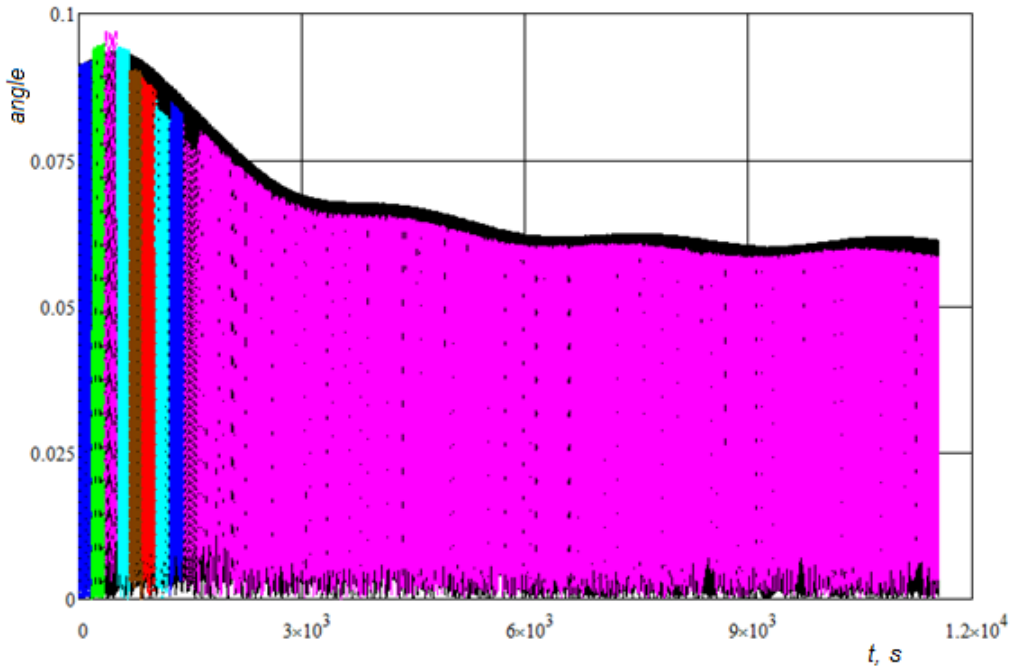

Figure 7.11 – Angle between longitudinal axis of the spacecraft and the tether

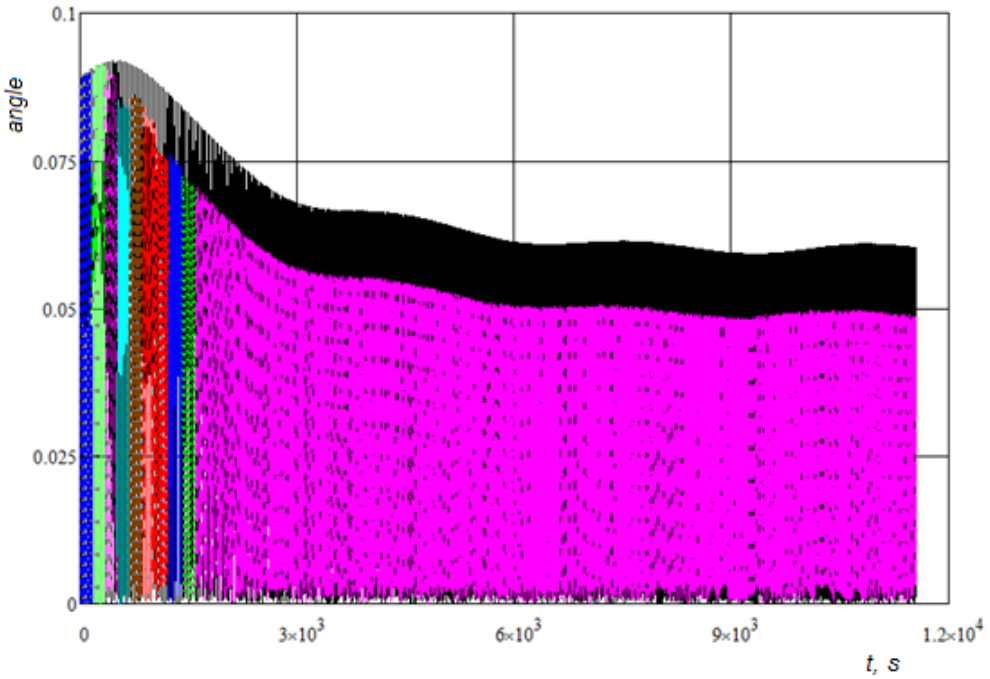

Figure 7.12 – Angle between longitudinal axis of the stabilizer and the tether

The trajectory of the stabilizer relative to the spacecraft is shown in Figure 7.14. The solid line depicts the motion calculated using the two-point model, and the dashed line represents the motion predicted by the multi-point model. The spacecraft is placed in the

upper right corner of the graph, and the stabilizer, affected by the aerodynamic and gravitational forces, moves away from the spacecraft as the tether is being deployed.

The shape of the tether during the motion is of great interest. Figure 7.15 illustrates how the shape of the tether changes during deployment. Each circle on the tether depicts an intermediate node, and different lines show the state of the tether system at the moment of inserting each new node. The tether is almost straight at every moment of deployment, and only when the tether is almost fully deployed and is, therefore, long, is there is a slight curvature near the stabilizer end. The modelling was also made for a simpler model, with fewer intermediate points. The increase in number of intermediate points from 5 to 8 has shown that, for this shape of tether and specified deployment model, there is no significant difference in parameters of the motion of the system.

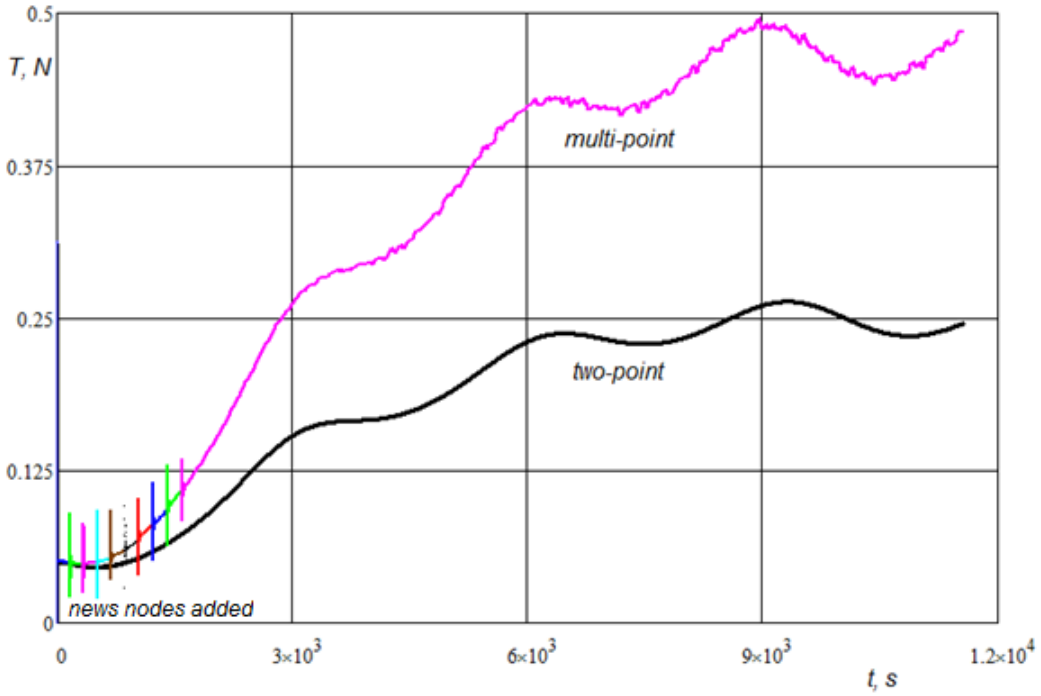

Figure 7.13 – Tension of the tether

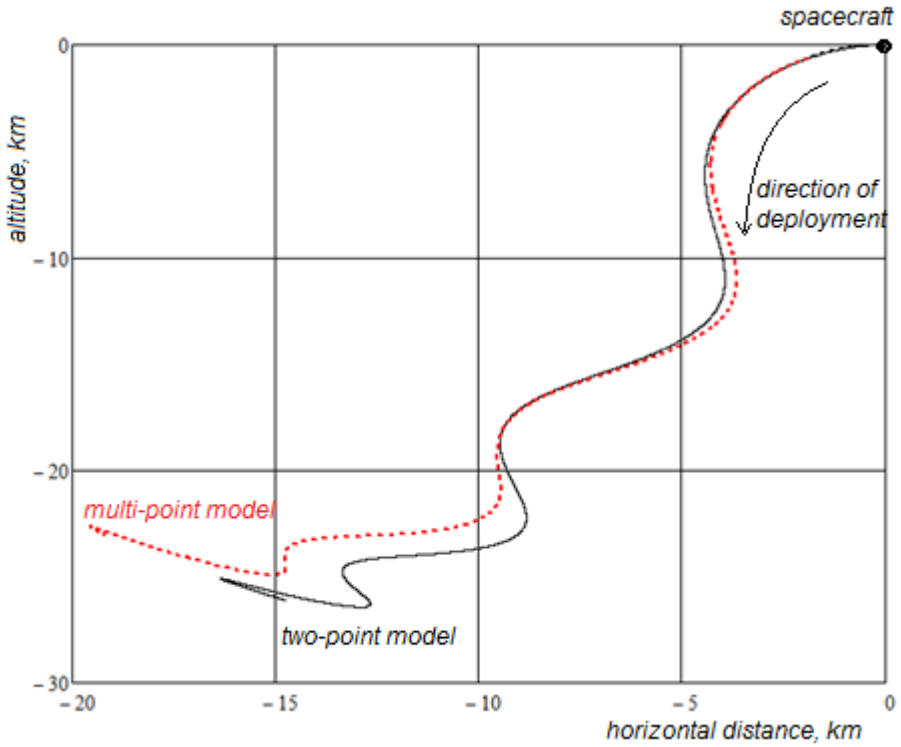

Figure 7.14 – The trajectory of the stabilizer relative to spacecraft

Figure 7.15 also confirms that the altitude of the spacecraft decreases as a result of the influence of the atmosphere. The spacecraft is shown by the dot at the right-hand end of each line describing the tether, and its position goes down as the tether length is increased.

The numerical calculations show that choosing a tether material with a lower Young's modulus leads to a decrease in shock loads after adding new node as well as after the separation of a stabilizer from the spacecraft in two-point model. As an example, Figure 7.16 shows the tension of a tether with Young's modulus equal to 10 MPa during first 2000 seconds of deployment. Compared to Figure 7.13, the shock loads are low. The increase in rigidity of the tether leads to the opposite effect.

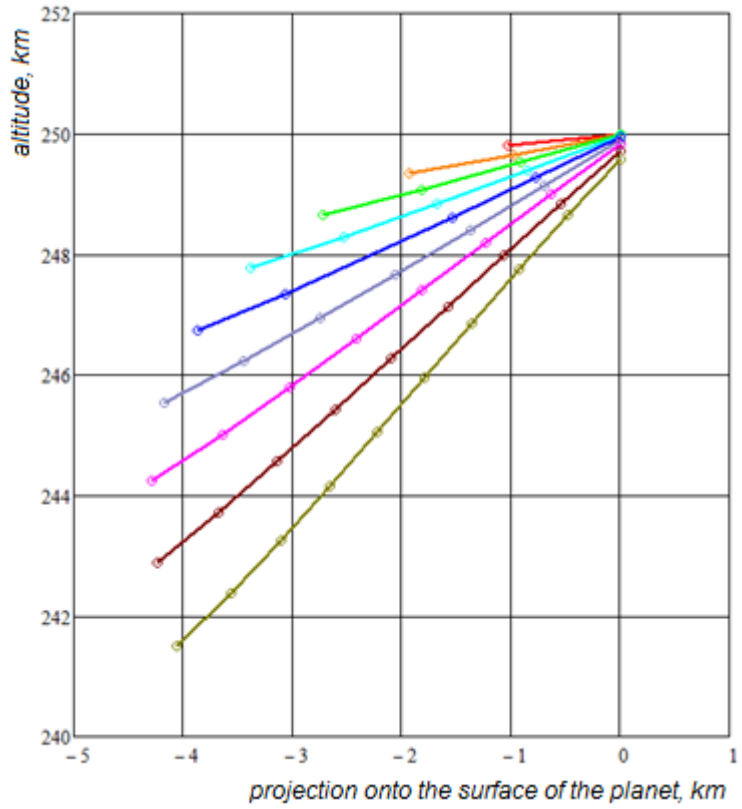

Figure 7.15 – Shape of the tether – the spacecraft is located at the top right of each trace

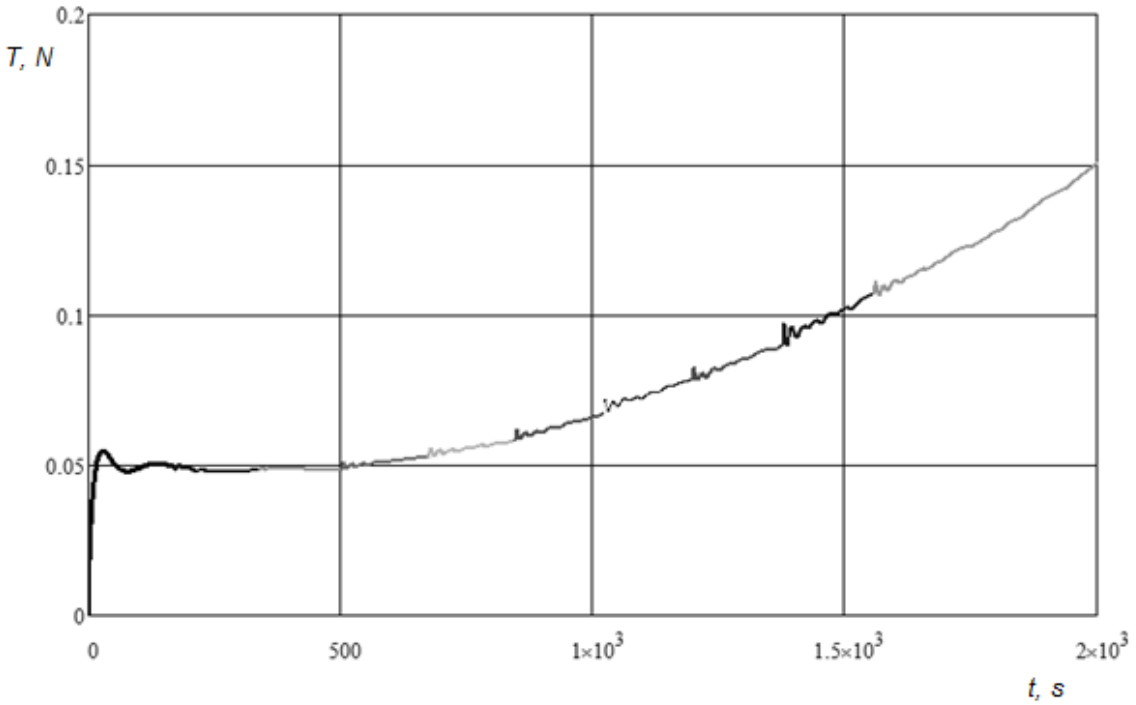

Figure 7.16 – Tension of the tether with small Young's modulus

7.5. Review of opportunities and caveats of the multi-point approach

The multi-point model of the tether system allows the examination of the deformation and flexure of the tether during and after the deployment.

Compared to two-point model, the multi-point model takes into consideration the mass of the tether and the aerodynamic forces acting on the tether. For modelling purposes, these forces were treated as acting on the nodes.

A comparison of the results of modelling tether system deployment, for different tether lengths, using both the previous two-point model and the new multi-point model was made. There is a difference in the motion parameters obtained by these two models. The tension of the tether calculated using the multi-point model is approximately two times higher than that calculated using the two-point model, and the angles defining orientation of the tether system are also lower in this case. This is explained by the fact that the multi-point model represents the aerodynamic forces as acting not only on the stabilizer, but also on the tether, thus predicting a higher tension force than predicted by the two-point model, where only the stabilizer aerodynamic forces were modelled. According to the properties of material from which the tether is made, the value of tension force is admissible in both cases.

It is also necessary to mention that the multi-point model is more computationally expensive than the two-point model. As the results obtained by the more complex method agree with those obtained by two-point model, it can be concluded that the two-point model can be relied on, not only for the particular modelling of the deployment of the tether system, but also for automated calculations and selection of parameters of the tether system at the design stage.

On the other hand, the multi-point model does show the motion of the tether and the tether system as the system with distributed parameters.

It is necessary to note that the multi-point model, like the two-point model, can be used with any admissible model for controlling the deployment of the tether. Here, in the result presented in this chapter, the kinematic deployment model was used, and this model has been developed to prevent the sag of the tether. When the shape of the tether is close to the straight line, it is possible to reduce the number of intermediate nodes used. Under such circumstances, modelling with half the number of intermediate nodes does not lead to significant change in parameters of motion of the tether system. The non-physical shock loads occur after inserting each new node because the model is discrete, whereas the real

tether system is continuous, it is necessary to include damping and corrective forces to get closer to the real parameters of the unreeling process.

During the real process of the deployment, there can be emergency situations such as a breakage of the tether or jamming in the unreeling device. In these cases the multi-point model would allow the parameters for the resulting motion of the system to be calculated: the two-point model would not be capable of providing this information about the flight.

Further development of the multi-point model could enable the modelling of the motion of a body with an attached tether for the case that the tether is broken apart or cut off from the spacecraft in order to initiate the motion of a second body into the dense layers of the atmosphere.

7.6. Summary

1. The multi-point model of the tether confirms the validity of the simplifications made in the mathematical model of the deployment.
2. Usage of the multi-point model enables more accurate values of the parameters of the tether system during motion through the atmosphere to be obtained. These parameters include tension of the tether, parameters of angular motion of the spacecraft and the stabilizer relative to the direction of the tether.
3. Comparison of the performance of the models, for different parameters and different numbers of intermediate tether nodes, shows that a discretisation of the tether into six equal lengths is sufficient for modelling purposes if shape of the tether is close to a straight line.
4. The multi-point model is discrete, and unfortunately, as the algorithm currently stands, introduces non-physical shock loads into the system after inserting each new node. Increasing the number of tether nodes leads to significantly higher model complexity without giving any noticeable improvement in the result accuracy.
5. The multipoint model allows to model the motion of the centre of mass of the tether system by considering gravity and aerodynamic forces acting on the tether.
6. In contingency situations like jamming in an unreeling device, the multi-point model would allow the modelling of the subsequent motion of the system.

8. DISCUSSION

8.1. Conclusions

The following results were obtained:

In ***Chapter 2*** the information about history of tether systems, existing mathematical models of motion of the tether system and deployment, and real tether space experiments are gathered and justified.

In ***Chapter 3*** the definition of stability of motion is made here. The terms and ideas for different types of stabilization are included there as well as the description of models of the atmosphere and numerical methods used for calculations.

In ***Chapter 4***, describing the descent of a deployed tether system in the atmosphere, the mathematical model of spatial motion has been derived. The three coordinate systems used for the derivation of the equations of motion of the tether system are described. The model takes into consideration aerodynamic and gravity forces, tension of the tether, mass and shape asymmetry of the bodies. The assumptions and simplifications made are also described and justified. The mathematical model of motion of the tether system is tested by usage of the integrals of the undisturbed motion of the tether system.

In ***Chapter 5*** the stability for the motion is defined in terms of the parameters of the deployed tether system during its descent. The parameters include mass, stabilizer shape and dimensions, and tether length. The dependencies of stability and natural frequencies on the parameters of the system are determined. It is found that the tension of the tether depends most significantly on the geometrical dimensions of the stabilizer, while the length of the tether has only a slight influence on this force. The algorithm for choosing the parameters of the tether system is proposed; this algorithm enables a significant reduction of the frequencies of oscillations in most cases. It is found, that the deployment of a tether during descent can increase the stability of the system.

Chapter 6 is concentrated on the deployment of the tether system with an elastic massless tether. It is found that the torque arising from the tension force has a major influence on the system dynamics. The dynamic methods are used to control the deployment, because it was shown, that unguided deployment leads to shock loads at the end of the deployment process and, these are accompanied by the sag of the tether and lead to the instability of

motion of the tether system after the deployment. The usage of systems of regulations of release of the tether allows stability of motion to be reached even then there are perturbations in the initial conditions of the separation.

In ***Chapter 7*** the tether system is modelled as a system with distributed parameters. The tether is represented as a set of nodes with elastic connections. The model takes into consideration the mass of the nodes and the aerodynamic forces acting on the tether. The comparison of results obtained by the two-point and multi-point models show that the change in mass after adding each node and the influence of aerodynamic forces acting on the tether leads to differences in values of the tension force and angles describing the orientation of the bodies. The multi-point model obtains more accurate values of the parameters of the tether system during motion through the atmosphere. Increasing the number of nodes leads to significantly higher model complexity without giving any noticeable improvement in the result accuracy compared to the model with fewer number of intermediate nodes. In contingency situations like jamming in the unreeling device, the multi-point model would allow the modelling of the subsequent motion of the system.

8.2. Discussion of errors, perturbations and model inadequacies

The descent of a tether system from the orbit includes two stages. During the first stage it is necessary to deploy the tether system, and the second stage is the motion of the deployed system in the atmosphere.

The modelling of motion of the tether during these stages encounters similar problems. The first group of problems refer to the manufacture process. The second group comprises the perturbations due to the influence of the surrounding medium, and the third one comprises the perturbations not taken into consideration by the mathematical model of motion.

The manufacture of any spacecraft assumes that there can be deviations from pre-determined values due to inaccuracy, lack of quality control or comparatively high manufacturing tolerances. Examples of such deviations are mass and shape asymmetry of the spacecraft, flaws in the unreeling mechanism or non-uniformity of the tether material. These deviations lead to perturbations in the parameters of the tether system.

When modelling the deployment of the tether system, the multipoint model shows that the elasticity of the tether leads to the error in the control of the deployment model based on

the tether length. The shock loads after inserting a new node are perturbations generated by the mathematical model itself, and should not occur in the real system because the real system is in contradistinction to the mathematical modelling and simulation is not discrete.

The influence of the surrounding medium can lead to perturbations due to simplifications made in the model of the atmosphere. The existing models of the atmosphere do not provide full information about the surrounding medium because of the chaotic character of local flows. The most vivid example of atmospheric perturbation is wind. Wind is a natural phenomenon and can take place about every location of Earth, but it is highly problematic to take it into consideration. There is also a difference in the properties of the atmosphere due to the change of days and nights, activity of Sun, etc.

The influence of the surrounding medium as well as manufacturing errors can lead to perturbations during the deployment process or motion of deployed system. For example, there can be errors in the absolute value or the direction of the vector of the velocity of separation at the beginning of the deployment, and the model of deployment is intended to ignore these perturbations. The methods of stabilization like spinning or usage of the tether system instead of a single spacecraft, allows the conditions of stable motion to be reached.

The magnetic field of the Earth was not taken into consideration in this research, but depending on the materials the spacecraft is made from there can be an influence from appropriate forces.

There are other forces acting on the spacecraft during its motion in the atmosphere, including the pressure from sunlight, gravity forces from space objects and others. Their magnitudes are small and usually these forces are not included into mathematical models.

The motion in the surrounding medium can be accompanied by erosion effects that can change the properties of materials that the spacecraft and stabilizer are made from, leading to the destruction of the bodies or changes in their parameters.

It is also necessary to mention about the cross influence of the bodies on each other. The perturbations in airflow produced by the bodies change the regime of airflow thus changing the values and directions of the aerodynamic forces.

The models described in previous chapters use diffuse models of gas reflection, but rarefied gas flow has a component of specular reflection. Taking into account this type of reflection leads to changes in aerodynamic characteristics of a spacecraft according to the change in angle of attack.

Every real system has dissipative forces acting on or within the system, and damping is of great importance during the motion. Damping reduces the amplitudes of oscillations thus making motion more stable. The dissipative forces cannot destroy the stability of motion of the system, but it is important to include damping to get the mathematical model closer to the real system. The problem here is the damping is one of the most complex processes for mathematical modelling. Nowadays there is no explicit opinion which model of damping is best for use in the modelling of space tether systems, and different damping models are used in different researches (Mantellato, R., 2015, Aslanov, V.S., 2015).

Another issue about the tether system is the shape of cross-section of the tether. The considered Dyneema® fibre has a circular cross-section. On the other hand, the usage of tape tether (Mantellato, R., 2015) can make the tether less vulnerable to the influence of micrometeorite attack.

8.3. Validations and recommendations for further work

The mathematical models described in previous chapters can be validated in different ways. The best validation of a mathematical model and results of simulation is to perform a real experiment. The cost of space tether system experiment is very high and would require the demand and funding from an organization with the resources and interest to develop the usage of small landing modules. Since such practical validation is currently unfeasible, the validation can instead be made by simulation using the provided mathematical models, for which predictable results can be presumed for particular initial conditions. Such investigations were made during this research, described in Chapters 4 and 7, and include research concerning the integrals of motion for the undisturbed motion of deployed tether system, modelling of deployment in the absence of atmosphere, and a comparison between rigid and elastic tether models.

Another way to validate a mathematical model and its simulation results is to compare these with the result obtained by another mathematical model. For example, a comparison with other research results shows that there are characteristic likenesses in the trajectories of the relative motion of the spacecraft and stabilizer during deployment (Ishkov, 2006).

The multi-point model represents a tether as a series of nodes with elastic connections taking into consideration the aerodynamic forces acting on the tether. Therefore, the tether

can be used as a stabilizer itself, and the small spacecraft can be stabilizer by using a tether represented by number of nodes during its motion in the atmosphere.

In this case, after the deployment, the tether should be cut at the spacecraft end, and the secondary body – in this case, a landing module – would continue its motion through the dense layers of the atmosphere, where the tether is used for the stabilization purposes. The length of the stabilizer should be sufficiently high to provide the necessary aerodynamic force, and the difference in the altitudes of the parts of the tether should be taken into consideration because of the variation in the density of the atmosphere.

The descent in the denser layers of the atmosphere with significant velocities is accompanied by thermal heating. This means that there should be thermal protection on the spacecraft and stabilizer, but the amount of protection required can be defined only if the temperatures during descent are known. The knowledge of temperature regimes during the descent is a subject for further investigations. Another reason for temperature variations is the influence of the Sun.

The models used in this thesis for the modelling of the motion of the tether system, starting from the simplest rigid rod tether model, makes it possible to calculate the tension in the tether. The more complex model takes into consideration the elasticity of the tether thus providing with the information about the elastic deformation of the tether. The multi-point model, in addition to the factors listed above, includes the aerodynamic forces acting along the length of tether and the flexibility of the tether. Unfortunately, these models do not take the internal torsion of the tether into consideration.

The comparison of possible shapes of the cross-section of the tether is also of interest because different shapes have their advantages. When the cross-section is not circular, and the tether has, for example, tape form, its aerodynamic characteristics are dependent on the angle between its surface and the oncoming airflow. Therefore, it is necessary to include the torsion and rotation of the tether and its parts around its longitudinal axis.

At the moment of separation, the second body can receive a torque which leads to a rotation around its longitudinal axis. If the connection of the tether to the rigid body does not include a swivel, then the tether will twist. This can cause a change in the aerodynamic and elastic characteristics of the tether, and lead to jamming of the unreeling devices. Contrariwise, the torsion force from the tether could cause the lightweight bodies to rotate. Therefore, the torsion of the tether is of significant interest and should be included in a advanced mathematical model.

A model describing the full dynamics within the tether should also include damping. As the damping is a mechanism for dissipating energy within a system, it should provide additional stabilization for the motion of the tether and, as a result, affect the motion of the whole tether system.

The model of deployment should also include the description of the unreeling process. The method by which the tether is put into the unreeling device is important because any possible residual effect will affect the properties of the tether. The friction of the tether during the deployment process affect the deployment process itself.

There is also a problem in the modelling of the unreeling device. It is important to determine how the tether is put into it, and this is a current open question for research. The method of putting the tether in would depend on the shape and material of the tether, for example a yo-yo winding principle can be used for thin tethers with circular cross-section, or a Z-fold method might be more appropriate for tape shaped tethers.

Next, there is a possibility to combine the aerodynamic method of stabilization of the tether system with other methods. For example, a tether system with electrically conducted tether might allow to use advantages of both types of stabilization with one tether. Of course, the combination of these methods require a tether made from proper materials.

REFERENCES

Alary, D., Andreev, K., Boyko, P., Ivanova, E., Pritykin, D., Sidorenko, V., Tourneur, C., Yarotsky, D. (2015) *Dynamics of multi-tethered pyramidal satellite formation.* Acta Astronautica. Vol. 117, pp. 222-230.

Alekseev, K.B. and Bebenin, G.G. (1974). *Spacecraft control*. Moscow: Mashinostroenie [In Russian]

Alpatov, A.P., Beletsky, V.V., Dranovskii, V.I., Khoroshilov, V.S., Pirozhenko, A.V., Troger, H., Zakrzhevskii, A.E. (2010). *Dynamics of tethered space systems.* Boca Raton, FL: CRC Press. http://mech.spbstu.ru/images/c/c3/Dynamics_of_Tethered_Space_Systems.pdf [Accessed 15 Jan. 2019]

Anderson, J. (1989). *Hypersonic and high temperature gas dynamics*. New York: McGraw-Hill.

Anselmo, L. and Pardini, C. (2005). The survivability of space tether systems in orbit around the earth. *Acta Astronautica*, 56(3), pp.391-396.

Artsutanov, Y. (1960) *V Kosmos na Electrovoze.* Komsomolskaya Pravda, July 31, 1960 [In Russian]Aslanov, V.S. and Ledkov, A.S. (2015) *Dynamics of Tethered Satellite Systems.* Beijing: National Defense Industry Press, 2015. – 179 pp.

Aslanov, V.S., and Yudintsev, V.V. (2013) *Behavior of tethered debris with flexible append ages*. Acta Astronautica. V. 104. P. 91–98.

Babuscia A., Van de Loo M., Wei Q. J., Pan S., Mohan S., and Seager S. (2014) *Inflatable Antenna for CubeSat: Fabrication, Deployment and Results of Experimental Tests*. IEEE Aerospace Conference, Big Sky, Montana.

Beletskii, V.V., Ivanov, M.B., and Otstavnov E.I. (2005) *Model problem of a space elevator*. Cosmic Research. Vol. 43. № 2. pp. 152–156.

Beletsky, V.V., Kasatkin, G.V. and Starostin E.L. (1996) *The pendulum as a dynamical billiard*. Chaos, Solutions & Fractals. Vol. 7, № 8., pp. 1145-1178.

Bertin, J.J., and Cummings, R. M. (2009) *Aerodynamics for Engineers*. Pearson Prentice Hall, Upper Saddle Brook.

Butcher J.C. (2003) *Numerical Methods for Ordinary Differential Equations, 2nd ed*. Wiley

Bouwmeester, J. G. H., Marissen, R., and Bergsma, O.K. (2008) Carbon/Dyneema® Intralaminar hybrids: new strategy to increase impact resistance or decrease mass of carbon fiber compositer. 26th International Conference Of The Aeronautical Sciences. https://www.dsm.com/content/dam/dsm/dyneema/en_GB/Downloads/v2-science/Abstract%20CarbonDyneema%20intralaminar%20hybrids.pdf [Accessed 15 Jan. 2019].

Carroll, J. and Oldson, John C. (1995) *Tethers for Small Satellite Applications.* AIAA/USU Small Satellite Conference Logan, Utah. https://digitalcommons.usu.edu/cgi/viewcontent.cgi?httpsredir=1&article=2532&context=smallsat [Accessed 15 Jan. 2019]

Chen, Y., Huang, R., He, L., Ren, X. and Zheng, B. (2014). Dynamical modelling and control of space tethers: a review of space tether research. *Nonlinear Dynamics*, 77(4), pp.1077-1099.

Clancy, L. J. (1975). *Aerodynamics*, Pitman Publishing Limited, London.

Colombo, G., Gaposchkin, E. M., Grossi, M. D., and Weiffenbach, G. C. (1975) *The 'Skyhook': A Shuttle-Borne Tool for Low Orbital Altitude Research.* Meccanica, Vol. 10, No. 1, Mar. 1975.Contopoulos, G. (1963). *A Classification of the Integrals of Motion.* Astrophysical Journal, vol. 138, pp.1297-1305

Cosmo, M. L. and Lorenzini, E. C. (1997) *Tethers in Space Handbook. Third edition*. Smithsonian Astrophysical Observatory. http://www.tethers.com/papers/TethersInSpace.pdf

Cutler, C. (2015). *The 3 Types Of Static And Dynamic Aircraft Stability*. [online] Boldmethod.com. Available at: https://www.boldmethod.com/learn-to-fly/aerodynamics/3-types-of-static-and-dynamic-stability-in-aircraft/ [Accessed 15 Jan. 2019].

Dong, Z., Zabolotnov, Y. M., and Wang, C. (2017) *Modeling and analysis of deployment dynamics of a distributed orbital tether system with an atmospheric sounder*. 3rd IAA Conference on Dynamics and Control of Space Systems: pp. 1053-1063.

Donovan, Allen (1957) *Aerodynamic Components of Aircraft at High Speeds,* Princeton University Press.

Daydkin, A.A., Kozlov, S.S., Lapygin, V.I., Lipnitskiy Y.M., Nikitin N.D., Petrov V.I., and Ryabova S.V. (2002) *Study of aerodynamic aspects of the problem of reducing the areas of falling flaps fairings of launch vehicles*. Cosmonavtika i raketostroenie, Vol. 3(28), pp. 17-25 [In Russian]

Elenev, D., and Zabolotnov, Y. (2017) *Modeling and analysis of motion of a spacecraft with a tether aerodynamic stabilizer.* CEUR Workshop Proceedings. Vol. 1904, pp. 85-88

Elenev, D.V., Zabolotnov, Y.M., and McMillan, A.J. (2017) *Deployment and stabilization of an aerodynamic space tether system.* Advances in the Astronautical Sciences Vol. 161, pp. 1023-1030.

Erofeev, A.I. (1969) *Interaction of molecules with the surface of a solid*. Journal of Applied Mechanics and Technical Physics. Volume 7, Issue 3, pp. 26-30.

Gantmacher, F.R. (1959). *The Theory of Matrices I*. American Mathematical Society, Chelsea

Greenwood, D. (2000). *Classical dynamics*. Mineola: Dover Publications.

Grossi, M. (1973) *A ULF Dipole Antenna on a Spaceborne Platform of the PPEPL Class.* Report on NASA Contract NAS8-28203, May 1973

Halliday, D., Resnick, R. and Walker, J. (2011). *Fundamentals of physics*. Hoboken, NJ: Wiley.

ISO 2533:1975 (1975). *ISO 2533:1975 Standard Atmosphere*. [online] ISO 2533:1975. Available at: https://www.iso.org/standard/7472.html [Accessed 15 Jan. 2019].

Jin, D.P. and Hu, H.Y. (2006) *Optimal control of a tethered subsatellite of three degrees of freedom.* Nonlinear Dynamics. Vol. 46, № 1–2. pp. 161–178.

Johnson, L., Fujii, H.A. and Sanmartin, J.R. (2010) *Electrodynamic Propulsion System Tether Experiment (T-Rex)*. 57th JANNAF Joint Propulsion Meeting, Colorado. https://ntrs.nasa.gov/archive/nasa/casi.ntrs.nasa.gov/20100024214.pdf

Johnson L., Gilchrist B., Estes R. D., and Lorenzini E. (1999) *Overview of future NASA tether applications.* Adv. Space Research Vol. 24. № 8. pp. 1055–1063.

Ishkov, S.A., and Naumov, S.A. (2006) Control over orbital tether system unfolding Vestnik SSAU Vol. 1 (9) pp. 77-85.

Kruijff, M., Heide, E., and Stelzer, M. (2008) *Applicability of Tether Deployment Simulation and Tests based on YES2 Flight Data.* AIAA-2008-7036.

Kruijff, M., Van Der Heide, E.J., Ockels, W.J., and Gill, E. (2008) *First mission results of the YES2 tethered SpaceMail experiment.* AIAA/AAS Astrodynamics Specialist Conference and Exhibit 2008-7385

Kruijff, M. (2011) *Tethers in Space*. Netherlands: Delta-Utec Space Research, 2011.

Kane, T.R.; and Levinson, D.A. (1980). *Formulation of Equations of Motion for Complex Spacecraft.* Journal of Guidance and Control. 3: pp. 99–112.

Kumar, K.D., Yasaka, T. and Sasaki, T. (2004) *Orbit transfer of service vehicle/payload through tether retrieval.* Acta Astronautica. Vol. 54, № 9. pp. 687-698.

Kumar, K. (2006) *Review of dynamics and control of nonelectrodynamic tethered satellite systems*. Journal of Spacecraft and Rockets. Vol. 43. № 4. pp. 705–720.

Landau, L. D. and Lifschitz, E. M. (1976) *Mechanics, 3rd ed*. Oxford, England: Pergamon Press.

Lang, D.D., and Nolting, R.R. (1967). *Operations with Tethered Space Vehicles.* Gemini Summary Conference, Houston, Texas, 1967, pp. 55–66.

Lee, T., Leok, M. and McClamroch, N. (2010). *Computational dynamics of a 3D elastic string pendulum attached to a rigid body and an inertially fixed reel mechanism.* Nonlinear Dynamics, 64(1-2), pp.97-115.

Levin, E. (2007). *Dynamic analysis of space tether missions*. San Diego, Calif: Univelt.

Lorenzini, E.C. , Cosmo, M.L., Kaiser, M., Bangham, M.E., Vonderwell, D.J., Johnson, L. (2000) *Mission analysis of spinning systems for transfers from low orbits to geostationary*. Journal of Spacecraft and Rockets. Vol. 37, № 2. pp. 165-172.

Lurie, A. (2002). *Analytical Mechanics*. Berlin, Heidelberg: Springer Berlin Heidelberg.

Lyapunov, A.M. (1992) *The general problem of the stability of the motion*, Taylor & Fransis Ltd.

Mankala, K.K., and Agrawal, S.K. (2008) *Dynamic modeling of satellite tether systems using Newton's laws and Hamilton's principle*. Journal of Vibration and Acoustics. Vol. 130. № 1. pp. 014501-1–014501-6.

Mantellato, R., Valmorbida, A., and Lorenzini, E. (2015) *Thust-aided librating deployment of tape tethers*. Journal of Guidance, Control, and Dynamics. Vol. 52. № 5. – pp. 1395-1406.

Mantri, P. (2007). *Deployment dynamics of space tether systems*. Ph.D. North Carolina State University.

Mason, W. (2016). *Hypersonic Aerodynamics*. [online] Dept.aoe.vt.edu. Available at: http://www.dept.aoe.vt.edu/~mason/Mason_f/ConfigAeroHypersonics.pdf [Accessed 15 Jan. 2019].

Maxwell, J. C. (1867) *On the Dynamical Theory of Gases*. Philosophical Transactions of the Royal Society of London

Mennon, C., Kruijff, M., and Vavonliotis, A. (2007) *Design and Testing of a Space Mechanism for Tether Deployment Journal of Spacecraft and Rockets.* Vol.44, No.4. pp.703-709.

Moravec H. (1977) *A Non-Synchronous Orbital Skyhook.* J. Astron. Sci. - 25, No 4. pp. 307-322.

NASA Science. (2016). *TSS | Science Mission Directorate*. [online] Available at: https://science.nasa.gov/missions/tss/ [Accessed 15 Jan. 2019].

Onoda, J., and Watanabe, N. (1988) *Tethered Subsatellite Swinging from Atmospheric Gradients*. Journal of Guidance, Control and Dynamics. Vol. 11. № 5. pp. 477–479.

Pasca, M., and Lorenzini, E. (1991) *Collection of Martian Atmospheric Dust with a Low Altitude Tethered Probe*. Advances in the Astronautical Sciences. Vol. 75. № 2. pp. 1121–1139.

Pradeep, S., and Kumar, K. (2003) *Extension of tethered satellites in the atmosphere.* Acta Astronautica. Vol. 52, №1, pp. 1–10.

Peraire, J. and Widnall, S. (2009). *Lecture L28 - 3D Rigid Body Dynamics: Equations of Motion; Euler's Equations.* [online] Ocw.mit.edu. Available at: https://ocw.mit.edu/courses/aeronautics-and-astronautics/16-07-dynamics-fall-2009/lecture-notes/MIT16_07F09_Lec28.pdf [Accessed 14 Apr. 2019].

Pugno, N., Schwarzbart, M., Steindl, A. and Troger H. (2009). *On the stability of the track of the space elevator*. Acta Astronautica. Vol. 64. pp. 524-537.

Puig-Suari, J. and Longuski, J.M. (1991) *Modeling and Analysis of Tethers in an Atmosphere.* Acta Astronautica. Vol. 25. № 11, pp. 679–686.

Reb, S. (1991). *Tether satellite systems. Part 1/ Orbital and relative motion.* Technische Universitat Munchen. Munchen, 1991.

Sabatini, M., Gasbarri, P. and Palmerini, G.B. (2016). *Elastic issues and vibration reduction in a tethered deorbiting mission.* Advances in Space Research. Vol. 57. pp. 1951-1964.

Space primer. (2009). Maxwell Air Force Base, Ala.: Air University Press. http://space.au.af.mil/au-18-2009/ [Accessed 15 Jan. 2019]

Tjavaras, A. (1996). *The dynamics of highly extensible cables*. Ph.D. Massachusetts Institute of Technology.

TSNIImash (2017). *TSNIImash*. [online] Available at: http://www.tsniimash.ru [Accessed 15 Jan. 2019].

U.S. Standard Atmosphere (1976). U.S. Standard Atmosphere. [online] Available at: https://ntrs.nasa.gov/archive/nasa/casi.ntrs.nasa.gov/19770009539.pdf [Accessed 15 Jan. 2019].

Van Der Heide, E.J., Kruijff, M., Avanzini, A., Liedtke, V., and Karlovsky, A. (2003) *Thermal protection testing of the inflatable capsule for YES2*. 54th International Astronautical Congress of the International Astronautical Federation (IAF), the

International Academy of Astronautics and the International Institute of Space Law. Volume 1, pp. 1719-1726.

Wen, H., Jin, D.P., Hu, H.Y. (2008) *Advances in dynamics and control of tethered satellite systems.* Acta Mechanica Sinica. Vol. 24. № 3. pp. 229–241.

Williams, P. (2006) *In-plane payload capture with an elastic tether.* Journal of Guidance, Control, and Dynamics. Vol. 29, № 4, pp. 810–821.

Williams, P., Hyslop, A. and Kruijff, M. (2006). *Deployment control for the YES2 Tether-assisted Re-entry Mission.* Advance in the Astronautical Sciences. Volume 123, part 2, pp. 1101-1120.

Williams, P. (2008) Deployment/retrieval optimization for flexible tethered satellite systems. Nonlinear Dynamics. V. 52. № 1–2. P. 159–179.

Williams, P., Hyslop, A., Stelzer, M. and Kruijff, M. (2009) *YES2 optimal trajectories in presence of eccentricity and aerodynamic drag.* Acta Astronautica. V. 64. № 7-8. P. 745–769.

Williams, P. (2010) *Electrodynamic tethers under forced-current variations part 2: Flexible-tether estimation and control*. Journal of Spacecraft and Rockets. V. 47. № 2. P. 320–333.

Wilson A. (1981) *A history of ballon satellites*. J. of Brit. Interplanet. Soc. 1981. Vol. 34, No. 1. pp. 10-22.

Yaroshevskiy, V.A. (1978) *Motion of Uncontrolled Body in the Atmosphere.* Mashinostroenie, Moscow [In Russian].

Zabolotnov, Y.M. (2003) *Movement of Light Re-entry Capsule around of the Centre of Mass in an Atmosphere*. Netherlands: ESA.

Zabolotnov, Yu.M., and Naumov, O.N. (2012) *Motion of a Descent Capsule Relative to Its Center of Mass when Deploying the Orbital Tether System.* Cosmic Research 50 (2), pp. 177-187.

Zabolotnov, Y. M. (2013) *Introduction to Dynamics and Control in Space Tether System.* Beijing: Science Press, 2013.

Zabolotnov, Y.M. (2015) *Control of the deployment of a tethered orbital system with a small load into a vertical position*. Journal of Applied Mathematics and Mechanics. Vol. 79. Issue 1. pp. 28-34.

Zander, F.A. (1977). *Selected Papers.* Riga [In Russian]

Zhong, R., and Zhu, Z. (2011) *Dynamic analysis of deployment and retrieval of tethered satellites using a hybrid hinged–rod tether model*. International Journal of Aerospace and Lightweight Structures. Vol. 1. № 2. pp. 239–259.

Zhu, L., Wang, J. and Ding, F. (2016). The Great Reduction of a Carbon Nanotube's Mechanical Performance by a Few Topological Defects. *ACS Nano*, 10(6), pp.6410-6415.

Zhu, R., Misra, A.K., and Modi, V. J. (1994) *Dynamics and Control of Coupled Orbital and Librational Motion of Tethered Satellite Systems*. Journal of the Astronautical Sciences. Vol. 42. № 3. pp. 319–342.

APPENDIX A. MATRICES OF EQUATIONS

A.1. Dynamic matrixes

Dynamic equations for motion of the system in the atmosphere are

$$A \cdot \dot{\bar{\omega}} = B,$$

where $A = [A_{ij}]$ - matrix of variable coefficients which are dependent from angles and angular velocities of both bodies, measured 9x9, $\dot{\bar{\omega}} = [\dot{\omega}_{x_1}, \dot{\omega}_{y_1}, \dot{\omega}_{z_1}, \dot{\omega}_{x_2}, \dot{\omega}_{y_2}, \dot{\omega}_{z_2}, \dot{\omega}_{x3}, \dot{\omega}_{y_3}, \dot{\omega}_{z_3}]^T$ is a vector of components of angular, and $B = [B_j]$ - vector of right parts of differential equations.

Matrix *A* components are as follows:

$A_{11} = I_{x1} + \frac{m_1 m_2}{m_1+m_2}(y_1^2 + z_1^2)$, $A_{12} = A_{21} = -\frac{m_1 m_2}{m_1+m_2} x_1 y_1$,

$A_{13} = A_{31} = -\frac{m_1 m_2}{m_1+m_2} x_1 z_1$, $A_{22} = I_{y1} + \frac{m_1 m_2}{m_1+m_2}(x_1^2 + z_1^2)$,

$A_{23} = A_{32} = -\frac{m_1 m_2}{m_1+m_2} y_1 z_1$, $A_{33} = I_{z1} + \frac{m_1 m_2}{m_1+m_2}(x_1^2 + y_1^2)$,

$A_{14} = A_{41} = \frac{m_1 m_2}{m_1+m_2}[(y_1 L_{32} - z_1 L_{22})z_2 - (y_1 L_{33} - z_1 L_{23})y_2]$,

$A_{15} = A_{51} = \frac{m_1 m_2}{m_1+m_2}[(y_1 L_{33} - z_1 L_{21})x_2 - (y_1 L_{31} - z_1 L_{21})z_2]$,

$A_{16} = A_{61} = \frac{m_1 m_2}{m_1+m_2}[(y_1 L_{31} - z_1 L_{21})y_2 - (y_1 L_{32} - z_1 L_{22})x_2]$,

$A_{24} = A_{42} = \frac{m_1 m_2}{m_1+m_2}[(z_1 L_{12} - x_1 L_{32})z_2 - (z_1 L_{13} - x_1 L_{33})y_2]$,

$A_{25} = A_{52} = \frac{m_1 m_2}{m_1+m_2}[(z_1 L_{13} - x_1 L_{33})x_2 - (z_1 L_{11} - x_1 L_{31})z_2]$,

$A_{26} = A_{62} = \frac{m_1 m_2}{m_1+m_2}[(z_1 L_{11} - x_1 L_{13})y_2 - (z_1 L_{12} - x_1 L_{32})x_2]$,

$A_{34} = A_{43} = \frac{m_1 m_2}{m_1+m_2}[(x_1 L_{22} - y_1 L_{12})z_2 - (x_1 L_{23} - y_1 L_{13})y_2]$,

$A_{35} = A_{53} = \frac{m_1 m_2}{m_1+m_2}[(x_1 L_{23} - y_1 L_{13})x_2 - (x_1 L_{21} - y_1 L_{11})z_2]$,

$A_{36} = A_{63} = \frac{m_1 m_2}{m_1+m_2}[(x_1 L_{21} - y_1 L_{11})y_2 - (x_1 L_{22} - y_1 L_{12})x_2]$,

$A_{44} = I_{x2} + \frac{m_1 m_2}{m_1+m_2}(y_2^2 + z_2^2)$, $A_{45} = A_{54} = -\frac{m_1 m_2}{m_1+m_2} x_2 y_2$,

$A_{55} = I_{y2} + \frac{m_1 m_2}{m_1+m_2}(x_2^2 + z_2^2)$,

$A_{46} = A_{64} = -\frac{m_1 m_2}{m_1+m_2} x_2 z_2$, $A_{56} = A_{65} = -\frac{m_1 m_2}{m_1+m_2} y_2 z_2$,

$$A_{66} = I_{z2} + \frac{m_1 m_2}{m_1+m_2}(x_2^2 + y_2^2),$$

$$A_{17} = A_{71} = -\frac{m_1 m_2}{m_1+m_2}(L_{33}^{13} y_1 - L_{32}^{13} z_1)x_3,\ A_{37} = A_{73} = -\frac{m_1 m_2}{m_1+m_2}(L_{32}^{13} x_1 - L_{31}^{13} y_1)x_3,$$

$$A_{47} = A_{74} = -\frac{m_1 m_2}{m_1+m_2}(L_{33}^{23} y_2 - L_{32}^{23} z_2)x_3,\ A_{57} = A_{75} = -\frac{m_1 m_2}{m_1+m_2}(L_{31}^{23} z_2 - L_{33}^{23} x_2)x_3,$$

$$A_{67} = A_{76} = -\frac{m_1 m_2}{m_1+m_2}(L_{32}^{23} x_2 - L_{31}^{23} y_2)x_3,\ A_{77} = \frac{m_1 m_2}{m_1+m_2}x_3^2,$$

$$A_{78} = A_{87} = 0,\ A_{18} = A_{81} = -\frac{m_1 m_2}{m_1+m_2}(L_{23}^{13} y_1 - L_{22}^{13} z_1)x_3,$$

$$A_{28} = A_{82} = -\frac{m_1 m_2}{m_1+m_2}(L_{21}^{13} z_1 - L_{23}^{13} x_1)x_3,\ A_{38} = A_{83} = -\frac{m_1 m_2}{m_1+m_2}(L_{22}^{13} x_1 - L_{22}^{13} y_1)x_3,$$

$$A_{48} = A_{84} = -\frac{m_1 m_2}{m_1+m_2}(L_{23}^{23} y_2 - L_{22}^{23} z_2)x_3,$$

$$A_{58} = A_{85} = -\frac{m_1 m_2}{m_1+m_2}(L_{21}^{23} z_2 - L_{23}^{23} x_2)x_3,\ A_{68} = A_{86} = -\frac{m_1 m_2}{m_1+m_2}(L_{22}^{23} x_2 - L_{21}^{23} y_2)x_3,$$

$$A_{88} = -\frac{m_1 m_2}{m_1+m_2}x_3^2,\ A_{99} = 1,\ A_{i9} = 0,\ A_{9j} = 0,$$

where $i, j = 1,2,\ldots 9$.

Matrix ***B*** components are:

$$B_1 = \left(\Delta\vec{r}_1 \times \vec{R}_1\right)_{x_1} + \frac{m_1}{m_1+m_2}\left(\vec{r}_1 \times \vec{R}_2\right)_{x_1} - \frac{m_2}{m_1+m_2}\left(\vec{r}_1 \times \vec{R}_1\right)_{x_1} + \\ + \frac{m_1 m_2}{m_1+m_2}\{\vec{r}_1 \times [\vec{\omega}_2 \times (\vec{\omega}_2 \times \vec{r}_2) - \vec{\omega}_1 \times (\vec{\omega}_1 \times \vec{r}_1)]\}_{x_1},$$

$$B_2 = \left(\Delta\vec{r}_1 \times \vec{R}_1\right)_{y_1} + \frac{m_1}{m_1+m_2}\left(\vec{r}_1 \times \vec{R}_2\right)_{y_1} - \frac{m_2}{m_1+m_2}\left(\vec{r}_1 \times \vec{R}_1\right)_{y_1} + \\ + \frac{m_1 m_2}{m_1+m_2}\{\vec{r}_1 \times [\vec{\omega}_2 \times (\vec{\omega}_2 \times \vec{r}_2) - \vec{\omega}_1 \times (\vec{\omega}_1 \times \vec{r}_1)]\}_{y_1},$$

$$B_3 = \left(\Delta\vec{r}_1 \times \vec{R}_1\right)_{z_1} + \frac{m_1}{m_1+m_2}\left(\vec{r}_1 \times \vec{R}_2\right)_{z_1} - \frac{m_2}{m_1+m_2}\left(\vec{r}_1 \times \vec{R}_1\right)_{z_1} + \\ + \frac{m_1 m_2}{m_1+m_2}\{\vec{r}_1 \times [\vec{\omega}_2 \times (\vec{\omega}_2 \times \vec{r}_2) - \vec{\omega}_1 \times (\vec{\omega}_1 \times \vec{r}_1)]\}_{z_1},$$

$$B_4 = \left(\Delta\vec{r}_2 \times \vec{R}_2\right)_{x_2} + \frac{m_2}{m_1+m_2}\left(\vec{r}_2 \times \vec{R}_1\right)_{x_2} - \frac{m_1}{m_1+m_2}\left(\vec{r}_2 \times \vec{R}_2\right)_{x_2} + \\ + \frac{m_1 m_2}{m_1+m_2}\{\vec{r}_2 \times [\vec{\omega}_1 \times (\vec{\omega}_1 \times \vec{r}_1) - \vec{\omega}_2 \times (\vec{\omega}_2 \times \vec{r}_2)]\}_{x_2},$$

$$B_5 = \left(\Delta\vec{r}_2 \times \vec{R}_2\right)_{y_2} + \frac{m_2}{m_1+m_2}\left(\vec{r}_2 \times \vec{R}_1\right)_{y_2} - \frac{m_1}{m_1+m_2}\left(\vec{r}_2 \times \vec{R}_2\right)_{y_2} + \\ + \frac{m_1 m_2}{m_1+m_2}\{\vec{r}_2 \times [\vec{\omega}_1 \times (\vec{\omega}_1 \times \vec{r}_1) - \vec{\omega}_2 \times (\vec{\omega}_2 \times \vec{r}_2)]\}_{y_2},$$

$$B_6 = \left(\Delta\vec{r}_2 \times \vec{R}_2\right)_{z_2} + \frac{m_2}{m_1+m_2}\left(\vec{r}_2 \times \vec{R}_1\right)_{z_2} - \frac{m_1}{m_1+m_2}\left(\vec{r}_2 \times \vec{R}_2\right)_{z_2} + \\ + \frac{m_1 m_2}{m_1+m_2}\{\vec{r}_2 \times [\vec{\omega}_1 \times (\vec{\omega}_1 \times \vec{r}_1) - \vec{\omega}_2 \times (\vec{\omega}_2 \times \vec{r}_2)]\}_{z_2},$$

$$B_7 = 0,$$

$$B_8 = \frac{m_1}{m_1+m_2}\left(\vec{R}_2\right)_{z3} - \frac{m_2}{m_1+m_2}\left(\vec{R}_1\right)_{z3} + \\ + \frac{m_1 m_2}{m_1+m_2}\{[\vec{\omega}_3 \times (\vec{\omega}_3 \times \vec{r}_3) - \vec{\omega}_1 \times (\vec{\omega}_1 \times \vec{r}_1) + \vec{\omega}_2 \times (\vec{\omega}_2 \times \vec{r}_2)]\}_{y3},$$

$$B_9 = \frac{m_1}{m_1+m_2}\left(\vec{R}_2\right)_{y3} - \frac{m_2}{m_1+m_2}\left(\vec{R}_1\right)_{y3} +$$
$$+\frac{m_1 m_2}{m_1+m_2}\{[\vec{\omega}_3 \times (\vec{\omega}_3 \times \vec{r}_3) - \vec{\omega}_1 \times (\vec{\omega}_1 \times \vec{r}_1) + \vec{\omega}_2 \times (\vec{\omega}_2 \times \vec{r}_2)]\}_{z3}.$$

Additional summands in vector B, related to the change of the tether length, are

$$\Delta B_1 = \frac{m_1 m_2}{m_1+m_2}\left\{\vec{r}_1 \times \left[2\left(\vec{\omega}_3 \times \frac{\tilde{d}\vec{r}_3}{dt}\right) + \frac{\tilde{d}^2\vec{r}_3}{dt^2}\right]\right\}_{x1},$$

$$\Delta B_2 = \frac{m_1 m_2}{m_1+m_2}\left\{\vec{r}_1 \times \left[2\left(\vec{\omega}_3 \times \frac{\tilde{d}\vec{r}_3}{dt}\right) + \frac{\tilde{d}^2\vec{r}_3}{dt^2}\right]\right\}_{y1},$$

$$\Delta B_3 = \frac{m_1 m_2}{m_1+m_2}\left\{\vec{r}_1 \times \left[2\left(\vec{\omega}_3 \times \frac{\tilde{d}\vec{r}_3}{dt}\right) + \frac{\tilde{d}^2\vec{r}_3}{dt^2}\right]\right\}_{z1},$$

$$\Delta B_4 = \frac{-m_1 m_2}{m_1+m_2}\left\{\vec{r}_2 \times \left[2\left(\vec{\omega}_3 \times \frac{\tilde{d}\vec{r}_3}{dt}\right) + \frac{\tilde{d}^2\vec{r}_3}{dt^2}\right]\right\}_{x2},$$

$$\Delta B_5 = \frac{-m_1 m_2}{m_1+m_2}\left\{\vec{r}_2 \times \left[2\left(\vec{\omega}_3 \times \frac{\tilde{d}\vec{r}_3}{dt}\right) + \frac{\tilde{d}^2\vec{r}_3}{dt^2}\right]\right\}_{y2},$$

$$\Delta B_6 = \frac{-m_1 m_2}{m_1+m_2}\left\{\vec{r}_3 \times \left[2\left(\vec{\omega}_3 \times \frac{\tilde{d}\vec{r}_3}{dt}\right) + \frac{\tilde{d}^2\vec{r}_3}{dt^2}\right]\right\}_{z2},$$

$$\Delta B_7 = 0,$$

$$\Delta B_8 = \frac{m_1 m_2}{m_1+m_2}\left\{\left[2\left(\vec{\omega}_3 \times \frac{\tilde{d}\vec{r}_3}{dt}\right) + \frac{\tilde{d}^2\vec{r}_3}{dt^2}\right]\right\}_{y3},$$

$$\Delta B_9 = \frac{m_1 m_2}{m_1+m_2}\left\{\left[2\left(\vec{\omega}_3 \times \frac{\tilde{d}\vec{r}_3}{dt}\right) + \frac{\tilde{d}^2\vec{r}_3}{dt^2}\right]\right\}_{z3}.$$

A.2. Matrices for coordinate systems

Let us consider the position of the bound coordinate system relative to the trajectory (figure A1). Matrices of elementary rotations occurring in the process of transition between the trajectory and the bound coordinate systems are as follows

$$L_{\gamma_1} = \begin{bmatrix} 1 & 0 & 0 \\ 0 & \cos\gamma_1 & \sin\gamma_1 \\ 0 & -\sin\gamma_1 & \cos\gamma_1 \end{bmatrix}, L_{\alpha_1} = \begin{bmatrix} \cos\alpha_1 & \sin\alpha_1 & 0 \\ -\sin\alpha_1 & \cos\alpha_1 & 0 \\ 0 & 0 & 1 \end{bmatrix}, L_{\phi_1} = \begin{bmatrix} 1 & 0 & 0 \\ 0 & \cos\phi_1 & \sin\phi_1 \\ 0 & -\sin\phi_1 & \cos\phi_1 \end{bmatrix},$$

$$L_{\alpha_2} = \begin{bmatrix} \cos\alpha_2 & \sin\alpha_2 & 0 \\ -\sin\alpha_2 & \cos\alpha_2 & 0 \\ 0 & 0 & 1 \end{bmatrix}, L_{\gamma_2} = \begin{bmatrix} 1 & 0 & 0 \\ 0 & \cos\gamma_2 & \sin\gamma_2 \\ 0 & -\sin\gamma_2 & \cos\gamma_2 \end{bmatrix}, L_{\phi_2} = \begin{bmatrix} 1 & 0 & 0 \\ 0 & \cos\phi_2 & \sin\phi_2 \\ 0 & -\sin\phi_2 & \cos\phi_2 \end{bmatrix},$$

$$L_{\gamma_3} = \begin{bmatrix} 1 & 0 & 0 \\ 0 & \cos\gamma_3 & \sin\gamma_3 \\ 0 & -\sin\gamma_3 & \cos\gamma_3 \end{bmatrix}, L_{\alpha_3} = \begin{bmatrix} \cos\alpha_3 & \sin\alpha_3 & 0 \\ -\sin\alpha_3 & \cos\alpha_3 & 0 \\ 0 & 0 & 1 \end{bmatrix}, L_{\phi_3} = \begin{bmatrix} 1 & 0 & 0 \\ 0 & \cos\phi_3 & \sin\phi_3 \\ 0 & -\sin\phi_3 & \cos\phi_3 \end{bmatrix}.$$

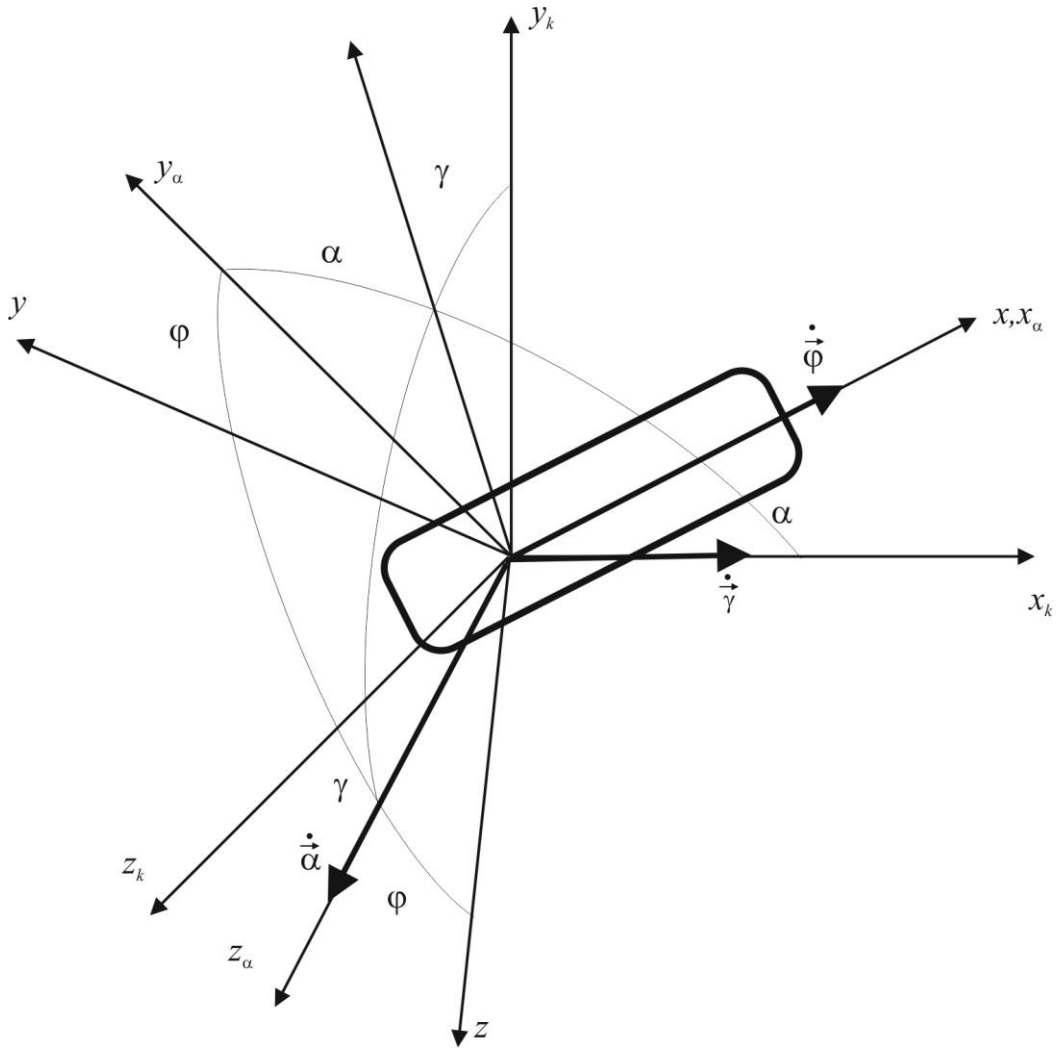

Figure A1 – Coordinate systems

Thereafter

$$\underset{1\leftarrow \mathrm{tr}}{L} = L_{\phi_1} \cdot L_{\alpha_1} \cdot L_{\gamma_1}, \quad \underset{2\leftarrow \mathrm{tr}}{L} = L_{\phi_2} \cdot L_{\alpha_2} \cdot L_{\gamma_2}, \quad \underset{3\leftarrow \mathrm{tr}}{L} = L_{\phi_3} \cdot L_{\alpha_3} \cdot L_{\gamma_3}, \qquad (A.1)$$

where $\underset{1\leftarrow \mathrm{tr}}{L}$ - transition matrix from the trajectory coordinate system to the coordinate system, related to the first body, $\underset{2\leftarrow \mathrm{tr}}{L}$ - transition matrix from the trajectory coordinate system to the coordinate system, related to the second body, $\underset{3\leftarrow \mathrm{tr}}{L}$ - transition matrix from the trajectory coordinate system to the coordinate system, related to the third body (tether).

Making use of relations (A1), it is possible to write down the transition matrix L from the coordinate system, related to the second body, to the coordinate system, related to the first body.

$$L = \underset{1\leftarrow 2}{L} = \underset{1\leftarrow \mathrm{tr}}{L} \cdot \underset{2\leftarrow \mathrm{tr}}{L^T}..$$

Analogously we obtain the expression for the L^{13} transition matrix from the coordinate system related to the tether, to the coordinate system related to the first body, and for the L^{23} transition matrix from the coordinate system related to the second body.

$$L^{13} = \underset{1\leftarrow 3}{L} = \underset{1\leftarrow \mathrm{tr}}{L} \cdot \underset{3\leftarrow \mathrm{tr}}{L^T}$$

$$L^{23} = \underset{2\leftarrow 3}{L} = \underset{2\leftarrow tr}{L} \cdot \underset{3\leftarrow \mathrm{tr}}{L^T}.$$

APPENDIX B. AERODYNAMIC CHARACTERISTICS FOR A CONE WITH ROUNDED APEX

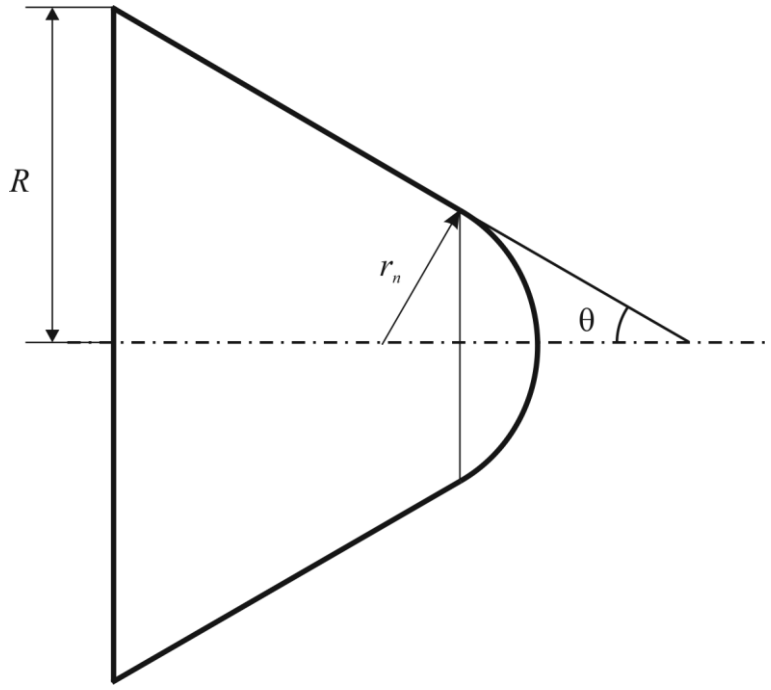

Figure B.1 – Geometric shape of the capsule

For the segment of a sphere force coefficients in Oxy_nz_n coordinate system, related to the plane of full angle of attack α, run over the following formulae.

When $0 \le \alpha \le \theta$

$C_{yn}^s = \frac{1}{2}\cos^4\theta \ \sin(2\alpha),\ C_x^s = 2\cos^2\theta \quad [1 - \frac{1}{2}\cos^2\theta - (1 - \frac{3}{4}\cos^2\theta)\sin^2\alpha] \quad .$

When $\theta < \alpha < \frac{\pi}{2}$

$C_{yn}^s = \frac{1}{4}\cos^4\theta \ \sin(2\alpha) \ (1 + \frac{2}{\pi}\beta) + \frac{\gamma}{\pi}\sin\alpha + \frac{1}{3\pi}\sin\alpha\sin\theta \ [\sin^2\theta(3 - \sin^{-2}\alpha) - 5]\, A,$

$C_x^s = (1 + \frac{2}{\pi}\beta) \quad [1 - \frac{1}{2}\cos^2\theta - (1 - \frac{3}{4}\cos^2\theta)\sin^2\alpha]\cos^2\theta + \frac{\gamma}{\pi}\cos\alpha +$

$+ \frac{\cos\alpha}{2\pi}\sin\theta(1 - 3\sin^2\theta) \ A$,

where $\beta = \arcsin(\ \frac{tg\theta}{tg\alpha}\ ), \quad \gamma = \arccos(\ \frac{\sin\theta}{\sin\alpha}\ )$, $A = \sqrt{\sin^2\alpha - \sin^2\theta}$.

Analogical formulae for the body of specified shape (conoid) are as follow:

when $0 \le \alpha \le \theta$ $C_{yn}^c = \frac{1}{2}\cos^2\theta \ \sin(2\alpha)$, $C_x^c = 2\sin^2\theta + \ (1 - 3\sin^2\theta)\sin^2\alpha$;

when $\theta < \alpha < \frac{\pi}{2}$

$C_{yn}^c = \frac{1}{2}\cos^2\theta \ \sin(2\alpha) \ [1 + \frac{2}{\pi}\beta + \frac{2}{3\pi}\sqrt{1 - \frac{tg^2\theta}{tg^2\alpha}} \ \ (2\frac{tg\alpha}{tg\theta} + \frac{tg\theta}{tg\alpha})]$,

$C_x^c = \frac{1}{2}(1 + \frac{2}{\pi}\beta) \ \ [2\sin^2\theta + (1 - 3\sin^2\theta)\sin^2\alpha] + \frac{3}{4\pi}\sqrt{1 - \frac{tg^2\theta}{tg^2\alpha}} \ \ \sin(2\alpha)\sin(2\theta)$.

Aerodynamic force coefficients for cone with spherical front part are obtained from force coefficients of the segment and of the conoid in this way

$$C_{yn}^c = C_{yn}^s \, \bar{r}_n^2 + C_{yn}^c(1 - \bar{r}_n^2\cos^2\theta), \ C_x^c = -C_x^s \, \bar{r}_n^2 - C_x^c(1 - \bar{r}_n^2\cos^2\theta),$$

where $\bar{r}_n = \frac{r_n}{R}$, r_n - radius of the spherical front part, R - radius of the bottom part of the capsule.

The restoring aerodynamic moment coefficient relative to the front part of the capsule is calculated by formula

$m_{zn} \ = -C_{yn}^s \frac{tg\theta}{L_o}\bar{r}_n^3 - \frac{C_{yn}^c}{L_o}(1 - \bar{r}_n^2\cos^2\theta) \ [x_d \frac{L_c}{L} + (1 - \frac{L_c}{L})]$,

where $L_o = \frac{L}{R}tg\theta$, $L = \frac{R}{tg\theta} + r_n - \frac{r_n}{\sin\theta}$ – the capsule length, $L_c = (R - r_n\cos\theta) \ ctg\theta$ – conoid length, $x_d = \frac{2}{3\cos^2\theta} \ \frac{(1+R_L+R_L^2)}{1-R_L^2} - \frac{R_L}{1-R_L}$ - value, determining the position of the centre of aerodynamic forces for conoid; $R_L = \frac{r_n}{R}\cos\theta$.

Thereafter the aerodynamic moment relative to the centre of mass of the capsule is determined by the expression

$$m_{zc} = m_{zn} - C_{yn}x_c,$$

where $x_c < 0$ – the position of centre of mass relative to the front part of the capsule.

The position of the point of aerodynamic force application for the capsule relative to the front part is determined by the formula

$$x_D = \frac{m_{zn}}{C_{yn}}.$$